

UNIVERSITY OF BIRMINGHAM

ELECTROCATALYSIS IN AQUEOUS BRINES AND AT LOW TEMPERATURES

by

Elizabeth Sargeant

A thesis submitted to the University of Birmingham for the degree of

Doctor of Philosophy

School of Chemistry
College of Engineering and Physical Sciences
The University of Birmingham
December 2022

UNIVERSITY OF
BIRMINGHAM

University of Birmingham Research Archive

e-theses repository

This unpublished thesis/dissertation is copyright of the author and/or third parties. The intellectual property rights of the author or third parties in respect of this work are as defined by The Copyright Designs and Patents Act 1988 or as modified by any successor legislation.

Any use made of information contained in this thesis/dissertation must be in accordance with that legislation and must be properly acknowledged. Further distribution or reproduction in any format is prohibited without the permission of the copyright holder.

ABSTRACT

This work investigates electrocatalytic reduction of CO_2 in concentrated electrolytes at temperatures below zero. In $Mg(ClO_4)_2$ and KOH brines the reduction of CO_2 at these low temperatures is promoted in favour of the main competing reaction, hydrogen evolution. These results discuss potential scenarios for CO_2 reduction in non-standard conditions, such as in the freezing, CO_2 rich environment on the Martian surface. In an aim to understand the reason for the increase in CO_2 reactivity at low temperature, so that the system can be refined and improved, further studies on physiochemical parameters and computational calculations are also presented. The change in viscosity with temperature is measured and its consequent effect on the diffusion of CO_2 discussed. The role of the electrolyte in stabilising reactant intermediates is probed using computational calculations. Together these results provide preliminary insights into the CO_2 reduction reaction at these low temperatures.

ACKNOWLEDGEMENTS

First and foremost, I would like to thank everyone who has supervised this research, without whom, this thesis would not exist. Dr Paramaconi Rodriguez had the original idea for this work and his passion and helpful suggestions have continued to be of great assistance. I would also like to thank him for the personal support he has shown me during difficult times, without which I would have struggled to continue. I extend profound thanks to Dr Federico Calle-Vallejo for teaching me everything I know about DFT calculations, for all of the opportunities he has offered me, and for all of the enjoyable discussions we have had. Without him my visits to the University of Barcelona and the opportunity to author papers would not have happened and so I am very grateful. Prof Tim Albrecht generously took over secondary supervision of my project and then later made room in his lab for me when Para moved abroad for different opportunities. I will always be appreciative for this and for his willingness to be involved in my work. Dr Cécile Le Duff is indispensable to the whole of the School of Chemistry, but I would like to thank her for the individual help she has given me. Finally, I would like to thank the late Prof Roy Johnston. He was a lovely man and an excellent scientist whose support with computational work at the beginning of my project will not be forgotten.

All members of the Ampere group, past and present, deserve a thank you for their scientific aid and discussions but also for making working in the lab an enjoyable experience (sometimes…). In particular, thanks to Nashwa, Matthew, Jake, and Adam for being friends as well as lab mates. Outside of my research group, my lunch crew have helped make me a better scientist and crossword solver! I will always be thankful that I met my friend Menisha – our coffee dates and phone calls have helped with all aspects of my life during the PhD.

My housemates and friends, David, Joe, and George have helped me get through this PhD. It has been really tough at times but living with them meant it will always be one of the best periods of my life. My habebtis also deserve thanks for their longstanding friendship and

support. Phone calls with Charanpreet and Duaa have kept me going numerous times when I have been struggling. Deep gratitude also goes to Andrea, without whom, I would not be where I am today. Oliver gets my love and thanks for all the innumerable ways he has supported me during this time.

Lastly, without all the help from my family I would not be who I am and where I am. Thank you to my mum, Helen, my grandma, Jane, and my brothers, James and Robert, for their love.

CONTENTS

Introduction .……1

References ……..……10

Chapter 1: Electrochemical conversion of CO_2 in non-conventional electrolytes: Recent achievements and future challenges ……..……12

Chapter 2: Electrochemical conversion of CO_2 and CH_4 at Sub-zero Temperatures ……..…13

Supporting Information ……14

Chapter 3: Determination of kinematic viscosity of $Mg(ClO_4)_2$ and KOH brines saturated with CO_2 at Sub-Zero Temperatures ……..……34

Abstract ……..……35

3.1 Introduction ……..35

3.2 Methodology ……..……..……38

3.3 Results and Discussion ……..……40

3.4 Conclusions ……..……45

3.5 Acknowledgments ……..…46

3.6 References ……..…47

Chapter 4: Investigating the stabilising effects of the electrolyte on CO2 reduction intermediates using DFT calculations ……..……49

4.1 Introduction ……..50

4.2 Methodology ……52

4.3 Results and Discussion ……..56

4.4 Conclusions and Future Work ……. 62

4.5 References ……..63

Final Conclusions and Future Work ……65

5.1 Conclusion ……..……..66

5.2 Future Work ……..68

INTRODUCTION

Introduction

As humanity continues its exploration of the solar system, the next goal in the journey is to send human astronauts to other planets. There are a number of obstacles which need to be overcome for this to be a reality. Long travel times currently limit interstellar travel to nearby planets and celestial bodies in our native solar system such as Venus, Mercury, Mars, Jovian and Saturnian moons, and our Moon. However, another huge obstacle is the provision of materials for an extended stay on another planet. It costs 12-13 tons of fuel to transport 1 ton of material out of Earth's atmosphere,[1] and so *in-situ* utilisation of planetary resources to synthesise oxygen and fuels is a rich and vital area of research.

Electrolysers will be a key technology for *in-situ* resource utilisation (ISRU). Electrolysers work by applying a potential to a material which then catalyses the conversion of reactants. The efficient synthesis of any substance is heavily influenced by the environmental conditions, and so the atmospheric conditions of other planetary bodies must be taken into account when planning reactions. Figure 1 and Table 1 show that the atmospheric composition and conditions vary wildly on different planets.[2] Mars and Venus have atmospheres very unlike our own, there the atmosphere is mostly CO_2 and there is no significant O_2 or H_2O present. Both are a necessity for life and will need to be synthesised if either of these planets is to be colonised. On Venus, floating colonies would have to be in the upper atmosphere due to incredibly high temperatures and pressures on the surface[3] and so, of these target planets, Mars is the favourite for scientists due to its favourable travel times and the fact that surface conditions are most similar to Earth. On Mars, prototypes of ISRU are already being used to compress the sparse, but CO_2 rich, atmosphere and then heating it to over 1000 K to convert it to syngas using a solid oxide fuel cell.[1,4] As of March 2022, MOXIE (Mars Oxygen ISRU Experiment) has been used to generate around 50 g of O_2 which would be used to provide breathable air for astronauts and for fuelling the Mars Ascent Vehicle (MAV).[1]

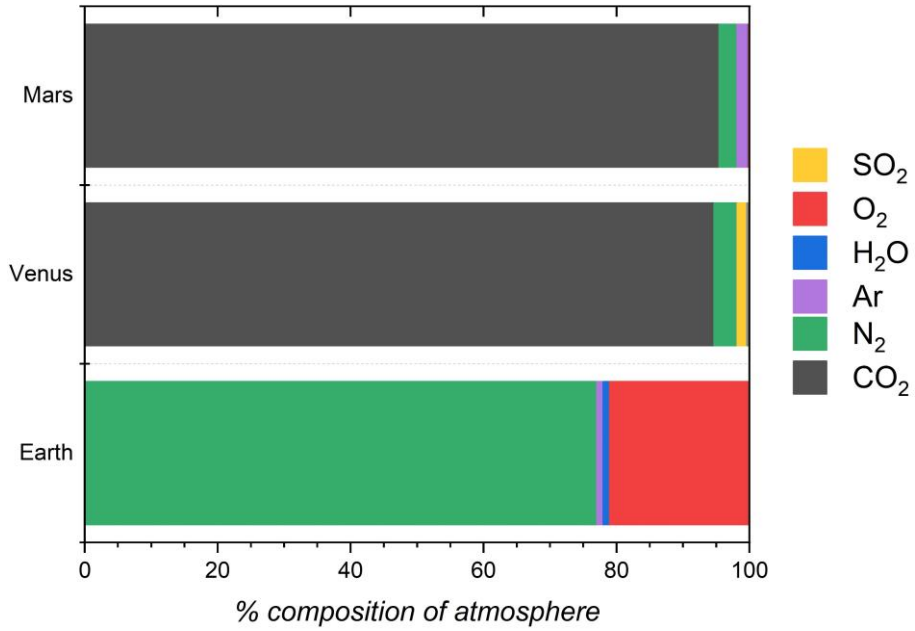


Figure 1. *The composition of gases that make up the atmosphere on various planets within our solar system. Adapted from reference 2*

Table 1. *Values for parameters important to consider for colonisation of planets in our solar system. Also adapted from reference 2*

	Earth	**Mars**	**Venus**
year	1	1.88	0.615
solar day	1	1.03	117
surface T / K	288	220	730
surface pressure / atm	1	0.007	91
surface gravity / m s^{-2}	9.8	3.72	8.87

Pressure and temperature are parameters often altered to improve the yield and efficiency of reactions, and on other planets, the ambient conditions may help or hinder these reactions. High pressure and/or low temperatures generally favour the increased solubility of gases in water[5] and so, if water can be found or synthesised, the different conditions on other planets may, in fact, greatly improve the efficiency of certain reactions. Any evidence of liquid water on Mars, has pointed to the presence of liquids with very high salt concentrations, brines, which only occur under specific conditions.[6–11] CO_2 solubility increases as temperature decreases[5] and since the atmosphere on Mars is mostly CO_2 and the average surface temperature is 220 K, it stands to reason the brines present on the surface may have high concentrations of dissolved CO_2.

The parameters of pressure, temperature, and electrolyte salinity are a rich area of research for the electrocatalytic conversion of CO_2 on Earth.[12–14] The ever-increasing concentration of CO_2 in our atmosphere is causing climate change at an alarming rate.[15] One avenue of mitigating these effects is to capture CO_2 at major production sites and either store it underground or in deep sea aquifers, or to convert it to value added products. Electrocatalytic reduction of CO_2 is one of many potential methods of CO_2 conversion.

Table 2. *Common CO_2RR target products and the standard potential, E°, at 25 °C and 1 atm.*[34] *An example catalyst is provided for each product and the faradaic efficiency, FE, and overpotential, ɖ, using that catalyst in 0.1 M $KHCO_3$ (pH å 6.8).*[14]

product	***E°* / V**	**electrocatalyst**	**FE / %**	***ɖ* / V**
HCOOH	-0.250	Pb	97.4	-1.19
CO	-0.106	Au nanoparticles	97	-0.58
CH_4	0.169	Cu poly-faceted	40.4	-1.34
C_2H_4	0.064	Cu poly-faceted	26.0	-1.13
CH_3CH_2OH	0.084	Cu_2O	9-16	-1.08

The CO_2 reduction reaction (CO_2RR) was first studied in depth by Yoshio Hori in the 1980s. He showed that although many metal catalysts will reduce CO_2, copper is unique in producing hydrocarbons in appreciable amounts[16,17] and later work by Kuhl *et al*. identified up to 16 different reaction products, including very small amounts of acetone, ethylene glycol and methanol.[18] Table 2 shows some of the common products of CO_2RR and their standard potentials and illustrates the number of issues that need to be solved if the CO_2RR is to be used in an electrolyser. CO_2RR requires large overpotentials, for example around 1.3 V for methane formation, and the faradaic efficiency (FE) for hydrocarbon products is low. The low FE is due to the aforementioned abundance of different potential products but also due to the concurrent hydrogen evolution reaction (HER).[19,20] Competition from the HER is a major issue in aqueous electrolytes since under CO_2 reduction conditions, the main pathway is via reduction of water which is of course, readily available.[19]

There are various avenues to try and mitigate some of these issues, some of which are shown in Figure 2. On the macroscale Figure 2(a), increasing the concentration of the

electrolyte can improve the buffering capability of the electrolyte near the surface.[21] This lowers the rate of the depletion of protons next to the surface and maintains a higher concentration of CO_2. The use of alkali metal cations has been shown to affect the selectivity of the reaction, where larger cations promote the production of C_2 products. There is debate as to whether this promoting effect is due to accumulation of the cations in the Helmholtz plane modifying the electric field, direct stabilisation of reduction intermediates, or the hydration shell of the cations contributing to the buffering of the interfacial pH. However, evidence seems to support direct stabilisation having the most influential role[22–24] which is of particular interest to this research, since the electrolytes used are of such high salinity. On the nanoscale, Figure 2(b), the surface orientation of the electrode can have large effects on the selectivity of the reaction. As an

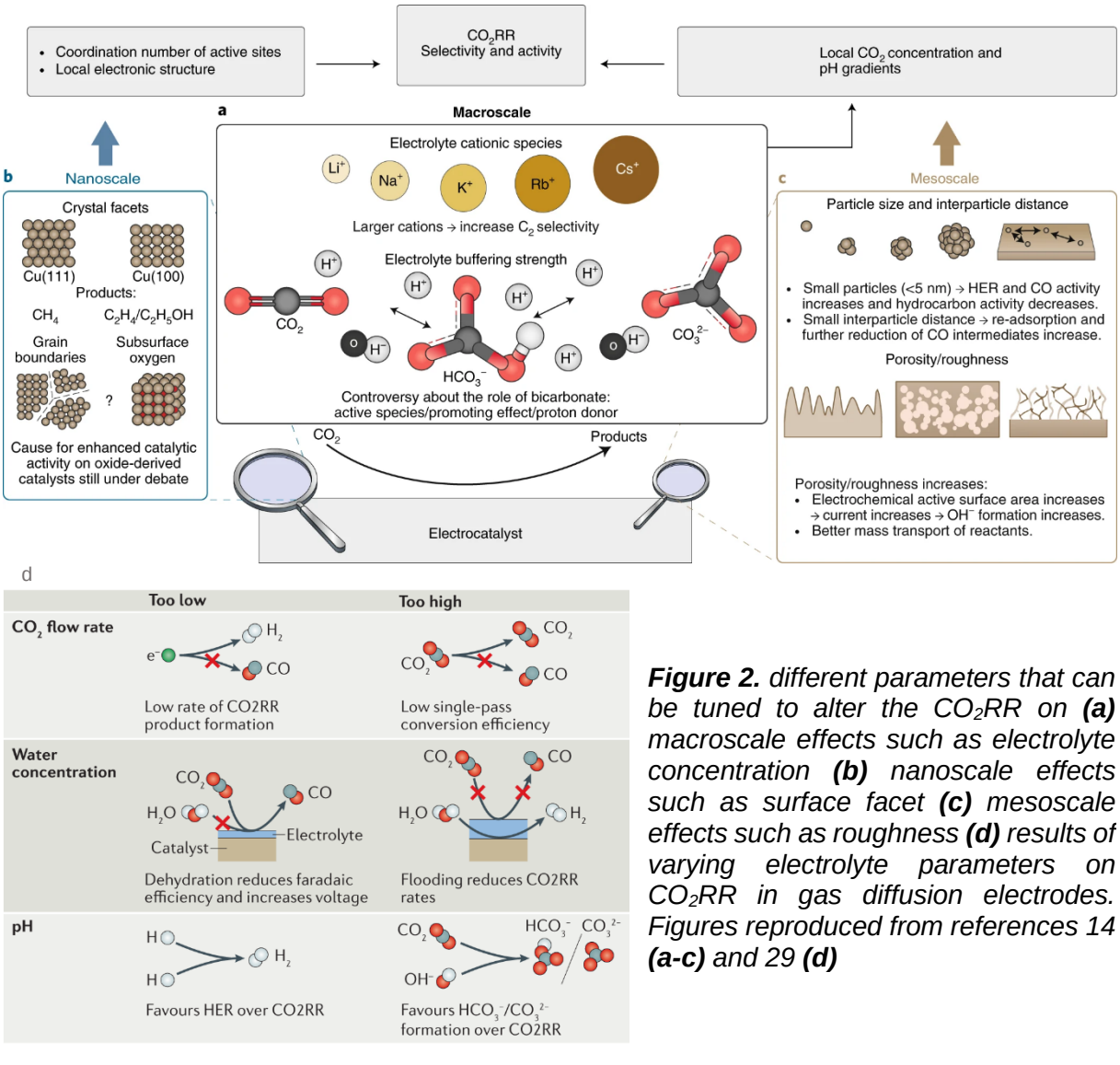


Figure 2. *different parameters that can be tuned to alter the CO_2RR on* ***(a)*** *macroscale effects such as electrolyte concentration* ***(b)*** *nanoscale effects such as surface facet* ***(c)*** *mesoscale effects such as roughness* ***(d)*** *results of varying electrolyte parameters on CO_2RR in gas diffusion electrodes. Figures reproduced from references 14* ***(a-c)*** *and 29* ***(d)***

example, Cu(100) surfaces promote the production of C_2 products rather than C_1.[25,26] On the mesoscale, roughening the surface of the electrode increases the surface area which has the dual benefits of increasing undercoordinated sites and reducing the mass transport of water, which both contribute to higher CO_2RR rates.

Another bottleneck to the reaction efficiency is that at standard temperature and pressure, CO_2 is only sparingly soluble in water, 34 mM at 25 °C and 1 atm. Work using gas diffusion electrodes or rotating disk electrodes, where the mass transport is strictly controlled, has shown that high concentrations of CO_2 are essential for inhibiting HER in favour of CO_2RR, Figure 2(d).[19,27–29] High concentrations of CO_2 at the surface are reduced to CO which then blocks surface sites for water adsorption and so HER is limited and the product selectivity can change. High concentration of CO_2 in solution is therefore desirable for high faradaic efficiencies. This has been achieved through pressurisation[30] but this is not the only method and a different avenue is discussed below.

Water with high concentrations of dissolved gases can be found on in various environments on Earth. At high pressures or low temperatures, gas clathrates are formed where cages of water molecules encapsulate gas molecules.[31] These phases are well known since in the mining industry they can form in gas pipelines, causing costly blockages, and since CH_4 versions are found in the permafrost or in the deep ocean. The CH_4 hydrates in the ocean and permafrost are a double edged sword, they could be a huge reservoir of energy if

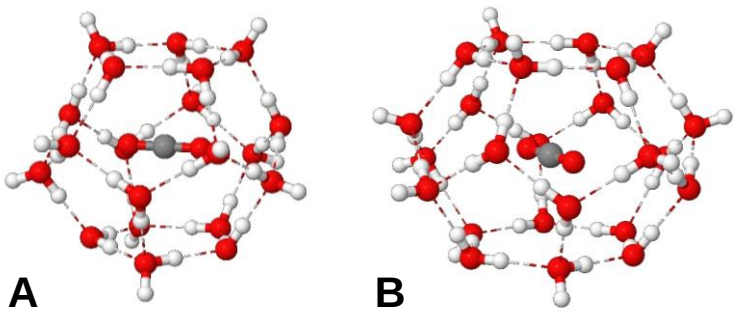


Figure 3. *Cages present in sI type clathrate with CO_2 occupant. (A) 20 water molecule cage, 5^{12} (B) 24 water molecule cage, $5^{12}6^2$*

electrocatalytic technology can be developed to exploit them but there is a small possibility that if oceanic temperatures continue to rise, the hydrates may become unstable, releasing CH_4 into the atmosphere leading to runaway warming.[32,33] When CO_2 is the guest molecule, an sI type clathrate is formed which is made up of two types of cages, shown in Figure 3, where the smaller 5^{12} cage is made of 12 pentagons and the larger $5^{12}6^2$ cage is made up of 12 pentagons and 2 hexagons. If these structures form at the electrode, then there will be consequent effects on the mobility of the water molecules and the mass transport of reactants and products which will in turn affect the CO_2RR, and HER from water reduction. This research will contribute to the understanding of electrocatalytic processes involving clathrate hydrates.

Using concentrated electrolytes and low temperature for CO_2RR is another avenue to increase CO_2 solubility. Up to a point, addition of salts to water lowers the freezing point which means that electrocatalytic reactions can be carried out in the liquid phase at sub-zero temperatures. The main idea behind this work is to perform the electrochemical reduction of CO_2 at sub-zero temperatures in brines. By decreasing the temperature, the concentration of CO_2 is expected to increase, resulting in changes to the product selectivity and efficiency of the reaction. This thesis aims to provide greater understanding of, and context to, the electrocatalytic conversion of CO_2 at low temperatures in brines.

Chapter 1 is a literature review of the electrochemical reduction of CO_2 to hydrocarbons in brines but also in other non-aqueous electrolytes, accepted for publication in Electrochemical Science Advances. These other electrolytes, such as organic solvents, molten carbonates, and ionic liquids, aim to alleviate the problems associated with CO_2RR in aqueous electrolytes, namely low CO_2 solubility, low selectivity, and competition from the HER. Overall, there is no perfect electrolyte which eliminates these issues and there are specific downsides associated with each. The downside in common with all the alternative electrolytes reviewed, is that in order to produce hydrocarbons from CO_2 a source of protons is needed which invariably reintroduces competition from the HER. To summarise CO_2RR in brines is an

emerging field with many questions still to be answered, but that concentrated aqueous electrolytes can increase the current density of the reaction and low temperatures can change the selectivity.

Chapter 2 of this thesis presents the preliminary studies carried out within our research group on CO_2 reduction in $Mg(ClO_4)_2$ and KOH brines at temperatures of around -20 °C. This work is published in ACS Catalysis. This work showed that the HER was suppressed, and the selectivity of the reaction changed as temperature decreased. Part of the work carried out by this author specifically focused on the identification and quantification of the liquid products of these reactions, the supporting information is included directly after. ^1H NMR is a common technique integral for the identification of chemicals and when used in conjunction with other NMR techniques can be used to elucidate structures of complex molecules. Since the electrocatalysis is carried out in aqueous electrolyte, albeit very concentrated, the signal from protons within the surrounding water need to be suppressed or they dwarf the signals from the products. Refinement of NMR parameters was needed since the high concentration of electrolyte ions affected the T1 relaxation of ^1H. To observe the effects of temperature on CO_2RR, accurate quantification of the products is needed.

Chapter 3 of this thesis is a paper submitted to Journal of Physical and Chemical Reference Data and focuses on how temperature affects the physiochemical properties of $Mg(ClO_4)_2$ and KOH brines. The current recorded at an electrode during an electrochemical reaction is dependent on both the kinetics of the reaction occurring and on the mass transport of species to and from the electrode. The mass transport encompasses the diffusion, convection, and migration processes, all of which are dependent on the diffusion coefficient of the species, which is in turn dependent on the viscosity of the medium. The viscosity as a function of temperature is presented before and after saturation with CO_2. From these results, conclusions about the diffusion and concentration of CO_2 in both brines are drawn.

Chapter 4 presents computational calculations which aim to understand how the energies of intermediate species in the CO_2RR are affected by the high concentration of the electrolyte. The protonation of CO_2 to from adsorbed COOH is generally considered to be the potential limiting step in and certain key intermediates are stabilised similarly by the surface which build in intrinsic scaling relations which must be broken in order to lower the overpotential of the reaction. For CO_2RR in dilute aqueous electrolyte, research focuses on optimising the structure of the catalyst, but work presented in this chapter shows that stabilisation by cations can also reduce these issues.

This thesis provides insights into electrocatalytic conversion of CO_2 at extremes of temperature and concentration. If electrocatalysis in these unusual conditions is to be used, for example for inter-planetary exploration or for sensing concentrations of clathrates in deep oceans, a fuller understanding of how the reaction and analysis of its results are affected by them is essential. Herein, an overview of the current knowledge is provided, and the importance of questioning how high concentrations can affect properties, which might be assumed to be unchanged, is highlighted.

References

1 J. A. Hoffman, M. H. Hecht, D. Rapp, J. J. Hartvigsen, J. G. SooHoo, A. M. Aboobaker, J. B. McClean, A. M. Liu, E. D. Hinterman, M. Nasr, S. Hariharan, K. J. Horn, F. E. Meyen, H. Okkels, P. Steen, S. Elangovan, C. R. Graves, P. Khopkar, M. B. Madsen, G. E. Voecks, P. H. Smith, T. L. Skafte, K. R. Araghi and D. J. Eisenman, *Sci. Adv.*, 2022, **8**, 1–7.

2 F. W. Taylor, *Planetary atmospheres / F.W. Taylor*, Oxford : Oxford University Press, Oxford, 2010.

3 G. A. Landis, in *AIP Conference Proceedings*, AIP, 2003, vol. 654, pp. 1193–1198.

4 M. Hecht, J. Hoffman, D. Rapp, J. McClean, J. SooHoo, R. Schaefer, A. Aboobaker, J. Mellstrom, J. Hartvigsen, F. Meyen, E. Hinterman, G. Voecks, A. Liu, M. Nasr, J. Lewis, J. Johnson, C. Guernsey, J. Swoboda, C. Eckert, C. Alcalde, M. Poirier, P. Khopkar, S. Elangovan, M. Madsen, P. Smith, C. Graves, G. Sanders, K. Araghi, M. de la Torre Juarez, D. Larsen, J. Agui, A. Burns, K. Lackner, R. Nielsen, T. Pike, B. Tata, K. Wilson, T. Brown, T. Disarro, R. Morris, R. Schaefer, R. Steinkraus, R. Surampudi, T. Werne and A. Ponce, *Space Sci. Rev.*, 2021, **217**, 9.

5 D. R. Lide, *CRC handbook of chemistry and physics*, CRC press, 85th edn., 2004.

6 M. H. Hecht, S. P. Kounaves, R. C. Quinn, S. J. West, S. M. M. Young, D. W. Ming, D. C. Catling, B. C. Clark, W. V. Boynton, J. Hoffman, L. P. DeFlores, K. Gospodinova, J. Kapit and P. H. Smith, *Science.*, 2009, **325**, 64–67.

7 P. H. Smith, L. K. Tamppari, R. E. Arvidson, D. Bass, D. Blaney, W. V. Boynton, A. Carswell, D. C. Catling, B. C. Clark, T. Duck, E. DeJong, D. Fisher, W. Goetz, H. P. Gunnlaugsson, M. H. Hecht, V. Hipkin, J. Hoffman, S. F. Hviid, H. U. Keller, S. P. Kounaves, C. F. Lange, M. T. Lemmon, M. B. Madsen, W. J. Markiewicz, J. Marshall, C. P. McKay, M. T. Mellon, D. W. Ming, R. V. Morris, W. T. Pike, N. Renno, U. Staufer, C. Stoker, P. Taylor, J. A. Whiteway and A. P. Zent, *Science.*, 2009, **325**, 58–61.

8 J. D. Toner and D. C. Catling, *Earth Planet. Sci. Lett.*, 2018, **497**, 161–168.

9 K. M. Primm, R. V. Gough, V. F. Chevrier and M. A. Tolbert, *Geochim. Cosmochim. Acta*, 2017, **212**, 211–220.

10 V. F. Chevrier, A. B. Fitting and E. G. Rivera-Valentín, *Planet. Sci. J.*, 2022, **3**, 125.

11 G. M. Marion, D. C. Catling, K. J. Zahnle and M. W. Claire, *Icarus*, 2010, **207**, 675–685.

12 M. König, J. Vaes, E. Klemm and D. Pant, *iScience*, 2019, **19**, 135–160.

13 M. Papasizza, X. Yang, J. Cheng and A. Cuesta, *Curr. Opin. Electrochem.*, 2020, **23**, 80–88.

14 Y. Y. Birdja, E. Pérez-Gallent, M. C. Figueiredo, A. J. Göttle, F. Calle-Vallejo and M. T. M. Koper, *Nat. Energy*, 2019, **4**, 732–745.

15 V. Masson-Delmotte, P. Zhai, A. Pirani, S. L. Connors, C. Péan, S. Berger, N. Caud, Y. Chen, L. Goldfarb, M. I. Gomis, M. Huang, K. Leitzell, E. Lonnoy, J. B. R. Matthews, T. K. Maycock, T. Waterfield, O. Yelekçi, R. Yu and B. Zhou, Eds., in *Climate Change 2021: The Physical Science Basis. Contribution of Working Group I to the Sixth Assessment Report of the Intergovernmental Panel on Climate Change*, Cambridge University Press, 2021.

16 Y. Hori, K. Kikuchi and S. Suzuki, *Chem. Lett.*, 1985, **14**, 1695–1698.

17 Y. Hori, H. Wakebe, T. Tsukamoto and O. Koga, *Electrochim. Acta*, 1994, **39**, 1833–1839.

18 K. P. Kuhl, E. R. Cave, D. N. Abram and T. F. Jaramillo, *Energy Environ. Sci.*, 2012, **5**, 7050–7059.

19 H. Ooka, M. C. Figueiredo and M. T. M. Koper, *Langmuir*, 2017, **33**, 9307–9313.

20 Y. Zhang, V. Sethuraman, R. Michalsky and A. A. Peterson, *ACS Catal.*, 2014, **4**, 3742–3748.

21 N. Gupta, M. Gattrell and B. MacDougall, *J. Appl. Electrochem.*, 2006, **36**, 161–172.

22 J. Resasco, L. D. Chen, E. Clark, C. Tsai, C. Hahn, T. F. Jaramillo, K. Chan and A. T.

Bell, *J. Am. Chem. Soc.*, 2017, **139**, 11277–11287.
23 L. D. Chen, M. Urushihara, K. Chan and J. K. Nørskov, *ACS Catal.*, 2016, **6**, 7133–7139.
24 M. C. O. Monteiro, F. Dattila, B. Hagedoorn, R. García-Muelas, N. López and M. T. M. Koper, *Nat. Catal.*, 2021, **4**, 654–662.
25 Y. Hori, I. Takahashi, O. Koga and N. Hoshi, *J. Phys. Chem. B*, 2002, **106**, 15–17.
26 S. Hanselman, M. T. M. Koper and F. Calle-Vallejo, *ACS Energy Lett.*, 2018, **3**, 1062–1067.
27 T. Möller, T. Ngo Thanh, X. Wang, W. Ju, Z. Jovanov and P. Strasser, *Energy Environ. Sci.*, 2021, **14**, 5995–6006.
28 C.-T. Dinh, T. Burdyny, M. G. Kibria, A. Seifitokaldani, C. M. Gabardo, F. P. García de Arquer, A. Kiani, J. P. Edwards, P. De Luna, O. S. Bushuyev, C. Zou, R. Quintero-Bermudez, Y. Pang, D. Sinton and E. H. Sargent, *Science.*, 2018, **360**, 783–787.
29 E. W. Lees, B. A. W. Mowbray, F. G. L. Parlane and C. P. Berlinguette, *Nat. Rev. Mater.*, 2022, **7**, 55–64.
30 J. P. Edwards, Y. Xu, C. M. Gabardo, C.-T. Dinh, J. Li, Z. B. Qi, A. Ozden, E. H. Sargent and D. Sinton, *Appl. Energy*, 2020, **261**, 1–7.
31 E. D. Sloan and C. A. Koh, *Clathrate hydrates of natural gases*, CRC Press/Taylor & Francis, Boca Raton, FL., 3rd edn., 2007.
32 J. F. Dean, *Science .*, 2020, **367**, 846–848.
33 C. D. Ruppel and J. D. Kessler, *Rev. Geophys.*, 2017, **55**, 126–168.
34 J. Qiao, Y. Liu, F. Hong and J. Zhang, *Chem. Soc. Rev.*, 2014, **43**, 631–675.

CHAPTER 1

Electrochemical conversion of CO_2 in non-conventional electrolytes: Recent achievements and future challenges

Sargeant, E., Rodríguez, P., *Electrochem Sci Adv*. 2022, e2100178.

doi: 10.1002/elsa.202100178
As of December 2022, to be published in a future issue.

Declaration

E.S. and P.R. conceived the manuscript. E.S wrote the manuscript and both authors contributed to discussion and revision of the manuscript.

1 of 16 Electrochemical Science Advances | REVIEW
doi.org/10.1002/elsa.202100178

Chemistry Europe
European Chemical Societies Publishing

Received: 5 October 2021
Revised: 18 January 2022
Accepted: 20 January 2022

Electrochemical conversion of CO_2 in non-conventional electrolytes: Recent achievements and future challenges

Elizabeth Sargeant | **Paramaconi Rodríguez**

School of Chemistry, University of Birmingham, Birmingham, UK

Correspondence
Paramaconi Rodríguez, School of Chemistry, University of Birmingham, Edgbaston, Birmingham B15 2TT, UK.
Email: p.b.rodriguez@bham.ac.uk

Abstract

Electrochemical reduction of CO_2 in traditional aqueous electrolytes suffers from low faradaic efficiency towards desired products which can be traced back to low CO_2 solubility and strong competition from the hydrogen evolution reaction. The use of non-conventional electrolytes aims to mitigate these issues. This review will give a focused overview summarizing some of the most recent contributions on the electrochemical conversion of CO_2 in organic solvents, ionic liquids, solid electrolytes, and brines. We summarize the findings in terms of activity, selectivity, and durability for each of the systems. In addition, it provides an outlook about the role of water, cations, and anions in the reaction. We also highlight the challenges of the electrochemical reduction of CO_2 in each of the electrolytes. All the studies referred to in this review contribute meaningfully to reaching the technical targets for CO_2 electrolyzers in non-conventional electrolytes.

KEYWORDS

CO_2 electrochemical reduction, highly concentrated electrolyte, ionic liquid electrolyte, molten carbonate electrolyte, organic electrolyte

1 | BACKGROUND AND BROADER CONTEXT

A recent survey found that worldwide two-thirds of people viewed climate change as a global emergency.[1] The 2021 IPCC report on climate change stated that "limiting human-induced global warming to a specific level requires limiting cumulative CO_2 emissions, reaching at least net zero CO_2 emissions, along with strong reductions in other greenhouse gas emissions."[2] In 2019, the level of CO_2 in the atmosphere was almost 410 ppm, the highest in the last 800,000 years, meanwhile, average global temperatures have risen 1°C compared to before the industrial revolution.[2] Via international agreements, such as the Paris Agreement, countries have committed to dramatically reducing their CO_2 emissions so that the rise in global temperature does not exceed this 2°C. Two of the priorities of the agreement are to decrease human activities that produce CO_2, as well as the development of technologies capable of reducing and converting CO_2 emissions into added-value products through a circular economy.

CO_2 can be converted to many useful products via many different methods. In the gas phase, at high pressures and temperatures, the reaction of CO_2 with H_2 yields CO and water via the reverse gas water-shift reaction,[3] methane and water via the Sabatier process,[4] and methanol via a hydrogenation reaction.[5] In the aqueous phase, the reaction between CO_2 and hydroxide salts produces carbonate salts such as $CaCO_3$ and Na_2CO_3 which are used in the glass industry, road construction, and cement production.[6] An alternative route to converting CO_2, is to mimic the natural processes. Nature is already extremely

This is an open access article under the terms of the Creative Commons Attribution License, which permits use, distribution and reproduction in any medium, provided the original work is properly cited.
© 2022 The Authors. *Electrochemical Science Advances* published by Wiley-VCH GmbH.

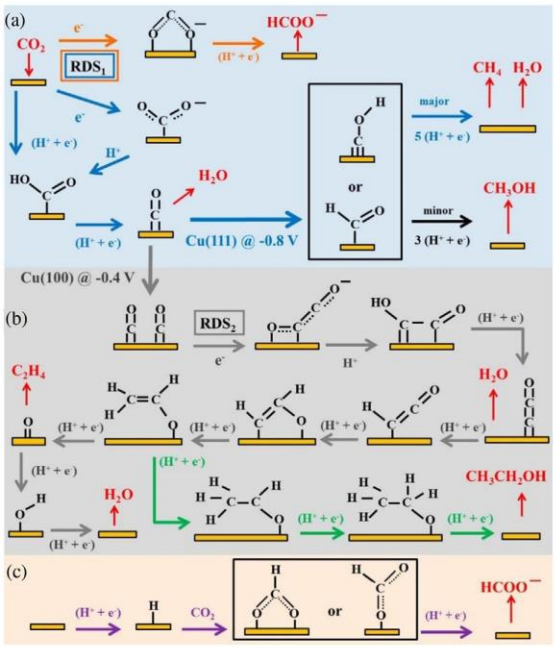


FIGURE 1 Proposed reaction pathways for the reduction of CO_2. (a) reduction pathway to CH_3OH (black arrows), CH_4 (blue arrows), $HCOO^-$ (orange arrows). (b) Reduction pathway to ethylene (grey arrows), ethanol (green arrows). (c) Alternative reduction pathway to $HCOO^-$ (purple arrows). Reprinted with permission.[15] Copyright 2015, the American Chemical Society

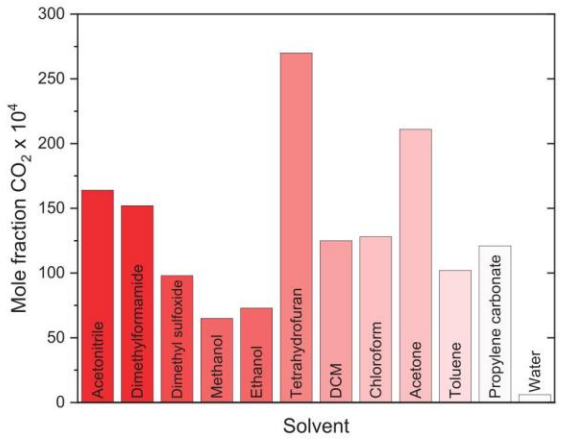


FIGURE 2 CO_2 solubility in some common organic solvents at 298 K and 101.3 kPa. Data from Gennaro et al.,[52] IUPAC data series,[53] and CRC Handbook of Chemistry and Physics[54]

effective at utilizing CO_2 from the atmosphere through photosynthesis to generate glucose and other carbohydrates. Designing enzymes that replicate this process in flue gas which is high temperature and has a high CO_2 concentration is a rich area of research with many technical challenges.[7–10]

One widely explored approach to the conversion of CO_2 into a variety of products is the electrochemical reduction of CO_2 (CO_2RR). Even though the CO_2RR was first reported in 1873 by Sir B. C. Brodie,[11] was not until 1985 that Hori et al. reported a systematic study for the electrochemical conversion of CO_2 to methane on copper electrodes.[12] For CO_2 electrolyzers to be economically feasible, Faradaic efficiency of 80%–90%, current density of greater than 300 mA cm^{-2}, cell voltage of less than 1.8 V, and stability of greater than 80,000 h are required.[13] Improving the selectivity of the CO_2RR has proven to be a challenging task.[14] Figures 1 shows the proposed reaction pathways to some of the main products in aqueous electrolytes.[15] Perhaps, a common belief is that the reduction to CO is an important step in the formation of CH_4, methanol, and C_2 products. In fact, research has shown that the protonation of the CO is the potential limiting step for the formation of C_1 products[16,17] and that the thermodynamic stability of either the COH or CHO intermediate depends on the metal catalyst determines the product selectivity.[18] The rate-determining step for the production of C_2 products is the formation of a CO-dimer intermediate which becomes thermodynamically stable at –0.40 V and needs to be stabilized via surface or solvent interactions.[19] The stabilization of different intermediates depends on the catalyst used and results in differing product selectivity for different metals.[17,20] Density functional theory (DFT) studies can be used to investigate the thermodynamic and kinetic modeling of the pathway.[19,21] Since Hori's 1985 study, extensive work has been reported on the CO_2RR, the main focus of those studies being the electrode material[14,19,22–35] and the composition of the aqueous electrolyte (cation effect and pH).[36–41]

A large proportion of CO_2RR research focuses on the development of new catalysts or the understanding of the electrochemical reactions in aqueous solutions.[19,42–44] The main advantage of an aqueous solution is the low cost and availability of the solvent, as well as its low toxicity. However, there are some major drawbacks that can be attributed to the use of an aqueous solution when studying the CO_2RR. The first is the poor CO_2 solubility in water, Figure 2. At 298 K and 1 atm, the maximum solubility of CO_2 is 34 mM,[45] and the addition of electrolyte salts causes a salting-out effect which reduces this further. It is also important to note that CO_2 solubility depends on the pH and the formation of carbonate salts.[36,46] One way to mitigate the low solubility, is to increase the pressure. Increasing up to around 6000 kPa, dramatically increases the mole fraction of CO_2 by around four times.[47] However, working at high pressure introduces energy costs and engineering challenges. Even if CO_2 electrolyzers are introduced at the exhaust of power plants or industrial

CO_2 sources such as cement and steel production, the flue gas is at atmospheric pressure so pressurization would be required.[48,49] The second main inconvenience in the use of water as a solvent, is that the hydrogen evolution reaction (HER) occurs in the same potential window and so H_2 production competes with CO_2 reduction.[50,51] To overcome these experimental inconveniences, reduction in alternative electrolytes such as ionic liquids (ILs), organic solvents, molten carbonates, and most recently brines have been investigated. This review will summarize the main findings on the CO_2RR to hydrocarbon products in these electrolytes and critically, from our point of view, propose the main challenges in the topic.

2 | CO_2RR IN ORGANIC SOLVENTS

Organic solvents were one of the first popular alternatives to the aqueous electrolyte for the CO_2RR. When the appropriate organic solvent is used, the solubility of CO_2 is higher than in water, for example, 314 mM of CO_2 can be dissolved in acetonitrile[52] and 151 mM in methanol[53] at 298 K in comparison with the 34 mM of CO_2 in water.[54] The CO_2RR in aprotic organic solvents overcomes the problem of the selectivity towards the formation of hydrogen and opens pathways to products such as oxalate.[55] In dry acetonitrile, CO is the main product.[56–58] Trace amounts of water can promote the formation of oxalic acid or formate[59,60] and spectroscopic investigations show that this residual water provides an alternative reduction pathway.[61] Again in propylene carbonate electrolytes, CO is the dominant product,[62,63] although oxalate has been detected using Single Potential Alteration Infrared Reflectance Spectroscopy on a lead electrode.[64]

However, in order to form hydrocarbons, protic solvents are needed.[65] Methanol is a popular choice of investigation since it is already used in the Rectisol process,[66,67] independently developed by Linde and Lurgi, to separate CO_2 from feed gases. Cu or Ni electrodes are the only metals that produce hydrocarbons at significant efficiencies in methanol.[68,69] Thus, most of the studies have been focused on these two metals, mainly on Cu catalysts, changing other physicochemical parameters such as temperature, pressure, and the supporting salt of the electrolyte.

In the early 90s, Naitoh et al. showed that lowering the temperature of methanol increases the faradaic efficiency (FE) of hydrocarbon formation on Cu.[70] When reducing the temperature of the methanol electrolyte with 80 mM benzalkonium chloride supporting electrolyte, from 0 to −15°C, the FE for CH_4 (FE_{CH4}) increased from 10.2% to 32.8% at −2.1 V versus SCE. However, FE for H_2 (FE_{H2}) also increased from 5.2% to 28.1%. Surprisingly, using the same electrolyte and catalyst material, Mizuno et al. reported improved FE_{CH4} up to 36% at −2.1 versus SCE while FE_{H2} remained below 10% when the temperature was reduced down to −30°C.[71]

Various studies from Kaneco et al. have looked at the product distribution of the reaction as a function of the composition of the supporting electrolyte, Table 1.[66,72–77] Two important parameters need to be described and discussed in this section: i) the solubility of the salts and ii) the cation and anion effect. Even though both can be treated and discussed separately, they are not exclusive. The solubility of the salts varies in methanol which results in changes to the conductivity and viscosity of the electrolyte. In general, it can be observed that a higher concentration of the electrolyte salt increases the current density of the reaction (j_{total}). There is also a clear effect of the cation on the reaction mechanism. Increasing the size of the cation decreases FE_{CH4} and similarly increases the production of CO and HCOOH. Larger cations (K^+, Rb^+, Cs^+) also tend to hinder the production of methane. Larger cations, which are weakly hydrated, adsorb to the surface of the electrode decreasing H^+ coverage which simultaneously encourages the dimerization of CH_2 intermediates and the production of less protonated products such as CO and HCOOH, Figure 3a.[73,74,76] Acetate anions do little to suppress HER and FE_{H2} is greater than 17.9% for all electrolytes tested. Generally, halide anions have high FE_{CH4}, especially for Li salts, and as the size of the anion increased FE_{H2} decreases. Thiocyanate ions promote the production of HCOOH and in these electrolytes, FE_{CO} increases as cation size increases. Hydroxide ions promote dimerization to form C_2H_4 but also produce significant amounts of CO. Carrying out electrolysis at more negative potentials can increase the yield of C_2H_4 for hydroxide supporting salts.[75,76,78] It is important to note, that the chemical nature of the salts used in the electrolyte, will also influence the solubility of the CO_2 in methanol. To our knowledge, such detailed studies have not been performed.

Cu is not the only electrode that has been investigated for hydrocarbon production. Ohya et al. used Cu_2O/Zn electrodes in methanol with 300 mM KOH as the supporting electrolyte at −30°C.[79] Increasing the wt% of Cu_2O in the catalyst had little effect on FE_{H2} which stayed around 20%. 2.5 wt% Cu_2O was determined to be the best electrode composition for hydrocarbon formation. FE_{CH4} was 7.5% and decreased at higher wt% and FE_{C2H4} did not significantly increase from around 6%.

The Rectisol process is carried out at high pressure and so research has been done to look at the effect of increasing pressure. Saeki et al. investigated the effect of pressure on the CO_2RR in methanol/0.1 M $TBABF_4$.[65] Figure 3b shows that as the pressure increases, the onset potential for CO_2 reduction on Cu moves to less negative potentials.

TABLE 1 Current density and faradaic efficiency for different products for CO_2 reduction on Cu electrode in methanol using various supporting salts. Electrolysis was performed at −30°C and −3.0 V versus Ag/AgCl sat. KCl. Data taken from references[66,72–77]

Electrolyte (mmol dm^{-3})	Current density (mA cm^{-2})	Faradiac efficiency (%)							Ref.
		CH_4	C_2H_4	C_2H_6	CO	HCOOH	H_2	total	
CH_3COOLi (500)	9.7	56.2	4.4		12	7.7	17.9	98.2	[73]
CH_3COONa (250)	7.6	43.4	5.1		1.1	4.6	34	88.2	[74]
CH_3COOK (500)	12.9	27	7.1	0.02	6.5	13	32.5	86.1	[77]
CH_3COOCs (500)	5.5	12.3	3.3		3.1	15.6	30.1	64.4	[66]
LiCl (500)	16.4	68.4	4		15.7	6.8	5.8	72.4	[73]
NaCl (250)	5.6	54.7	8.6		19.3	7.4	2.4	92.4	[74]
CsCl (30)	1.7	2.8	8.8	0.01	35.6	14.6	8.4	70.2	[66]
LiBr (500)	17	68.1	6.8		19.2	6.3	2.8	103.2	[73]
NaBr (250)	21.7	53.1	8		5.4	6.7	12.6	85.9	[74]
KBr (50)	3.2	6.4	9.8		35	17.4	3.6	72.2	[72]
CsBr (25)	1.5	0.1	5.9		54.1	13	7	80.1	[66]
LiI (500)	19.3	65.5	9		14.9	–	0.95	90.4	[73]
NaI (250)	16.7	63.1	5.2		2	7.2	9.1	86.6	[74]
KI (50)	4.2	15.8	19.9	0.17	15.2	–	3.5	54.6	[72]
CsI (30)	1.3	1	9.9	0.05	40	4.8	6.2	61.9	[66]
NaSCN (250)	8.9	49.8	7.9		2.7	15.2	1	77.4	[74]
KSCN (50)	2.6	22.4	12.6	0.23	21	–	15.3	71.5	[72]
CsSCN (30)	1.3	2.4	6		36.1	16.3	7.2	68	[66]
LiOH (80)	5.3	58	16.5		13.5	6.8	1.3	96.1	[73]
NaOH (80)	–	62	16		15.5	7.8	1.9	103.1	[75]
KOH (80)	4.5	10.8	27.9		13.9	8.5	2.6	63.7	[76]
RbOH (80)	3.9	3.5	24.3		33.8	12.8	3.6	78	[76]
CsOH (80)	5.4	5.5	25.7		7.4	13.4	23.3	75.3	[73]
$LiClO_4$ (500)	27	71.8	1.6		14.3	3.7	12	103.4	[73]
$NaClO_4$ (250)	22.7	70.5	3.1		3.2	4.2	17.9	99	[74]
0.005 M TEAP	1.6	5.9	1.2		54.2	20	6.7	88	[77]

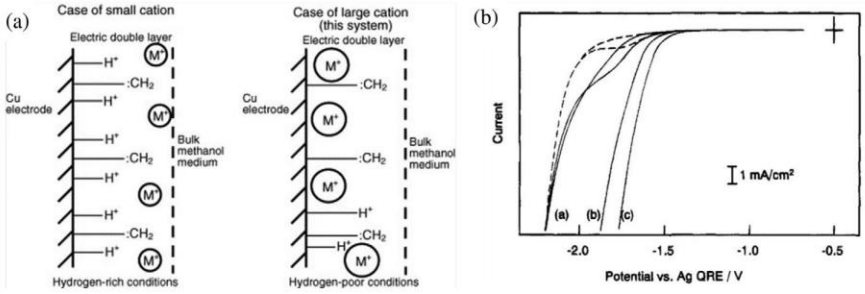


FIGURE 3 (a) Schematic showing how the size of cations affects the coverage of H^+ on the surface of Cu electrodes during electrochemical reduction of CO_2 (CO_2RR). Reprinted[76] Copyright (2016) with permission from Elsevier (b) Cyclic Voltammograms of Cu in methanol/0.1 M $TBABF_4$ in N_2 saturated electrolyte (dashed line) and CO_2 saturated solution at (a) 1 atm (b) 20 atm (c) 40 atm. Reprinted with permission.[65] Copyright (1995), the American Chemical Society

Increasing the pressure suppressed the HER but the main products were CO and formate, and hydrocarbon formation did not increase. Later work by Saeki et al., used various electrolytes at 40 atm and at ambient temperatures.[80] Under these high-pressure conditions either H_2 or CO were the main product and the current efficiency for CH_4 was below 10 %. In later work, Kaneco et al. showed the combination of high pressure and low temperature increased the efficiency of CH_4 production.[67] At 10 atm and -30°C with 500 mM LiCl supporting salt, the maximum efficiency for CH_4 was 20.2% at −3.0 V versus Ag quasi reference electrode (QRE). At more negative potentials, H_2 production dominates and FE_{CH4} decreased to less than 5%. Murugananthan et al. used 500 mM $LiClO_4$ at 4 atm and -30°C and FE_{CH4} increased at more negative potentials up to 37.4% at −4.0 V versus Ag QRE.[81] However, FE_{H2} increased under the same conditions up to 60.2%. In order to try and inhibit H_2 production, Kaneco et al. used 500 mM CsOH as a supporting salt.[82] Cs^+ is less hydrophilic than Li^+ which affords a less hydrogen-rich environment at the surface of the electrode. FE_{CH4} decreases dramatically at potentials more negative than −2.0 V versus Ag QRE but FE_{H2} production decreases concurrently. Instead, the production of C_2H_4 and CO increase as potential decreases. The suggested explanation for this trend is that the lack of protons makes desorption of CO or dimerization to form C_2 products more likely.

Very few investigations have pursued the fundamental aspects of the reaction from the atomistic view of the reaction mechanism. We, however, would like to highlight the work of Figueiredo et al. using in-situ Fourier-transform infrared spectroscopy (FTIR) to determine the role of the water and the supporting electrolyte in the electrochemical conversion of CO_2 in acetonitrile on different metal electrodes.[61] The authors concluded that in acetonitrile containing small amounts of water, the main reaction products of the electrochemical conversion of CO_2 are carbonate, bicarbonate, and CO. The authors concluded that the formation of carbonate and bicarbonate species is due to the formation of an electrochemically generated hydroxyl group from water reduction.

3 | CO_2RR IN ILs

ILs are flexible solvents as both anion and cation can be tailored to suit the needs of the reaction. As with organic solvents, the use of ILs aims to address the main problems of the aqueous systems, CO_2 solubility, and the competitive HER. They have a large capacity for CO_2 absorption, Figure 4, and functionalization can increase this further.[83] Hollingsworth et al. have suggested that the chemical absorption of CO_2 using a super-basic anion can also provide an alternative pathway of lower activation energy for the production of formate.[84] The intrinsic ionic conductivity of ILs and the wide potential window of stability makes them attractive solvents for the CO_2RR. Previous reviews by Alvarez-Guerra et al.[85] and Chen and Mu [86] have summarised IL solvents where CO_2 is reduced to valuable products such as CO or reacted with methanol and an alkylating agent to form dimethyl carbonate. However, there is less focus on the production of hydrocarbons in these systems which is what this review will highlight.

Kang et al., reported a broad study of the CO_2RR in pure [bmim][BF_4] using different metals as catalysts.[87] The results in Figure 5 show that on all metals, except Au, at −2.2 V versus Ag/Ag^+ the current density for CH_4 is higher than for CO or H_2. For Fe and Zn, the main overall product changes to CH_4. These results contrast with the selectivity commonly observed for the same metals in an aqueous solution. In aqueous electrolytes, Cu is known to be the only metal to reduce CO_2 to hydrocarbons. The CO_2RR on metals such as Au, Ag, and Zn stop after two-electron transfers to produce CO and the HER dominates on Pt and Fe. Despite the changes in selectivity, the total current density reported is generally lower than that reported in aqueous solvents.[19] For example, on Cu catalysts designed for methane production in 0.1 M $KHCO_3$, j_{total} of 5–7 mA cm^{-2} have been reported.[19]

N-doped graphene-like material (NGM) carbon electrodes in [bmim][BF_4] can produce CH_4 with very high efficiencies.[88] Sun et al. formed the NGM from different nitrogen-containing bases and the FE_{CH4} varied depending on the nitrogen content of the catalyst. The surface nitrogen content was measured by X-ray photoeletron spectroscopy (XPS) and the bulk content was measured by elemental analysis and in general, higher N content promoted CH_4 production. The NGM formed from 3-pyridinecarbonitrile had the highest FE_{CH4} (93.5%) and at −1.4 V versus NHE the main by-products were CO and H_2 (FE_{CO} = 4.2% and FE_{H2} = 2.1%). The performance of the NGM electrode was compared to Cu foil under the same conditions. In pure [bmim][BF_4], the FE_{CH4} was almost 20% greater for the NGM than for Cu foil, while in [bmim][BF_4] with 3 wt% H_2O the NGM was 45% more efficient than Cu foil.

Using the NGM electrode, Sun et al. compared the product selectivity and total current density of IL electrolytes with varied anions (BF_4, PF_5, TfO, Tf_2N, and DCA).[88] Within their choice of anions, product selectivity was largely unchanged but the overall current densities were larger for fluorinated anions, and the authors attributed this to strong interactions between CO_2 and fluorine. In addition, Sun et al. also investigated the effect of adding trace amounts of water to [bmim][BF_4] on FE_{CH4}. The addition of water steadily increased current density up

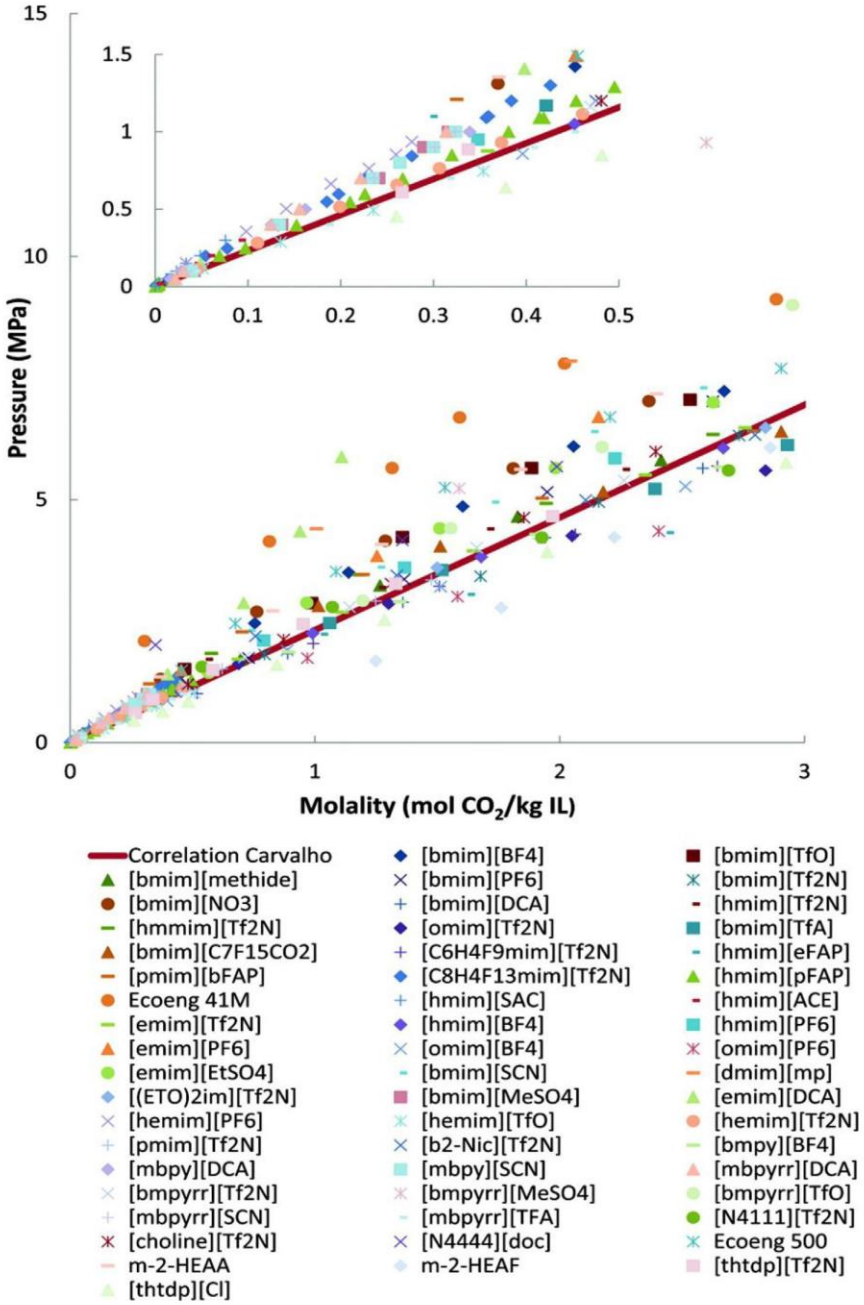


FIGURE 4 Solubility of carbon dioxide expressed as molality (mol CO_2/kg solvent) in different ionic liquids at 59.85°C. Figure reprinted with permission[83]

to 5% and maintained FE_{CH4} of greater than 80% for the NGM electrode. However, CO and H_2 were the major by-products of the addition of water with H_2 production increasing at higher overpotentials. The increase in current density was attributed to a decrease in viscosity and a decrease in pH due to the formation of hydroxide ions coordinating to the BF_3^-. Interestingly, using a similar electrolyte, [bmim][BF_4] and 0.5% water, Miao et al. found that the residence time of the electrolyte in a microscale electrochemical reactor results in changes in the products selectivity.[89] Using Ni-coated graphite sheets as the electrodes, they showed that longer mean residence times in

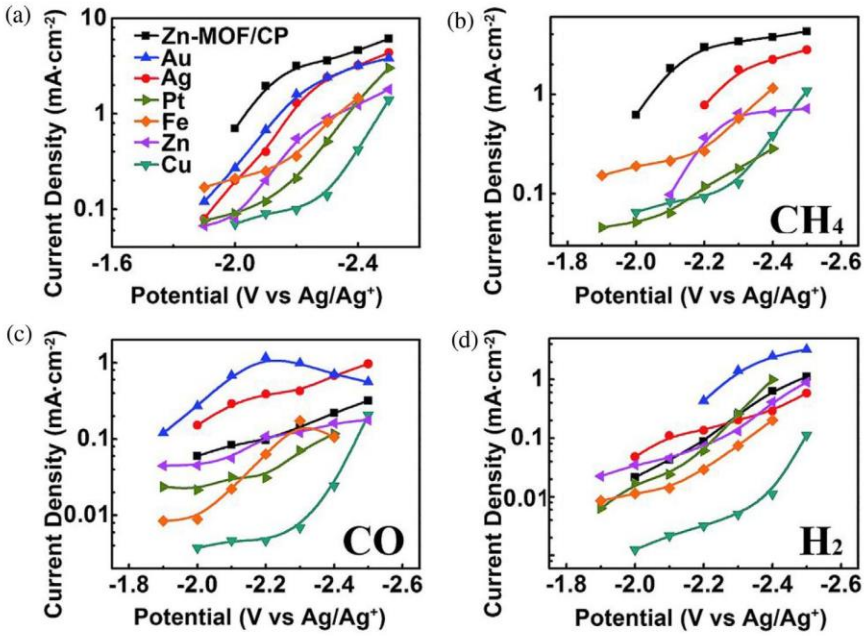


FIGURE 5 Current densities for different electrodes in pure [bmim][BF_4] as a function of potential. (a) total current density, (b) partial current density of CH_4, (c) partial current density of CO, and (d) partial current density of H_2. Reproduced[87] with permission from the Royal Society of Chemistry

the reactor, increased the product conversion to CH_4 while shorter residence times result in HCHO or CH_3OH being the major products.

To further illustrate the importance of the IL in enhancing the formation of CH_4, we recall the work of Liu et al. which evaluated the CO_2RR in [bmim][BF_4] with 4% water and in 0.1 M $KHCO_3$ using ultrathin layers of $MoTe_2$ as a catalyst. It was found that in [bmim][BF_4] with 4% water the $MoTe_2$ reduces CO_2 to CH_4 with $FE_{CH4} = 83\%$ at –1.0 V versus reversible hydrogen electrode (RHE) while in 0.1 M $KHCO_3$ and FE_{CH4} was only 20%.

Based merely on Tafel analysis, Sun et al. and Liu et al. suggest [88,90] that the rate-determining step is the formation of an adduct between the radical anion of CO_2 (CO_2•) adsorbed to the catalyst surface, however further DFT calculations and spectroscopic measurements are required to confirm the presence and stability of this reaction intermediate. Some work has been done to try and elucidate the mechanism but mainly focusing on the reduction of CO_2 to CO. DFT calculations by Niu et al. showed that the CO_2• is stabilized by the partial positive charges on nearby protons on the [bmim] cation.[91] They compared the onset potential of the reduction of CO_2 to CO on an Ag electrode in ILs with varied cations and argued that sterically hindered cations do not provide effective stabilization to the radical and so the overpotential is increased. Lau et al. used a series of imidazolium cations to show that the cation acts as a co-catalyst for reduction to CO on Ag electrodes.[92] The behavior depends on the availability of the protons at the C4 and C5 positions to interact with the CO_2• but their experiments showed that imidazolium cations still reduced the overpotential even when these positions were substituted and so suggested that the cation has some alternative method of binding. Other work by Vasilyev et al. compared the co-catalytic activity of different cations and they summarised that those which had an accessible localized positive charge were most effective at stabilizing the CO_2• and reduced the overpotential of the reaction.[93] They also carried out DFT calculations and found that the enthalpy of hydrogen bonds between the cation and the radical were too small to be solely responsible for the stabilization.

To this stage, it seems important to discuss the role of the water and the ionic liquid in the CO_2RR. Many questions have arisen in terms of conductivity, viscosity, proton availability, or co-catalysis. Golru et al. looked at the catalytic activity and selectivity during the CO_2RR in diluted solutions of different ILs in 0.1 M $KHCO_3$.[94] Using just 10 mM of IL with [bmim] as a cation and [Tf_2N], [TfO], [Ac], [Cl] and [DCA] as anions, the authors found that for all ILs, except [bmim][DCA], at –0.92 V versus RHE, formate was the major product while at –1.12 V versus RHE, CH_4 production dominated. For [bmim][DCA], H_2 was the main product which is likely due to [DCA] having a high affinity

for water which promotes the HER. The authors used electrochemical impedance spectroscopy (EIS) to help explain the changes in selectivity. The solution resistance (R_s) was similar for the aqueous 0.1 M $KHCO_3$ and all the added IL solvent systems and so product changes were attributed to differences in the double layer. The charge transfer resistance (R_{ct}) decreased for all electrolytes at more negative potentials as the energy barrier for reactions is lowered. At more negative potentials the electrolytes showed an inductive loop in the Nyquist plots, which indicates adsorption/desorption of ions on the electrode surface, and the R_{ct} increased signifying slower diffusion of CO_2 to the surface. At the more negative potentials, the IL accumulates on the surface which seems to stabilize the intermediate for CH_4 rather than HCOOH.

Similar to organic solvents, very few works have investigated the CO_2RR in ILs from the fundamental atomistic point of view, using in situ spectroscopic techniques or theoretical calculations.[95–97] We will mention the work of Papasizza et al. implementing in situ ATR SEIRAS to understand the changes in the structure of the double-layer during the CO_2RR to CO in ILs and ionic-liquid/water mixtures.[98] The in situ ATR SEIRAS experiments revealed two types of water in the [EMIM]BF4/water mixture, with different degrees of hydrogen bonding at the interface: water in water-rich regions (bulk-like water) and water in a [EMIM]BF4-rich environment. During the CO_2RR, only bulk-like water was observed at the electrochemical interface.

4 | CO_2RR IN MOLTEN CARBONATES

Molten carbonates are interesting electrolytes for the high-temperature CO_2RR for a number of reasons. At high temperatures, the kinetics of the reaction is quick, the overpotential for the reduction is relatively low, and non-precious metals can be used as catalysts.[99–104] In addition, the product selectivity at high temperatures is better for two reasons: i) HER is hindered because water is not usually present in the system, and ii) there is a wide potential gap between the reduction potential of the two main products, C and CO, over a large temperature range. Absorption of CO_2 into these systems is high since oxygen anions, react with CO_2 to generate carbonate ions which are then reduced, and the oxygen anion regenerated, Figure 6a.

$$CO_3^{2-} + 4e^- \rightarrow C + 3O^{2-} \quad (1)$$

$$CO_2 + O^{2-} \rightarrow CO_3^{2-} \quad (2)$$

Common electrolyte mixtures contain multiple types of carbonate or carbonate with chlorides in order to reduce the melting temperature of the electrolyte, Figure 6b. Cathodes are usually transition metals or steel and anodes are materials effective for oxygen evolution that can withstand the corrosive environment. Research is mostly focused on producing different morphologies of carbon such as nanoparticles, nanotubes, and graphite sheets. Work by Hu et al. showed that the addition of borates to the electrolyte acts as a buffer which lowers the overpotential of CO_2 reduction and that by changing the conditions of the electrolysis, the product can be tuned between CO and carbon nanofibers.[105] Yu et al.[106] and Jiang et al.[99] have reviewed the conditions used to generate different carbon morphologies and syngas. Here, the production of hydrocarbon fuels is highlighted but throughout the production of carbon products at the cathode is a competes.

Wu et al. reported that methane could be synthesized from the electrolysis of CO_2 and steam in an alkali carbonate with LiOH mix using a Fe cathode and a Ni anode.[108] They varied the concentrations of hydroxide and showed that with very low concentrations of LiOH, carbon was the only product whereas with higher concentrations of LiOH, hydrogen, from concurrent water splitting, was the main product. The optimum ratio of hydroxide to carbonate, n_{OH}:n_{CO3}, for methane production was 0.3:1 so $Li_{1.427}Na_{0.359}K_{0.214}CO_3$-0.3LiOH was used as the electrolyte. A range of temperatures (500–650°C) and operating currents (0.25–1.00 V) was tested. Increasing the temperature and the operating current both increased the production of H_2. The current efficiency was highest (97.4%) at 600°C and 0.25 V. These conditions had the highest gas composition of methane (64.9%) and lowest of hydrogen (34.8%). Longer chain hydrocarbons were also detected using gas chromatography-flame ionization detector (GC-FID) at the lower temperature of 500°C.

The results summarised in Figure 7 show the effect of different electrode materials (Fe, Cu, Ni, and graphite) on the product selectivity of the CO_2RR using $Li_{1.427}Na_{0.359}K_{0.214}CO_3$-0.15LiOH as the electrolyte.[109] While the cathode material did not affect the FE_{total}, Ji et al. found a large impact on the product distribution. It was found that a graphite cathode produced a significant amount of CO and Ni cathode promotes the production of H_2. Out of the four cathodes, Fe produces the greatest amount of CH_4 and the lowest amount of H_2.

An extensive study by Al-Juboori et al.[110] investigated the effect of temperature, applied voltage, and feed gas on the product distribution during the CO_2RR using titanium as the cathode. At higher temperatures, longer chain hydrocarbons were also formed, for example, C_7H_{16} which decreased the overall efficiency. In a molten carbonate mixture, Li_2CO_3–Na_2CO_3–K_2CO_3; 43.5:31.5:25.0 mol%, hydrocarbon production was promoted as the temperature increased from 425 to 500°C and the competing produc-

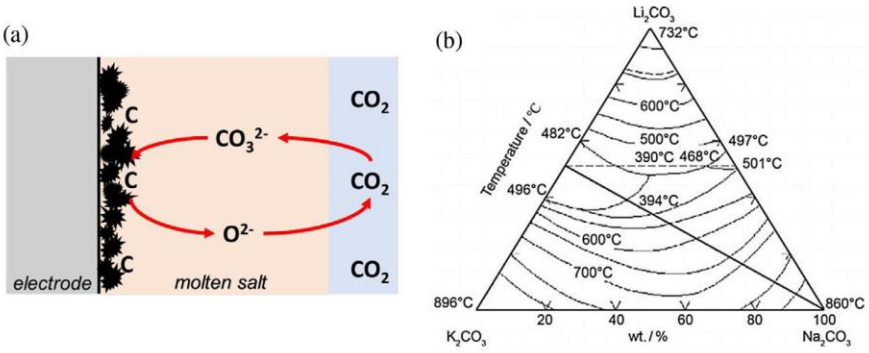


FIGURE 6 (a) Schematic diagram of the cycle of CO_2 absorption and C deposition in molten salt electrolytes, and (b) Phase diagram for alkali metal carbonates. Reproduced with permission[107]

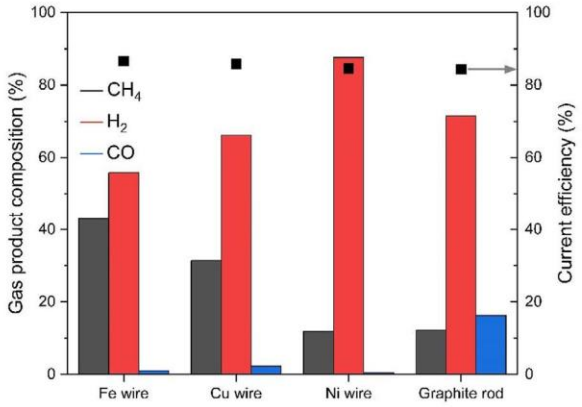


FIGURE 7 Results of the CO_2 electrolysis at a constant current of 0.25 A at 550°C in $Li_{1.427}Na_{0.359}K_{0.214}CO_3$-0.15LiOH for different cathode materials. Right axis, faradaic efficiency. Left axis, product composition, CH_4 (black), H_2 (red), CO (blue). Data taken from reference[109]

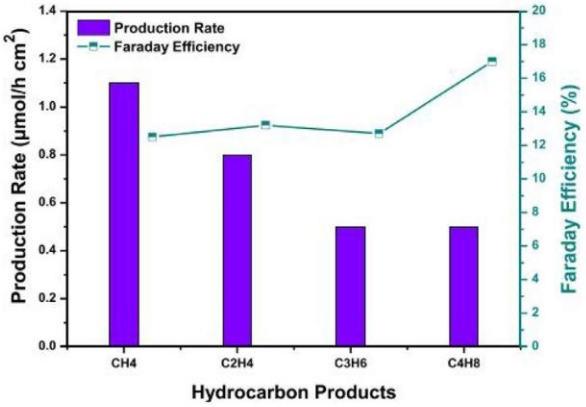


FIGURE 8 Production rates and faradaic efficiencies for various hydrocarbons products at 1.5 V and 425°C on a Ti electrode in Li_2CO_3–Na_2CO_3–K_2CO_3; 43.5:31.5:25 mol% Reproduced with permission,[111] Copyright (2020), American Chemical Society

tion of CO and H_2 decreased. Unsurprisingly, it was also found reported that higher water content in the feed-gas promoted H_2 evolution to the detriment of hydrocarbon production. Figure 8 shows the FE for the production of short-chain hydrocarbons which were reported in another study by Al-Juboori et al. under the same conditions illustrating that CH_4 is not the only hydrocarbon produced.[111] Wu et al. found a similar trend in $Li_{1.427}Na_{0.359}K_{0.214}CO_3$-0.3LiOH, where CH_4 production increased from 500 to 600°C.[108] However, at 650°C CH_4 productions reduced dramatically and they hypothesized that the LiOH dehydrated and so there was less water available to form hydrocarbons.

The voltage and the current are the key parameters in this reaction. Both Wu et al. and Ji et al. found that lower electrolysis currents favored the production of CH_4 over H_2.[108,109] Wu et al. found that in $Li_{1.427}Na_{0.359}K_{0.214}CO_3$-0.3LiOH at 0.25 A the yields of CH_4 and H_2 were 64.9% and 34.8%, respectively compared with 27.4% and 69.4% at 1.5 A. In another study by Al-Juboori et al.,[111] they found that electrolysis at 2 V produced no hydrocarbons and instead carbon was deposited.

5 | CO_2RR IN AQUEOUS BRINES

Although the addition of salt to the electrolyte contributes to the salting-out effect, reducing the solubility of CO_2, there are advantages to the use of highly concentrated brines. Water-in-salt electrolytes are electrolytes that are so concentrated that solvation shells for the ions are incomplete.[112] Brine electrolytes, while very concentrated, do not meet this requirement. The stability provided by ions to reaction intermediates changes the selec-

tivity of the reaction[113,37] and the addition of salts lowers the freezing point of the electrolyte allowing CO_2RR at low temperatures where CO_2 solubility is higher. Gas diffusion electrodes can be used to reduce the issue of low CO_2 solubility in these systems. However, the selection of ion exchange membranes for GDE systems is challenging, in particular at alkaline pH and low temperatures, for example, those expected in Mars. Research in this type of electrolyte is much less developed, thus this section not only summarises the CO_2RR in brines but also includes those findings where the local concentration of electrolytes near the surface mimics the brines and will contribute to the understanding of the field.

On an Ag electrode in a gas-diffusion electrode, increasing the concentration of KOH from 0.1 to 11 M increases the formation of formate in comparison to CO, due to the lack of H_3O^+ in solution.[114] Seifitokaldani et al. used DFT calculations to show that when H_3O^+ transferred the proton to CO_2, the transition state for *COOH, which is the intermediate for CO formation, was lower in energy whereas when the proton is directly transferred from the surface to CO_2, the transition state for *CHOO, which is the intermediate for HCOOH formation, was lower in energy. However, the authors do not account for how the pH of the electrolyte affects the $CO_2 \leftrightarrow HCO_3^- \leftrightarrow CO_3^{2-}$ equilibrium. At high pH, almost all CO_2 is in the CO_3^{2-} form but the DFT calculations still assume CO_2 is the active species. Figure 9 shows that as the electrolyte concentration increases FE_{HCOO^-} increases. At $[H_3O^+] = 10^{-7}$, which equates to pH = 7, the CO/formate ratio is around 50 while at $[H_3O^+] = 10^{-15}$, which equates to pH = 15, the ratio is 0.69. In order to demonstrate that the changes in selectivity were due to changes in H_3O^+ concentration, and not associated with K^+ concentration, KI was used as an electrolyte in the concentration range between 1 M and 7 M, where no change to the CO/formate ratio, in contrast to the results by Liu et al.[115] Similar results were obtained on Pd electrodes using an applied current density of 100 mA cm^{-2}. FE_{CO} decreased from 75 % in 1 M KOH to 6.5 % in 10 M KOH but FE_{HCOO^-} only increased from 1.8% to 8% for Pd electrodes due to competition from the HER.

Increasing the concentration of electrolytes increased the total current density for CO_2RR, independently of the anion used.[116] Verma et al. used Ag nanoparticles on a gas-diffusion electrode in different K-based electrolytes (KOH, $KHCO_3$, and KCl). One of the main contributions of this work was the study of the conductivity of the electrolyte. Using EIS the authors showed that R_s and R_{ct} decreased as electrolyte concentration increased. The conductivity of electrolytes increases with a concentration in the range between 0.5 and 3 M, accounting for the decrease in R_s, and they suggested the decrease in R_{ct} was due to K^+ stabilizing reaction intermediates in the rate-determining step, in agreement with Liu et al.[115] Increasing the concentration of KOH from 0.5 M to 3 M resulted in j_{total} increasing from 76.1 to 231.3 mA cm^{-2} at −2.5 V versus RHE. In $KHCO_3$ and KCl, j_{total} increased from 12.7 to 28.0 mA cm^{-2} and from 8.9 to 14.6 mA cm^2 respectively. However, in these electrolytes, FE_{CO} decreased with increasing concentration. For $KHCO_3$ there was a decrease from 99.2% to 82.5% and for KCl the decrease was from 86.3% to 73.6%. Given the similarities in conductivity, the decrease of the FE_{CO} was attributed to the lower solvation of the $KHCO_3$ and KCl in comparison with the KOH. The authors also proposed that the specific adsorption of the anions might be blocking adsorption sites for the CO_2RR. However, given the high negative potential, −2.5 V versus RHE, we believe that this is quite unlikely, and spectroscopic evidence of the adsorption of anions in this poten-

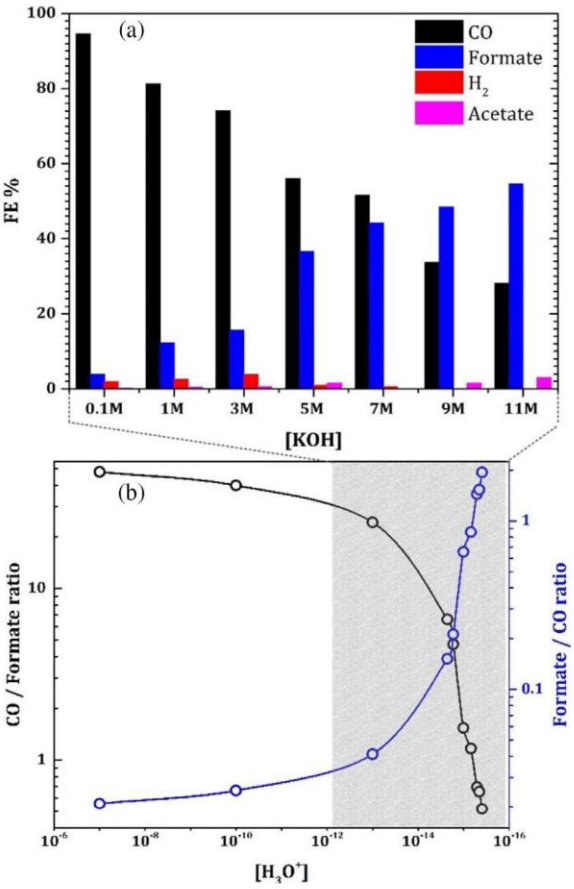


FIGURE 9 Effect of the KOH concentration on the product selectivity during the electrochemical reduction of CO_2 (CO_2RR) on Ag electrodes. (a) FE for different products from electrolysis at 300 mA cm^{-2} (b) CO:formate ratio (left y-axis) and its inverse (right y-axis) at different hydronium concentrations. Reprinted with permission,[114] Copyright (2018), the American Chemical Society

tial region would need to be proved. On the other hand, we propose that changes of the selectivity could be associated with other parameters such as changes in the local pH, thus the chemical equilibrium of the $CO_2 \leftrightarrow HCO_3^- \leftrightarrow CO_3^{2-}$, due to the HER at such negative potentials. This effect is certainly reduced in highly alkaline media or in a system with controlled mass transport.

Increasing the concentration of KOH from 1 to 10 M reduced the overpotential for CO_2 reduction on the Ag gas diffusion electrode.[117] While increasing the concentration had no effect on the onset of HER in KOH, Gabardo et al. found the onset potential for the CO_2RR moved from around −0.360 V versus RHE in 1 M KOH to −0.117 V versus RHE in 10 M KOH, Figure 10a. Likewise, the selectivity changed from mostly CO ($FE_{CO} = 84\%$ and $FE_{HCOO-} = 12\%$ at 1 M KOH) to a mix of CO and formate as concentration increased ($FE_{CO} = 42\%$ and $FE_{HCOO-} = 40\%$ at 10 M KOH). Following the findings of Seifitokaldani et al.,[114] Gabardo et al. attempted to study the effect of the CO_2 pressure in the CO_2RR in these electrolytes. They hypothesized that the increase in CO_2 pressure increased CO_2 coverage and so there were fewer protons on the surface able to directly protonate the CO_2 and form the *CHOO intermediate. The optimal system for almost 100 % FE_{CO} was obtained in 7 M KOH at 7 atm, Figure 10b,c.

Bhargava et al. investigated the CO_2RR on Ag nanoparticles on a gas diffusion electrode in CsOH solutions between 0.1 to 3 M.[118] Based on EIS results, the authors suggested that the increase in the kinetics of charge transfer and the increase in CO production at low overpotentials during the CO_2RR as a function of the concentration of CsOH was associated to the decreases of the thickness of the double layer and the stabilization of CO_2^- radicals by the cations in the double layer.

Although most of the research of the CO_2RR in brines has been focused on Ag and Au for the production of CO, other catalysts have been used to produce hydrocarbons. Dinh et al. used a Cu catalyst in a gas diffusion electrode to study the CO_2RR.[119] Increasing the concentration of KOH from 1 to 10 M had no effect on HER onset but moved the onset of CO_2 reduction to less negative potentials. In 7 M KOH, the authors reported an extraordinary $FE_{C2H4} = 70$ % at −0.55 V versus RHE over 150 h. At high OH concentrations, CO_2 diffusion into the electrolyte is inhibited which favors enhanced *CO formation and an increase in coverage which in turn favors dimerization. DFT results showed that the presence of OH on the surface lowers the binding energy of CO and increases the dipole interaction within the OCCO adsorbed intermediate.

Using Au electrodes with different morphologies can induce a 20-fold increase of K^+ ions near the surface of the electrode in order to look at the effect of such high ions concentrations on CO_2 reduction.[115] Liu et al. car-

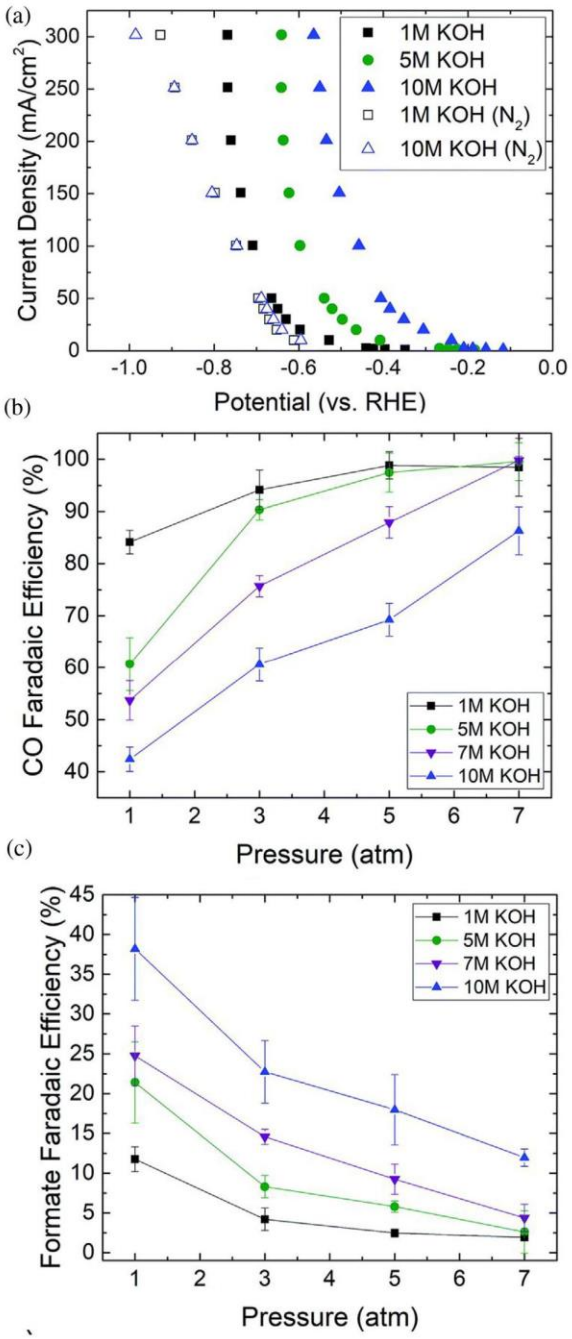


FIGURE 10 (a) Current/voltage curves in 1, 5, and 10 M KOH under CO_2 and N_2 streams using Ag as the electrocatalyst. (b) and (c) Effect of pressure on the (b) FE_{CO} and (c) $FE_{formate}$ during the electrochemical reduction of CO_2 (CO_2RR) at 300 mA cm^{-2} at different KOH concentrations. Republished with permission[118] conveyed through Copyright Clearance Center, Inc.

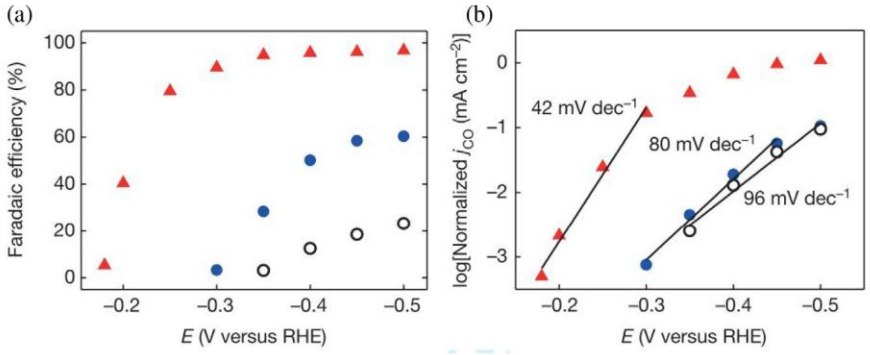


FIGURE 11 Results of CO_2 reduction on Au particles (black), rods (blue) and needles (red) in 0.5 M $KHCO_3$ (a) FE_{CO} dependence on potential (b) ECSA-normalised partial current density for CO production versus potential. Reprinted with permission from Springer Nature,[116] Copyright 2016

ried out investigations in 0.5 M $KHCO_3$ and found that high curvature of the electrode concentrates the electric field which in turn increases the concentration of K^+ ions at the surface. Au particles (radius curvature of around 140 nm), rods (radius curvature of 60 nm), and needles (curvature of around 5 nm) were used, and XPS, powder X-ray diffraction, and scanning electron microscopy were used to show that the electrodes were composed of regular Au lattices with no oxides before and after CO_2 reduction. Figure 11a shows that needles have the highest FE_{CO} (100% vs. 60% and 20% for rods and particles, respectively) at –0.5 V versus RHE and that at –0.2 V versus RHE, which corresponds to an overpotential of 0.09 V, the FE_{CO} was still 40%. Tafel slope analysis, Figure 11b, shows a decrease in the slope for Au needles compared to rods and particles indicating that the barrier for the rate-determining step, the transfer of the first electron to CO_2, is lowered. This field-induced reagent concentration-effect enhances CO_2 reduction. Ab-initio molecular dynamic simulations showed that the presence of K^+ increases the interaction between the CO_2 and the Au surface and DFT calculations show that reaction intermediates are stabilized by K^+ which lowers the thermodynamic energy barrier. The effect was enhanced in saturated $KHCO_3$ where FE_{co} was 95% and j_{CO} was 22 mA cm^{-2} at –0.35 V versus RHE. Pd was tested in the same way and for Pd needles at –0.2 V versus RHE, FE_{HCOOH} was 91% and j_{HCOOH} was 10 mA cm^{-2} compared to FE_{HCOOH} = 13% and j_{HCOOH} = 0.05 mA cm^{-2} for Pd particles.

Sargeant et al. used highly concentrated electrolytes to carry out the reduction of CO_2 at low temperatures.[28] They reported an anti-Arrhenius relationship for the reduction of CO_2 in 4.4 molal $Mg(ClO_4)_2$ below – 5°C. On a Cu(111) electrode at –0.45 V versus RHE, E_a = –1.52 kJ mol^{-1}. As the temperature was decreased to –18°C, H_2 production decreased while CO, CH_4, and ethanol production increased. When using a Pd polycrystalline electrode as the catalyst, the authors found the same trend in product distribution when decreasing the temperature. The authors suggested that the origin for the decrease in the HER activity was the formation of clathrate hydrate structures where the entropy of the water molecules is hindered due to the formation of cage-like structures.

6 | SUMMARY AND OUTLOOK

In summary, the reported literature postulates that the concentration of CO_2 has a large impact on the catalytic activity and selectivity for the CO_2RR, independently of if the reaction takes place in methanol or water. Even though the concentration of CO_2 in methanol is around five times larger than in aqueous media, operational parameters such as temperature, pressure, and composition of the electrolyte strongly affect the catalytic activity and the product selectivity of the reaction. It is important to note, that the use of protic solvents or the addition of water is, so far, essential to form hydrocarbons in organic media, thus even though the HER is minimized, it is still a concern. The electrochemical reduction of small traces of water in organic solvents, such as acetonitrile, might also result in the formation of hydroxyl species that react with the CO_2 at the interface producing carbonates and bicarbonates. Compared to aqueous solvents, organic solvents can be hazardous to health and they have many existing uses in industry and so can be expensive.

It is important to mention that, so far, ILs are expensive to manufacture at scale and can eventually degrade.[86] Despite the high CO_2 solubility and inherent conductivity of ILs, the implementation of IL in the CO_2RR also requires water as a co-reactant present in order to form hydrocarbons, thus the HER again becomes a competitive reaction.

In molten carbonates, even though the conversion of CO_2 does not require precious metals and the FE is higher than in organic media, ILs, and water, the disadvantage of these systems is the energy cost of running at high temperatures. In addition, as in the case of the CO_2RR in organic solvents and ionic liquid solvents, the CO_2RR in molten carbonate requires the addition of water vapor in order to tune the selectivity towards the formation of hydrocarbons which results in the simultaneous synthesis of H_2.

The studies on the electrochemical conversion of CO_2 in aqueous brines, suggest that the FE and selectivity towards the formation of hydrocarbons can be significantly improved. Parameters associated with the nature and concentration of the electrolyte need to be further studied. The electrochemical conversion of CO_2 from gas hydrates is very promising, however further studies on the effect of pressure and temperature are needed. In addition, as highlighted by the authors, the studies on the electrochemical conversion of CO_2 in brines at sub-zero temperatures are relevant for the exploration and colonization of Mars as demonstrated by the MOXIE experiments.[120,121]

The use of alternative electrolytes for CO_2 reduction has been summarised in this review. By using non-aqueous electrolytes, the main issue of poor CO_2 solubility can be mitigated. It can be alleviated even further by increasing the pressure or lowering the temperature. However, in order to produce hydrocarbon products, H_2O usually needs to be reintroduced, even in small quantities, which will cause competition from the HER, as in aqueous electrolytes. There is much scope for tailoring each system to try and increase the FE of the desired product.

The implementation of IL, organic solvents, and brines will require further fundamental studies, as well as feasibility studies using a gas-diffusion electrode configuration. Fundamental studies, both experimental and theoretical, are essential to understand the role of the hydration shell and the effect of the ions in the electrochemical interphase during the CO_2RR.[98,122–124] The application of in-situ spectro-electrochemical methods such as FTIR or Raman and other scanning electrochemical methods can provide information regarding the composition of the interface in real-time. They will not only provide information on the adsorbed species and intermediates but also could provide relevant information on the degradation of the electrolyte. In this regard, the long-term durability and possible catalyst/electrolyte degradation also need further studies. In particular, it is important to take into consideration that many IL contains halide ions that might accelerate the dissolution of the metal catalyst. Further studies with mixtures of IL and organic solvent might require the implementation of step-potential techniques that minimize the HER.[125–127]

The CO_2RR in molten carbonates on the other hand faces the challenge of reducing the operating temperature and the overpotential while keeping the high conversion rate and selectivity in long-term electrolysis and at high current densities. Although some work has been done to understand the mechanism and kinetics of carbon deposition in these systems,[128,129] research should also be carried out to understand the mechanism of hydrocarbon formation. The question of how the CO_3^{2-} is protonated to form hydrocarbons and whether the mechanism is similar to the aqueous electrolyte is as yet, unanswered.

CONFLICT OF INTEREST

The authors declare no conflict of interest.

DATA AVAILABILITY STATEMENT

Not applicable.

ORCID

Paramaconi Rodríguez https://orcid.org/0000-0002-1517-0964

REFERENCES

1. C. Flynn, E. Yamasumi, S. Fisher, D. Snow, Z. Grant, M. Kirby, P. Browning, M. Rommerskirchen, I. Russell *The Peoples' Climate Vote*. **2021**.
2. Intergovernmental Panel on Climate Change, *Climate Change 2021: The Physical Science Basis*, Cambridge University Press, Cambridge **2021**.
3. J. Xu, G. F. Froment, *AIChE J.* **1989**, *35*, 88.
4. P. Sabatier, J.-B. Senderens, *des séances l'Académie des Sci.* **1902**, *134*, 514.
5. F. Studt, M. Behrens, E. L. Kunkes, N. Thomas, S. Zander, A. Tarasov, J. Schumann, E. Frei, J. B. Varley, F. Abild-Pedersen, J. K. Nørskov, R. Schlögl, *ChemCatChem* **2015**, *7*, 1105.
6. R. Zevenhoven, S. Eloneva, S. Teir, *Catal. Today* **2006**, *115*, 73.
7. J. Shi, Y. Jiang, Z. Jiang, X. Wang, X. Wang, S. Zhang, P. Han, C. Yang, *Chem. Soc. Rev.* **2015**, *44*, 5981.
8. G. A. Aleku, G. W. Roberts, G. R. Titchiner, D. Leys, *ChemSusChem* **2021**, *14*, 1781.
9. P. C. Sahoo, M. Kumar, S. K. Puri, S. S. V. Ramakumar, *J. CO2 Util.* **2018**, *24*, 419.
10. S. K. Bhatia, R. K. Bhatia, J. M. Jeon, G. Kumar, Y. H. Yang, *Renew. Sustain. Energy Rev.* **2019**, *110*, 143.
11. B. C. Brodie II, *Proc. R. Soc. London* **1873**, *21*, 245.
12. Y. Hori, K. Kikuchi, S. Suzuki, *Chem. Lett.* **1985**, *14*, 1695.
13. M. G. Kibria, J. P. Edwards, C. M. Gabardo, C. Dinh, A. Seifitokaldani, D. Sinton, E. H. Sargent, *Adv. Mater.* **2019**, *31*, 1.
14. K. P. Kuhl, E. R. Cave, D. N. Abram, T. F. Jaramillo, *Energy Environ. Sci.* **2012**, *5*, 7050.
15. R. Kortlever, J. Shen, K. J. P. Schouten, F. Calle-Vallejo, M. T. M. Koper, *J. Phys. Chem. Lett.* **2015**, *6*, 4073.
16. W. J. Durand, A. A. Peterson, F. Studt, F. Abild-Pedersen, J. K. Nørskov, *Surf. Sci.* **2011**, *605*, 1354.
17. A. A. Peterson, J. K. Nørskov, *J. Phys. Chem. Lett.* **2012**, *3*, 251.

18. F. Calle-Vallejo, M. T. M. Koper, *ACS Catal.* **2017**, *7*, 7346.
19. Y. Y. Birdja, E. Pérez-Gallent, M. C. Figueiredo, A. J. Göttle, F. Calle-Vallejo, M. T. M. Koper, *Nat. Energy* **2019**, *4*, 732.
20. Y. Hori, H. Wakebe, T. Tsukamoto, O. Koga, *Electrochim. Acta* **1994**, *39*, 1833.
21. A. Rendón-Calle, S. Builes, F. Calle-Vallejo, *Curr. Opin. Electrochem.* **2018**, *9*, 158.
22. H. Mistry, Y. Choi, A. Bagger, F. Scholten, C. S. Bonifacio, I. Sinev, N. J. Divins, I. Zegkinoglou, H. S. Jeon, K. Kisslinger, E. A. Stach, J. C. Yang, J. Rossmeisl, B. Roldan Cuenya, *Angew. Chemie Int. Ed.* **2017**, *56*, 11394.
23. W. Zhu, Y.-J. Zhang, H. Zhang, H. Lv, Q. Li, R. Michalsky, A. A. Peterson, S. Sun, *J. Am. Chem. Soc.* **2014**, *136*, 16132.
24. A. Klinkova, P. De Luna, C.-T. Dinh, O. Voznyy, E. M. Larin, E. Kumacheva, E. H. Sargent, *ACS Catal.* **2016**, *6*, 8115.
25. S. Gao, Y. Lin, X. Jiao, Y. Sun, Q. Luo, W. Zhang, D. Li, J. Yang, Y. Xie, *Nature* **2016**, *529*, 68.
26. R. Kortlever, I. Peters, S. Koper, M. T. M. Koper, *ACS Catal.* **2015**, *5*, 3916.
27. A. Del Castillo, M. Alvarez-Guerra, J. Solla-Gullón, A. Sáez, V. Montiel, A. Irabien, *J. CO2 Util.* **2017**, *18*, 222.
28. E. Sargeant, A. Kolodziej, C. S. Le Duff, P. Rodriguez, *ACS Catal.* **2020**, *10*, 7464.
29. Y. Pu, M. J. Lawrence, V. Celorrio, Q. Wang, M. Gu, Z. Sun, L. A. Jácome, A. E. Russell, L. Huang, P. Rodriguez, *J. Mater. Chem. A* **2020**, *8*, 13340.
30. K. J. P. Schouten, Z. Qin, E. P. Gallent, M. T. M. Koper, *J. Am. Chem. Soc.* **2012**, *134*, 9864.
31. Y. Lum, J. W. Ager, *Nat. Catal.* **2019**, *2*, 86.
32. R. Reske, H. Mistry, F. Behafarid, B. Roldan Cuenya, P. Strasser, *J. Am. Chem. Soc.* **2014**, *136*, 6978.
33. F. Calle-Vallejo, M. T. M. Koper, *Angew. Chemie Int. Ed.* **2013**, *52*, 7282.
34. H. Mistry, A. S. Varela, C. S. Bonifacio, I. Zegkinoglou, I. Sinev, Y.-W. Choi, K. Kisslinger, E. A. Stach, J. C. Yang, P. Strasser, B. R. Cuenya, *Nat. Commun.* **2016**, *7*, 12123.
35. S. Liu, H. Tao, L. Zeng, Q. Liu, Z. Xu, Q. Liu, J.-L. Luo, *J. Am. Chem. Soc.* **2017**, *139*, 2160.
36. R. Kortlever, K. H. Tan, Y. Kwon, M. T. M. Koper, *J. Solid State Electrochem.* **2013**, *17*, 1843.
37. E. Pérez-Gallent, G. Marcandalli, M. C. Figueiredo, F. Calle-Vallejo, M. T. M. Koper, *J. Am. Chem. Soc.* **2017**, *139*, 16412.
38. K. J. P. Schouten, E. Pérez Gallent, M. T. M. Koper, *J. Electroanal. Chem.* **2014**, *716*, 53.
39. A. S. Varela, M. Kroschel, T. Reier, P. Strasser, *Catal. Today* **2016**, *260*, 8.
40. M. Moura de Salles Pupo, R. Kortlever, *ChemPhysChem* **2019**, *20*, 2926.
41. M. C. O. Monteiro, F. Dattila, B. Hagedoorn, R. García-Muelas, N. López, M. T. M. Koper, *Nat. Catal.* **2021**, *4*, 654.
42. S. Nitopi, E. Bertheussen, S. B. Scott, X. Liu, A. K. Engstfeld, S. Horch, B. Seger, I. E. L. Stephens, K. Chan, C. Hahn, J. K. Nørskov, T. F. Jaramillo, . *Chem. Rev.* **2019**, *119*, 7610.
43. R. Francke, B. Schille, M. Roemelt, *Chem. Rev.* **2018**, *118*, 4631.
44. W. Zhang, Y. Hu, L. Ma, G. Zhu, Y. Wang, X. Xue, R. Chen, S. Yang, Z. Jin, *Adv. Sci.* **2018**, *5*.
45. E. Wilhelm, R. Battino, R. J. Wilcock, *Chem. Rev.* **1977**, *77*, 219.
46. H. Zhong, K. Fujii, Y. Nakano, F. Jin, *J. Phys. Chem. C* **2015**, *119*, 55.
47. N. Spycher, K. Pruess, J. Ennis-King, *Geochim. Cosmochim. Acta* **2003**, *67*, 3015.
48. D. M. D. Alessandro, B. Smit, J. R. Long, *Angew. Chem. Int. Ed. Engl.* **2010**, *49*, 6058. https://doi.org/10.1002/anie.201000431.
49. X. Wang, C. Song, *Front. Energy Res.* **2020**, *8*.
50. H. Ooka, M. C. Figueiredo, M. T. M. Koper, *Langmuir* **2017**, *33*, 9307.
51. A. Goyal, G. Marcandalli, V. A. Mints, M. T. M. Koper, *J. Am. Chem. Soc.* **2020**, *142*, 4154.
52. A. Gennaro, A. A. Isse, E. Vianello, *J. Electroanal. Chem.* **1990**, *289*, 203.
53. SOLUBILITY DATA SERIES. in: *Carbon Dioxide in Non–Aqueous Solvents at Pressures Less than 200 KPA* (eds.: Fogg, P. G. T. B. T.-C. D. N. S. A. P. L. T. 200 K. P. A.) xElsevier, Amsterdam, NL **1992**, 484–485. https://doi.org/10.1016/B978-0-08-040495-0.50023-3.
54. D. R. Lide, *CRC Handbook of Chemistry and Physics*, CRC Press, Boca Raton, FL **2004**.
55. M. König, J. Vaes, E. Klemm, D. Pant, *iScience* **2019**, *19*, 135.
56. A. Aljabour, H. Coskun, D. H. Apaydin, F. Ozel, A. W. Hassel, P. Stadler, N. S. Sariciftci, M. Kus, *Appl. Catal. B Environ.* **2018**, *229*, 163.
57. N. E. Mendieta-Reyes, A. K. Díaz-García, R. Gómez, *ACS Catal.* **2018**, *8*, 1903.
58. N. E. Mendieta-Reyes, W. Cheuquepán, A. Rodes, R. Gómez, *ACS Catal.* **2020**, *10*, 103.
59. Y. Tomita, S. Teruya, O. Koga, Y. Hori, *J. Electrochem. Soc.* **2000**, *147*, 4164.
60. N. Hoshi, T. Murakam, Y. Tomita, Y. Hori, *Electrochemistry* **1999**, *67*, 1144.
61. M. C. Figueiredo, I. Ledezma-Yanez, M. T. M. Koper, *ACS Catal.* **2016**, *6*, 2382.
62. F. Shen, J. Shi, T. Chen, F. Shi, Q. Li, J. Zhen, Y. Li, Y. Dai, B. Yang, T. Qu, *J. Power Sources* **2018**, *378*, 555.
63. J. Shi, F. Shen, F. Shi, N. Song, Y.-J. Jia, Y.-Q. Hu, Q.-Y. Li, J. Liu, T.-Y. Chen, Y.-N. Dai, *Electrochim. Acta* **2017**, *240*, 114.
64. B. Eneau-Innocent, D. Pasquier, F. Ropital, J. M. Léger, K. B. Kokoh, *Appl. Catal. B Environ.* **2010**, *98*, 65.
65. T. Saeki, K. Hashimoto, A. Fujishima, N. Kimura, K. Omata, *J. Phys. Chem.* **1995**, *99*, 8440.
66. S. Kaneco, K. Iiba, K. Ohta, T. Mizuno, *Energy Sources* **2000**, *22*, 127.
67. S. Kaneco, K. Iiba, H. Katsumata, T. Suzuki, K. Ohta, *Electrochim. Acta* **2006**, *51*, 4880.
68. K. Ohta, M. Kawamoto, T. Mizuno, D. A. Lowy, *J. Appl. Electrochem.* **1998**, *28*, 717.
69. T. Saeki, K. Hashimoto, N. Kimura, K. Omata, A. Fujishima, *J. Electroanal. Chem.* **1996**, *404*, 299.
70. A. Naitoh, K. Ohta, T. Mizuno, H. Yoshida, M. Sakai, H. Noda, *Electrochim. Acta* **1993**, *38*, 2177.
71. T. Mizuno, A. Naitoh, K. Ohta, *J. Electroanal. Chem.* **1995**, *391*, 199.
72. S. Kaneco, K. Iiba, K. Ohta, T. Mizuno, *J. Solid State Electrochem.* **1999**, *3*, 424.
73. N. Deng, Y. Liu, Q. Li, J. Yan, L. Zhang, L. Wang, Y. Zhang, B. Cheng, W. Lei, W. Kang, *Ind. Eng. Chem. Res.* **2002**, *41*, 5165.
74. S. Kaneco, H. Katsumata, T. Suzuki, K. Ohta, *Energy Fuels* **2006**, *20*, 409.

75. S. Kaneco, K. Iiba, H. Katsumata, T. Suzuki, K. Ohta, *J. Solid State Electrochem.* **2007**, *11*, 490.
76. S. Kaneco, H. Katsumata, T. Suzuki, K. Ohta, *Electrochim. Acta* **2006**, *51*, 3316.
77. S. Kaneco, K. Iiba, K. Ohta, T. Mizuno, *Energy Sources* **1999**, *21*, 643.
78. S. Kaneco, K. Iiba, S. K. Suzuki, K. Ohta, T. Mizuno, *J. Phys. Chem. B* **1999**, *103*, 7456.
79. S. Ohya, S. Kaneco, H. Katsumata, T. Suzuki, K. Ohta, *Catal. Today* **2009**, *148*, 329.
80. T. Saeki, K. Hashimoto, N. Kimura, K. Omata, A. Fujishima, *J. Electroanal. Chem.* **1995**, *390*, 77.
81. M. Muruganantha, M. Kumaravel, H. Katsumata, T. Suzuki, S. Kaneco, *Int. J. Hydrogen Energy* **2015**, *40*, 6740.
82. S. Kaneco, K. Iiba, H. Katsumata, T. Suzuki, K. Ohta, *Chem. Eng. J.* **2007**, *128*, 47.
83. M. Ramdin, T. W. de Loos, T. J. H. Vlugt, *Ind. Eng. Chem. Res.* **2012**, *51*, 8149.
84. N. Hollingsworth, S. F. R. Taylor, M. T. Galante, J. Jacquemin, C. Longo, K. B. Holt, N. H. de Leeuw, C. Hardacre, . *Angew. Chemie Int. Ed.* **2015**, *54*, 14164.
85. M. Alvarez-Guerra, J. Albo, E. Alvarez-Guerra, A. Irabien, *Energy Environ. Sci.* **2015**, *8*, 2574.
86. Y. Chen, T. Mu, *Green Chem.* **2019**, *21*, 2544.
87. X. Kang, Q. Zhu, X. Sun, J. Hu, J. Zhang, Z. Liu, B. Han, *Chem. Sci.* **2016**, *7*, 266.
88. H. Liu, J. Guan, S. Yang, Y. Yu, R. Shao, Z. Zhang, M. Dou, F. Wang, Q. Xu, *Chem. Sci.* **2016**, *7*, 2883.
89. Y. Miao, N. Siri-Nguan, T. Sornchamni, G. N. Jovanovic, A. F. Yokochi, *Chem. Eng. J.* **2018**, *333*, 300.
90. X. Liu, H. Yang, J. He, H. Liu, L. Song, L. Li, J. Luo, *Small* **2018**, *14*, 1704049.
91. D. Niu, H. Wang, H. Li, Z. Wu, X. Zhang, *Electrochim. Acta* **2015**, *158*, 138.
92. G. P. S. Lau, M. Schreier, D. Vasilyev, R. Scopelliti, M. Grätzel, P. J. Dyson, *J. Am. Chem. Soc.* **2016**, *138*, 7820.
93. D. V. Vasilyev, S. Shyshkanov, E. Shirzadi, S. A. Katsyuba, M. K. Nazeeruddin, P. J. Dyson, *ACS Appl. Energy Mater.* **2020**, *3*, 4690.
94. S. S. Golru, E. J. Biddinger, *Electrochim. Acta* **2020**, *361*, 136787.
95. B. Braunschweig, P. Mukherjee, J. L. Haan, D. D. Dlott, *J. Electroanal. Chem.* **2017**, *800*, 144.
96. L. Zhang, Z. Zhang, W. Yuan, N. Zhao, Q. Zhu, L. He, G. Tao, *ChemPhysChem* **2019**, *20*, 3259.
97. V. O. Santos, I. R. Leite, A. G. Brolo, J. C. Rubim, *J. Raman Spectrosc.* **2016**, *47*, 674.
98. M. Papasizza, A. In Cuesta, *ACS Catal.* **2018**, *8*, 6345.
99. R. Jiang, M. Gao, X. Mao, D. Wang, *Curr. Opin. Electrochem.* **2019**, *17*, 38.
100. T. Lv, J. Xiao, W. Weng, W. Xiao, *Adv. Energy Mater.* **2020**, *2002241*, 28.
101. H. Yin, X. Mao, D. Tang, W. Xiao, L. Xing, H. Zhu, D. Wang, D. R. Sadoway, *Energy Environ. Sci.* **2013**, *6*, 1538.
102. H. V. Ijije, C. Sun, G. Z. Chen, *Carbon* **2014**, *73*, 163.
103. D. Tang, H. Yin, X. Mao, W. Xiao, D. H. Wang, *Electrochim. Acta* **2013**, *114*, 567.
104. V. Kaplan, E. Wachtel, K. Gartsman, Y. Feldman, I. Lubomirsky, *J. Electrochem. Soc.* **2010**, *157*, B552.
105. L. Hu, B. Deng, K. Du, R. Jiang, Y. Dou, D. Wang, *iScience* **2020**, *23*, 101607.
106. A. Yu, G. Ma, J. Ren, P. Peng, F. Li, *ChemSusChem* **2020**, *13*, 6229.
107. H. Wu, Y. Liu, D. Ji, Z. Li, G. Yi, D. Yuan, B. Wang, Z. Zhang, P. Wang, *J. Power Sources* **2017**, *362*, 92.
108. H. Wu, D. Ji, L. Li, D. Yuan, Y. Zhu, B. Wang, Z. Zhang, S. Licht, *Adv. Mater. Technol.* **2016**, *1*, 1600092.
109. D. Ji, Y. Liu, Z. Li, D. Yuan, G. Yang, M. Jiang, Y. Wang, Y. Yu, H. Wu, *Int. J. Hydrogen Energy* **2017**, *42*, 18156.
110. O. Al-Juboori, F. Sher, A. Hazafa, M. K. Khan, G. Z. Chen, *J. CO2 Util.* **2020**, *40*, 101193.
111. O. Al-Juboori, F. Sher, U. Khalid, M. B. K. Niazi, G. Z. Chen, *ACS Sustain. Chem. Eng.* **2020**, *8*, 12877.
112. L. Suo, Y. S. Hu, H. Li, M. Armand, L. Chen, *Nat. Commun.* **2013**, *4*, 1.
113. M. R. Singh, Y. Kwon, Y. Lum, J. W. Ager, A. T. Bell, *J. Am. Chem. Soc.* **2016**, *138*, 13006.
114. A. Seifitokaldani, C. M. Gabardo, T. Burdyny, C.-T. Dinh, J. P. Edwards, M. G. Kibria, O. S. Bushuyev, S. O. Kelley, D. Sinton, E. H. Sargent, *J. Am. Chem. Soc.* **2018**, *140*, 3833.
115. M. Liu, Y. Pang, B. Zhang, P. De Luna, O. Voznyy, J. Xu, X. Zheng, C. T. Dinh, F. Fan, C. Cao, F. P. G. de Arquer, T. S. Safaei, A. Mepham, A. Klinkova, E. Kumacheva, T. Filleter, D. Sinton, S. O. Kelley, E. H. Sargent, *Nature* **2016**, *537*, 382.
116. S. Verma, X. Lu, S. Ma, R. I. Masel, P. J. A. Kenis, *Phys. Chem. Chem. Phys.* **2016**, *18*, 7075.
117. C. M. Gabardo, A. Seifitokaldani, J. P. Edwards, C.-T. Dinh, T. Burdyny, M. G. Kibria, C. P. O'Brien, E. H. Sargent, D. Sinton, *Energy Environ. Sci.* **2018**, *11*, 2531.
118. S. S. Bhargava, F. Proietto, D. Azmoodeh, E. R. Cofell, D. A. Henckel, S. Verma, C. J. Brooks, A. A. Gewirth, P. J. A. Kenis, *ChemElectroChem* **2020**, *7*, 2001.
119. C. T. Dinh, T. Burdyny, M. G. Kibria, A. Seifitokaldani, C. M. Gabardo, F. P. García de Arquer, A. Kiani, J. P. Edwards, P. De Luna, O. S. Bushuyev, C. Zou, R. Quintero-Bermudez, Y. Pang, D. Sinton, E. H. Sargent, *Science* **2018**, *360*, 783.
120. NASA. Perseverance Mars rover extracts first oxygen from red planet. https://www.nasa.gov/press-release/nasa-s-perseverance-mars-rover-extracts-first-oxygen-from-red-planet **2021**.
121. M. Hecht, J. Hoffman, D. Rapp, J. McClean, J. SooHoo, R. Schaefer, A. Aboobaker, J. Mellstrom, J. Hartvigsen, F. Meyen, E. Hinterman, G. Voecks, A. Liu, M. Nasr, J. Lewis, J. Johnson, C. Guernsey, J. Swoboda, C. Eckert, C. Alcalde, M. Poirier, P. Khopkar, S. Elangovan, M. Madsen, P. Smith, C. Graves, G. Sanders, K. Araghi, M. de la Torre Juarez, D. Larsen, J. Agui, A. Burns, K. Lackner, R. Nielsen, T. Pike, B. Tata, K. Wilson, T. Brown, T. Disarro, R. Morris, R. Schaefer, R. Steinkraus, R. Surampudi, T. Werne, A. Ponce, *Space Sci. Rev.* **2021**, *217*.
122. H.-K. Lim, Y. Kwon, H. S. Kim, J. Jeon, Y.-H. Kim, J.-A. Lim, B.-S. Kim, J. Choi, H. Kim, *ACS Catal.* **2018**, *8*, 2420.
123. M. Papasizza, X. Yang, J. Cheng, A. Cuesta, *Curr. Opin. Electrochem.* **2020**, *23*, 80.
124. E. Vichou, Y. Li, M. Gomez-Mingot, M. Fontecave, C. M. Sánchez-Sánchez, *J. Phys. Chem. C* **2020**, *124*, 23764.
125. C. S. Le Duff, M. J. Lawrence, P. Rodriguez, *Angew. Chemie Int. Ed. 56*, **2017**, 12919 https://doi.org/10.1002/anie.201706463.

REVIEW
doi.org/10.1002/elsa.202100178
Chemistry Europe
European Chemical Societies Publishing

126. H. S. Jeon, J. Timoshenko, C. Rettenmaier, A. Herzog, A. Yoon, S. W. Chee, S. Oener, U. Hejral, F. T. Haase, B. Roldan Cuenya, *J. Am. Chem. Soc.* **2021**, *143*, 7578.
127. R. M. Arán-Ais, F. Scholten, S. Kunze, R. Rizo, B. Roldan Cuenya, *Nat. Energy* **2020**, *5*, 317.
128. B. Deng, M. Gao, R. Yu, X. Mao, R. Jiang, D. Wang, *Appl. Energy* **2019**, *255*, 113862.
129. M. Gao, B. Deng, Z. Chen, M. Tao, D. Wang, *Electrochem. Commun.* **2018**, *88*, 79.

AUTHOR BIOGRAPHIES



Elizabeth Sargeant received her MSci in Chemistry from the University of Birmingham in 2018. Since graduating, Elizabeth has been pursuing a Ph.D. in Electrochemistry under the supervision of Prof. Paramaconi Rodriguez. also at the University of Birmingham. Her current research focuses on electrochemical processes at low temperatures.



Prof. Paramaconi Rodriguez obtained his M.Sc. degree from the University Simón Bolivar (2003) and a Ph.D. from the University of Alicante (2007), before undertaking postdoctoral appointments at the University of Leiden and a research officer position at the Paul Scherrer Institute. He was awarded the Birmingham Research Fellow in 2012 and promoted to Associate Professor at Birmingham in 2018. He is currently an Ikerbasque Research Professor at the CIC energiGUNE in Spain and an honorary Associate Professor at the University of Birmingham in electrochemistry.

How to cite this article: E. Sargeant, P. Rodríguez. *Electrochem Sci Adv*. **2022**, e2100178. https://doi.org/10.1002/elsa.202100178

CHAPTER 2

Electrochemical conversion of CO_2 and CH_4 at Sub-zero Temperatures

Elizabeth Sargeant, Adam Kolodziej, Cécile S. Le Duff, and Paramaconi Rodriguez, *ACS Catal.* 2020, 10, 14, 7464–7474

doi: 10.1021/acscatal.0c01676

Declaration

P.R conceived the experiments. The electrochemical experiments were performed by E.S, A.K and P.R. **Note, E.S. carried out the electrochemical experiments in KOH during her Masterôs year and so should be assessing the data regarded this thesis**. Product characterisation by mass spectrometry experiments were carried out by P.R. NMR characterisation and analyses was performed by E.S and C.L.D. All authors contributed to the analysis of the results, discussion, writing and revision of the manuscript.

ACS Catalysis

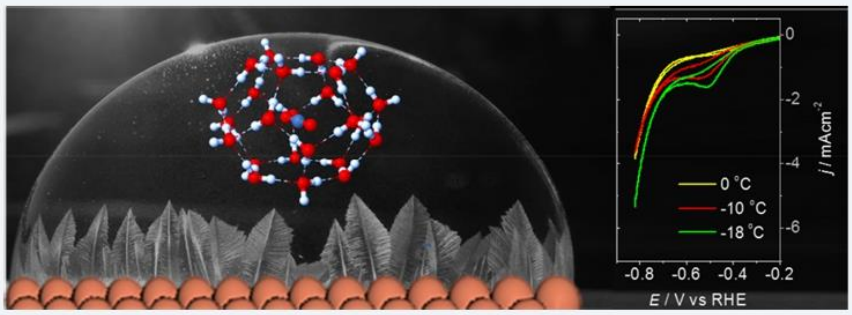
pubs.acs.org/acscatalysis Research Article

Electrochemical Conversion of CO_2 and CH_4 at Subzero Temperatures

Elizabeth Sargeant, Adam Kolodziej, Cécile S. Le Duff, and Paramaconi Rodriguez*

Cite This: ACS Catal. 2020, 10, 7464−7474 Read Online

ACCESS | Metrics & More | Article Recommendations | Supporting Information



ABSTRACT: By taking advantage of the high solubility of CO_2 and CH_4 at low temperature, we report the electrochemical conversion of these gases in aqueous media down to −40 °C. The 5-fold increase in the concentration of CH_4 in gas hydrate slurries makes its electrochemical oxidation feasible at temperatures below the freezing point of water. We also report the electrochemical conversion of CO_2 at low temperatures and demonstrate, unexpectedly, that its reduction in these conditions follows an anti-Arrhenius kinetics electrochemical environment. These findings open windows of investigation into electrocatalysis in brines below the freezing point of water.

KEYWORDS: *Electrocatalysis, CO_2 reduction, methane oxidation, brines, freezing point depletion, anti-Arrhenius*

Downloaded via UNIV OF BIRMINGHAM on August 11, 2020 at 09:45:51 (UTC).
See https://pubs.acs.org/sharingguidelines for options on how to legitimately share published articles.

1. INTRODUCTION

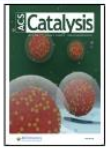
Gas hydrates, or clathrates, were discovered in 1810 in the laboratory of Sir Humphrey Davy by cooling a solution saturated with chlorine gas below −9 °C.[1] Since then, many other gas hydrates such as hydrates of hydrocarbons, sulfur dioxide (SO_2), and carbon dioxide (CO_2) have been discovered.[2,3] 200 years after the discovery of gas hydrates, they are barely used and there are very few examples of technical applications.[4] In particular, these systems have been disregarded for electrocatalytic applications.

However, the recent discovery of perchlorate brines on Mars at the Phoenix landing site[5] has renewed interest in the scientific community in gas hydrates and the chemistry of brines. Given that the composition of the Martian atmosphere is 96% CO_2 and, knowing the solubility of CO_2 increases with decreasing temperature, it is expected that such brines will have large amounts of carbonates and CO_2 hydrates.[6] Furthermore, the presence of CH_4 in the Martian atmosphere and formation of gas hydrates has recently been confirmed.[7]

NASA has continuously examined technologies that may enable Mars In-Situ Resource Utilization (ISRU).[8] Such technologies should provide practical and affordable ways to use the local resources during the missions instead of the costly transportation of resources to Mars. The technologies should have the ability to transform the resources into air, fuels, water for drinking, fine chemicals, plant growth, rocket propellants, building materials, etc. CO_2 and CH_4 hydrates could be considered basic elements for human establishment, as they could provide, directly or indirectly, fuel, water, and standard industrial chemicals for the manufacture of plastics. In fact, the ISRU program has focused on the production of methane from atmospheric CO_2 and hydrogen brought from Earth via the Sabatier reaction, and the synthesis of oxygen required for propellant usage.[8]

Developing and understanding electrocatalytic reactions of gas hydrates at low temperature will be relevant for the development of technology capable of producing electricity by converting CH_4 into CO_2 and then recycling CO_2 back into CH_4. These reactions can then be used as a sustainable energy cycle, in a reversible fuel cell,[9] under severe environmental conditions. This will be critical to ensure the availability of key

Received: April 14, 2020
Revised: June 9, 2020
Published: June 9, 2020



© 2020 American Chemical Society

https://dx.doi.org/10.1021/acscatal.0c01676
ACS Catal. 2020, 10, 7464−7474

in situ resources sustaining future human exploration and colonization of Mars (Figure 1). Such technology would be based on reversible fuel cell/electrolyzer technologies and preferentially taking place in water or gas hydrates.[10]

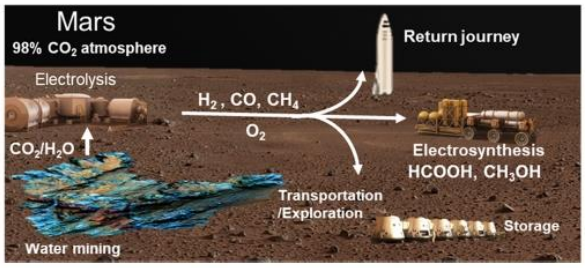


Figure 1. Electrochemical utilization of CO_2 and methane transformation on Mars. The figure has been prepared based on the In Situ Resource Utilization (ISRU) program from NASA. Adapted from ref 13.

So far, electrocatalytic processes in aqueous solution have been extensively studied as a function of temperature in the range 0−99 °C, but very little is known about electrocatalytic processes at temperatures below the freezing point of water or in gas hydrates.[11] The magnitude of freezing-point depression of the brine solution depends only on the solute concentration (m, molality) and the of number of ion particles per individual molecule of solute dissociated in the solvent (i, van't Hoff coefficient). The magnitude of freezing-point depression can be estimated by the linear relationship of these two parameters and the cryoscopic constant ($k_{freezing}$)

$$\Delta T = imk_{freezing}$$

Decreasing the temperature of water to subfreezing temperatures significantly increases the solubility of gases in water,[12] and, as such, the reaction rate of the oxidation or reduction reaction can be increased. As the concentration of the gas increases, the chemical potential increases, which might favor the adsorption of the reactive and intermediate species.

In this paper, we report the first electrochemical results for the oxidation of CH_4 and the reduction of CO_2 on platinum, palladium, gold, and copper electrodes in aqueous brines at subfreezing temperatures, down to −38 °C. The systems were evaluated in different brines such as 4.4 m $Mg(ClO_4)_2$, similar to those brines observed on Mars, 11 m NaOH and 10 m KOH solutions.

2. RESULTS AND DISCUSSION

2.1. Hydrogen UPD and Hydrogen Evolution Reaction (HER) in Brines. The current−potential curves (I−V) of Pt(111) and Pt(100) single-crystal electrodes in a 4.4 m $Mg(ClO_4)_2$ solution at different temperatures are shown in Figure 2A. Below 0.5 V vs RHE, the features are associated with the hydrogen adsorption/desorption process, and at potentials higher than 0.5 V vs RHE, the features are due to the formation and reduction of the surface oxides. The so-called hydrogen UPD is reversible for both electrodes at room temperature and becomes irreversible when the temperature is decreased down to −18 °C. Similarly, the voltammetric features associated with the oxidation and reduction of the surface change significantly when the temperature is reduced from room temperature to −18 °C. Such irreversibility in the hydrogen UPD and the surface oxides processes are not due to the presence of any type of contamination present in the electrolyte, but because larger overpotentials are required for processes to take place at lower temperature. The degree of

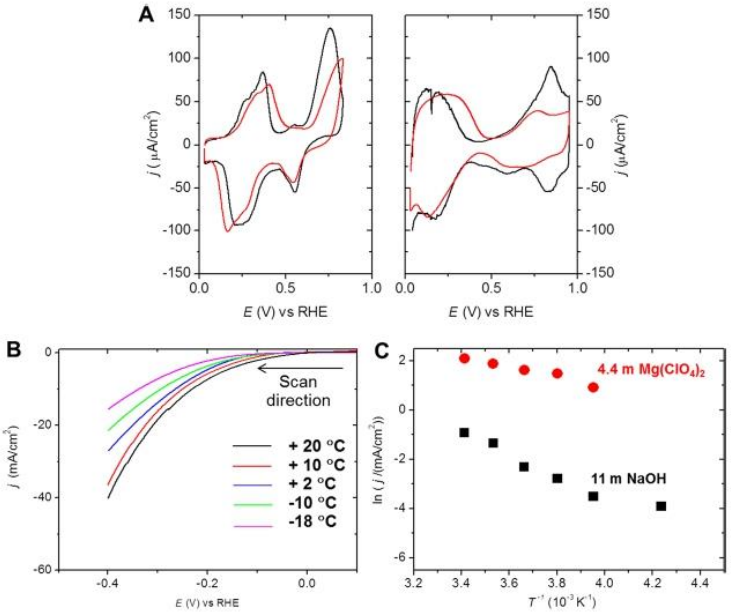


Figure 2. (A) Voltammetric profiles of Pt(100) and Pt(111) in 4.4 m solution of $Mg(ClO_4)_2$ at +20 °C (black curve) and −18 °C (red curve). (B) Voltammetric profiles of Pt(111) in 4.4 m $Mg(ClO_4)_2$; temperatures indicated in the figure. (C) Arrhenius plots for the HER on Pt(111) at −0.1 V vs RHE in 11 m NaOH and 4.4 m solution of $Mg(ClO_4)_2$.

https://dx.doi.org/10.1021/acscatal.0c01676
ACS Catal. 2020, 10, 7464−7474

cleanliness and the effect of the purity of the electrolyte are discussed in the Supporting Information, Figure S10.

The irreversibility of the hydrogen adsorption/desorption as a function of the temperature contrasts with previous results by Arvia et al.[11b,14] in concentrated sulfuric and perchloric acid. This can be attributed to the large difference in proton concentrations between the concentrated acid solutions and the $Mg(ClO_4)_2$ brines used in this work. For both electrodes, Pt(111) and Pt(100), the hydrogen desorption peak shifts to more positive potentials, 100 mV and 120 mV, respectively, when the temperature decreases from +20 to −18 °C. In the same range of temperature, the hydrogen adsorption peak shifts to more negative potentials, 56 and 90 mV, respectively. This corresponds to a temperature coefficient of approximately 2 mV K^{-1}, an average of the adsorption and desorption processes. This is larger than the calculated temperature coefficient of 0.65 mV K^{-1} for the reversible hydrogen electrode in 0.1 M H^+ solution[15] and the shift of 0.45 mV K^{-1} estimated from the adsorption isotherm of hydrogen on Pt(111) in 0.1 M $HClO_4$ by Markovic et al.[16] The variation can be attributed not only to differences in the proton concentration but also to the nature and concentration of the ions in solution as described by Debethune et al.[15] As a consequence of the shift in the hydrogen adsorption at low temperature, the onset of the hydrogen evolution reaction (HER) also shifts toward more negative potentials as shown in Figure 2B.

This is an important parameter to determine, as the HER is a competitive reaction during the electrochemical reduction of CO_2. Previous works by Frese et al.[17] showed that the HER on platinum electrodes at −45 °C in $HClO_4 \cdot 5.5H_2O$, close to the freezing point of the electrolyte, follows the Volmer−Tafel mechanism where the combination of two adsorbed hydrogen atoms to form H_2 is rate-determining

$$H_{aq}^{+} + e^{-} \Leftrightarrow H_{ad} \text{(Volmer reaction)}$$

$$2H_{ad} \Leftrightarrow H_2 \text{(Tafel reaction, RDS)}$$

In acidic media, the mechanism of HER is not dependent on the temperature as the Tafel slope is independent of T and a proton tunneling mechanism has been proposed.[11a,17] Our results show a Tafel slope of 40 mV dec^{-1} at +20 °C for the HER in 4.4 m solution of $Mg(ClO_4)_2$. This indicates that either the Tafel step is the rate-determining step or the rate-determining step is a chemical step preceded by a 2-electron transfer step. The chemical steps could be related to the reorganization of the water molecules in the presence of a high concentration of ions. Unlike in acidic media, the HER in $Mg(ClO_4)_2$ showed changes in the Tafel slope as a function of the temperature, from 40 mV dec^{-1} at +20 °C to 65 mV dec^{-1} at −18 °C. This result is consistent with the expected short-range structural rearrangement of water around both cations and anions.[18] In 11 m NaOH at 20 °C, a value of 135 mV dec^{-1} was found for the Tafel slope. This implies that the Volmer step, which is the first electron transfer, is the rate-determining step

$$H_2O + e^{-} \Leftrightarrow H_{ads} + OH^{-}$$

(Volmer step in alkaline media, RDS)

This is in agreement with previous results for the HER in alkaline media with much lower concentrations of hydroxide.[19] In acidic media, the anions occupy the large cavities in the water cage-like structure and the excess of delocalized protons act as charge carriers. In alkaline media, it is the cation that occupies the cavities of the water cage structure and the hydroxyl ions act as the charge carriers. Given the absence of free protons in alkaline solution, the protons for the hydrogen adsorption and HER come from the water molecules. It has been previously reported that water at the liquid/solid interface has a well-ordered structure which is lower in free energy than either ice or clathrate and higher in energy than liquid water under the same thermodynamic conditions.[20] This ordering increases on cooling, giving way to heterogeneous ice nucleation from the surfaces.[21] However, the water structure ordering results in a higher energy barrier that needs to be overcome for proton adsorption and subsequent HER.[20] The Tafel slopes in alkaline media are also temperature dependent,[18,22] increasing from 135 mV dec^{-1} at 20 °C up to 190 mV dec^{-1} at −35 °C. The decrease in catalytic activity as the temperature decreases follows an expected Arrhenius behavior, as shown in Figure 2C. The apparent activation energies (E_a) in $Mg(ClO_4)_2$ and NaOH obtained from the Arrhenius plots were 17.27 and 31.78 kJ mol^{-1}, respectively. Previous reports have shown E_a values for H on Pt electrodes in HCl/CH_3OH and 0.1 M KOH of 11.2[11a] and 28.9 kJ mol^{-1},[19c] respectively. The differences in E_a can be partly attributed to the different pH values but are mainly due to the coadsorption of cations (Na^+ vs Mg^{2+}).[23]

On palladium electrodes, in addition to the shift toward more negative potentials for the hydrogen adsorption/absorption process upon decreasing the temperature, the intensity of the peaks associated with the hydrogen oxidation also changed (Figure S11). This change is related to different rates of diffusion of the hydrogen through the two distinct palladium hydride phases, α- and β-, and the transformation between these phases.[24]

2.2. Electrochemical Reduction of CO_2 in Brines. Previous studies have shown that the changes in the lattice parameter of palladium and the hydrogen diffusion in the palladium structure influence the catalytic activity and selectivity of the electrochemical reduction of CO_2.[25] Therefore, it is expected that the changes to the absorption, diffusion, and desorption of the hydrogen in the palladium electrodes and the increased concentration of CO_2 at low temperatures will strongly influence the electrochemical catalytic activity and selectivity of the reduction of CO_2.[26] As mentioned before, the HER competes with CO_2 reduction on some metal electrodes, such as copper and palladium. In gas hydrate crystal structures, the arrangement of their hydrogen bond network is "ice-like" but slightly more distorted. Due to the formation of the ice-like ordered structure of water, the HER might be hindered, resulting in changes to the kinetics and selectivity of CO_2 reduction.[11b,d,17]

Figure 3A,B shows the electrochemical reduction of CO_2 on palladium electrodes in a 10 m KOH solution at two different temperatures. It shows that the CO_2 reduction, indicated by an arrow, is favorable at the lower temperature. Although seemingly counterintuitive, this behavior can be attributed to the increase in the solubility of CO_2 due to the formation of the water cages as the temperature decreases. As the concentration of CO_2 increases with decreasing temperature, the formation of carbonate species is favorable. Potassium was selected as the cation of choice over sodium, because when NaOH was used a white precipitate of $NaHCO_3$ formed at low temperatures. The measured pH after CO_2 saturation at −18

https://dx.doi.org/10.1021/acscatal.0c01676
ACS Catal. 2020, 10, 7464−7474

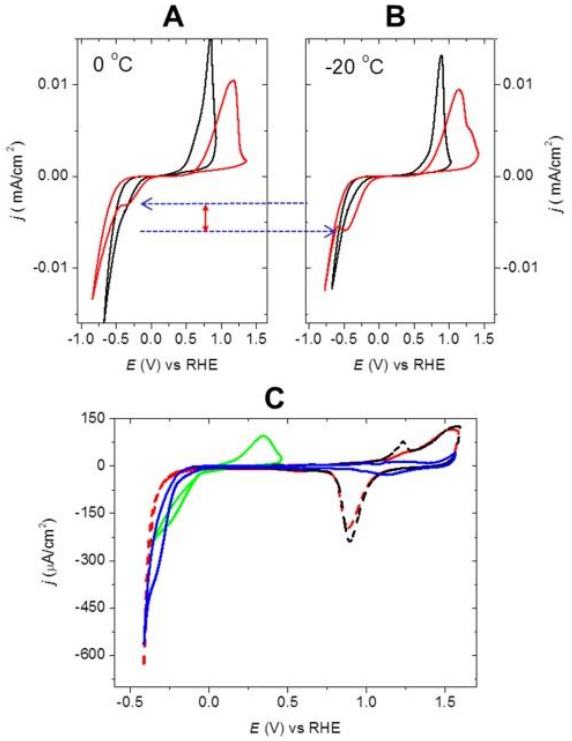


Figure 3. (A,B) Voltammetric profiles of a Pd polycrystalline electrode at 0 °C and −20 °C in an Ar-saturated solution of 10 m KOH (black curve) and in a CO_2-saturated solution of 10 m KOH (red curve) Scan rate, υ = 50 mV/s. (C) Voltammetric profiles of Au polycrystalline electrode in a CO_2-saturated solution of 4.4 m $Mg(ClO_4)_2$ at 0 °C (red curve), −10 °C (blue curve), and −18 °C (green curve). The voltammetric profile of the gold electrode at 0 °C in the absence of CO_2 (black dashed curve) was included for comparison. Scan rate, υ = 50 mV/s.

°C was 11, which indicates the formation of carbonate/bicarbonate species. It is important to note that such species are present in the Mars atmosphere and determine the oxidation/reduction potential of the Martian soil.[6e] All the CO_2 reduction reaction curves were corrected for the corresponding change of the pH at each temperature on the RHE scale.

The product distribution for this reaction was followed by online electrochemical mass spectrometry (Figure S1) and NMR (Table 1 and Figure S4−8). As can be seen in Figure 4A, the formation of hydrogen decreases when decreasing the temperature from 20 to −18 °C. At the same time, a small increase in the formation of other hydrocarbons was observed as the temperature decreased. It has been previously reported that the electrochemical reduction of CO_2 results in the formation of formic acid (formate) at low overpotentials.[25b] At this pH and temperature, the formate is not volatile and its detection was not possible by OLEMS. The formation of other gases, such as CO and other hydrocarbon species (C_xH_y), also increased upon decreasing the temperature. The liquid products were identified and quantified using water suppression NMR (Table 1).[27] The NMR spectra (Figure S6) show the different selectivity of the reduction of CO_2 at different temperatures. At the lower temperature, the formation of formic acid is enhanced, and ethanol, which is not observed at

Table 1. Summary of the Liquid Products Identified after 20 min of Electrolysis, at −0.6 V in a CO_2-Saturated Solution of 4.4 m $Mg(ClO_4)_2$ on Cu(111) and Pd (Polycrystalline)

electrode	temperature (°C)	species detected in the 1D ^{1}H spectrum[a]	species detected in the 1D ^{1}H-decoupled ^{13}C spectrum[a]
Pd	20	HCOOH − trace	None detected (10,000 scans)
	−18	**HCOOH** − 0.30 mM	**$HCOO^-$**
		EtOH − 0.06 mM	
Cu	20	**HCOOH** − 0.27 mM	**$HCOO^-$**
		EtOH − 0.02 mM	$CH_2(OH)_2$
	−18	**HCOOH** − 0.26 mM	**$HCOO^-$**
		EtOH − 0.13 mM	EtOH
		MeOH − trace	$CH_2(OH)_2$

[a]Species found in both types of spectra (^{1}H and ^{13}C) are highlighted in bold.

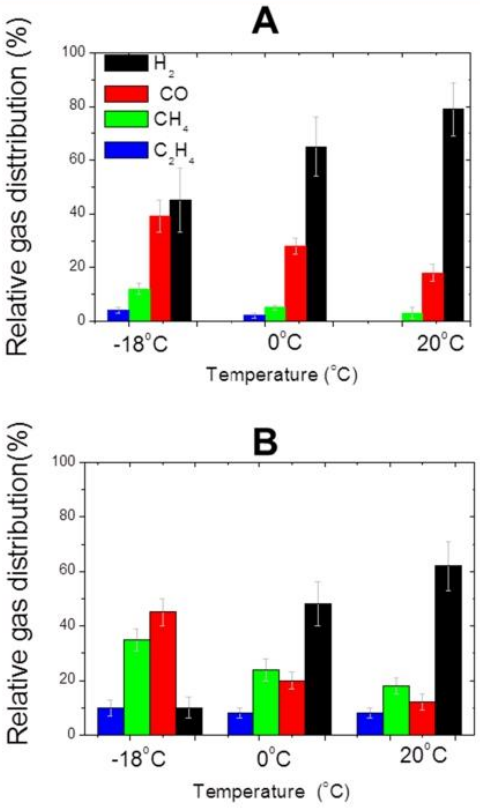


Figure 4. Gas product distribution during the CO_2 reduction on (A) Pd and (B) Cu electrodes after 15 min electrolysis at −0.6 V vs RHE in 4.4 m $Mg(ClO_4)_2$.

20 °C, is formed. Previous works have reported the formation of H_2, CO, and formic acid as the main products of the electrochemical reduction of CO_2 on Pd.[25b,28] Here for the first time, we report the formation of ethanol as one of the products of the reduction of CO_2. We believe that the C−C coupling is promoted by the increase of the surface coverage of CO at low temperatures and the change of the lattice of the palladium.

https://dx.doi.org/10.1021/acscatal.0c01676
ACS Catal. 2020, 10, 7464−7474

Figure 3C shows the electrochemical reduction of CO_2 on Au(111) electrodes in 4.4 m $Mg(ClO_4)_2$ at 0 and −18 °C. As in the case of Pd and Pt, the electrochemical reduction of CO_2 is favored at lower temperatures. Interestingly, the voltammetric profile at −18 °C showed an oxidation signal at 0.4 V vs RHE which is not present at 0 °C. Since the main product of the CO_2 reduction on gold is CO, this signal is likely due to the oxidation of CO. Earlier work has shown that CO oxidation takes place on gold electrodes at lower potentials in alkaline media.[29] As the CO_2 reduction reaction takes place, the local pH becomes more alkaline due to the HER favoring the adsorption and oxidation of CO. However, such an effect should also be observed at 20 °C. The presence of the signal only at low temperature can be attributed to the higher concentration of CO near the electrode at low temperature, resulting from the increased CO_2 reduction reaction.

The curves for the electrochemical reduction of CO_2 on Cu(111) in static conditions, as a function of the temperature, are shown in Figure 5A and B. It was found that the currents associated with the CO_2 reduction increased as the temperature decreased, likely due to the increase of the concentration of CO_2 in solution.

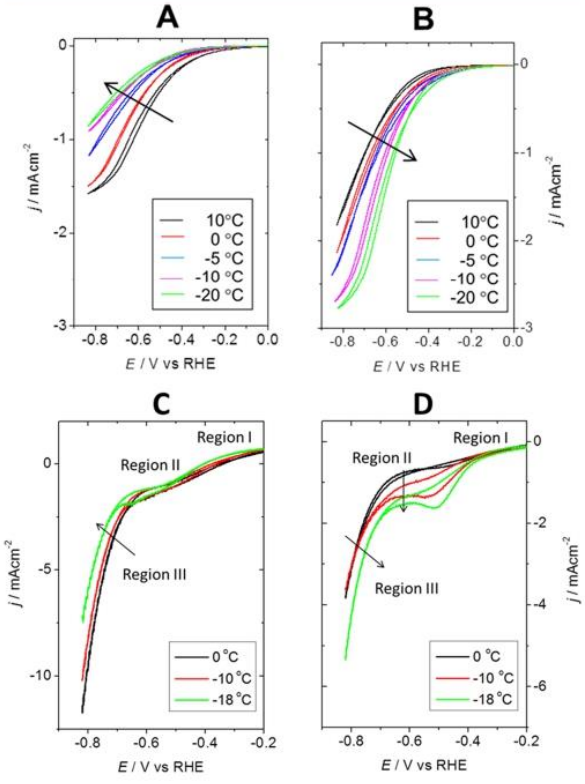


Figure 5. (A,B) Voltammetric profiles of Cu(111) electrode in (A) Ar-saturated and (B) CO_2 saturated 4.4 m $Mg(ClO_4)_2$. The solutions were saturated and the voltammetries were recorded with a stationary electrode and at different temperatures as indicated in the figure. The arrow indicates the trend as a function of the temperature. (C,D) HMRDE voltammograms of Cu(111) electrode in a (C) Ar-saturated and (D) CO_2-saturated solution of 4.4 m $Mg(ClO_4)_2$ at different temperatures. Rotation rate: 1600 rpm and scan rate, υ = 50 mV s^{-1}. The arrow indicates the trend as a function of the temperature.

It is well-known that mass transport gradients play an important role in the kinetics of the CO_2 reduction reaction and HER. The use of a hanging-meniscus rotating electrode during experiments on the Cu(111) enable strict control over the mass transport, diminishing the concentration gradients at the electrode interface, and minimizing changes of the pH at the surface.

Figure 5C,D shows cyclic voltammograms of a Cu(111) rotating disc electrode in a hanging meniscus configuration (HMRDE) in Ar-saturated and CO-saturated 4.4 m $Mg(ClO_4)_2$ electrolyte at different temperatures. Three well-defined regions can be distinguished. In Figure 5C, Ar-saturated solution, region I, between −0.2 and −0.45 V vs RHE is assigned to the hydrogen evolution reaction from proton reduction. Region II, between −0.45 and −0.7 V vs RHE, leads to a current plateau indicating mass transport limitation. In region III, at potentials more negative than −0.7 V vs RHE, the current increases independently from proton mass transport and can be assigned to HER from water reduction.

As can be seen in Figure 5C, Ar-saturated solution, the onset of the proton reduction current in region I, is slightly shifted to a more negative potential, and the diffusion current, region II, is almost unaltered when the temperature is decreased from 0 to −18 °C. This is an indication that the mass transport and reduction of protons is almost independent of the temperature. On the other hand, the HER from water reduction, region III, is shifted to more negative potentials as the temperature decreases. Interestingly, the larger overpotential was found at −18 °C where the crystallization of the water is expected at this concentration of the brine.

In contrast, the CO_2-saturated solution, Figure 5D, the voltammograms are strongly influenced by the temperature. The onset potentials in regions I and III shift toward more positive potentials, and the diffusion limiting currents increase as the temperature decreases. These results show that under well-defined mass transport conditions, the rate of the reduction of CO_2 is largely dependent on temperature and that the concentration of CO_2 at the interface is greater at low temperatures as confirmed in Figure S3.

Figure 6 shows the comparison between the voltammograms of Cu(111) HMRDE in an Ar-saturated and CO_2-saturated 4.4 m $Mg(ClO_4)_2$ electrolyte at different temperatures and different rotation rates.

Compared to the Ar-saturated solution, at temperatures above −10 °C the onset of reduction current in the CO_2-saturated solution in region III is slightly shifted to a more negative potential. However, as the temperature becomes more negative and the rotation rate increases, the onset of the reduction current shifts to more positive potentials. It is also important to note, at temperatures greater than 0 °C the diffusion current, region II is almost identical to the diffusion current in Ar-saturated electrolyte, independent of the rotation rate as previously reported for the reduction of CO_2 in acidic media.[30] This is in contrast to lower temperatures, −10 to −18 °C, where the diffusion current increases as the rotation rate increases. Since the diffusion current, from the Levich constant depends on the kinematic viscosity ($\upsilon^{-1/6}$) and the diffusion coefficient ($D^{2/3}$), where both factors decrease with temperature, the only possible factors that might result in an increase in the diffusion current are the number of electrons (n) and the concentration (C). It was previously proven that the concentration of CO_2 increased with decreasing temperature

https://dx.doi.org/10.1021/acscatal.0c01676
ACS Catal. 2020, 10, 7464−7474

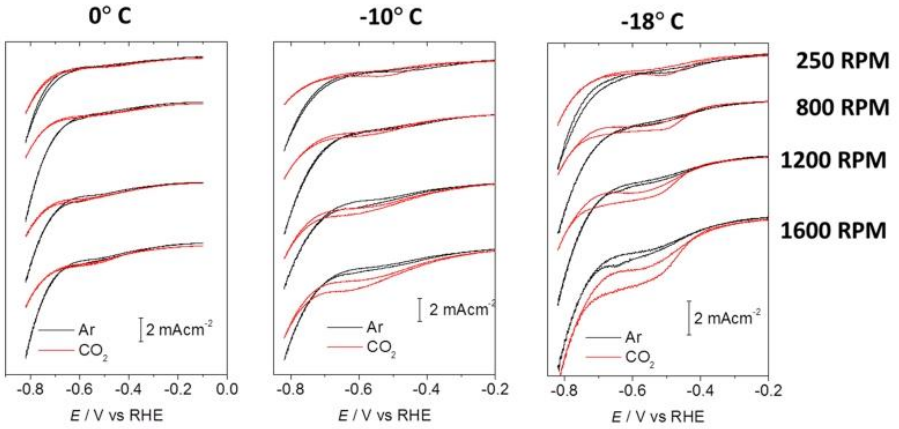


Figure 6. HMRDE voltammograms of Cu(111) electrode in (black curve) Ar-saturated, and (red curve) CO_2-saturated solution of 4.4 m $Mg(ClO_4)_2$ at different temperatures and rotation rate as indicated in the figure. Scan rate, υ = 50 mV s^{-1}.

(Figure S3). Below, we will discuss the changes in the product selectivity that result from the change in the number of electrons transferred. The increase in the limiting current, as a function of the rotation rate, at −18 °C, might also influence the onset of the reduction current in region III.

In order to determine the E_a of the process from the Arrhenius plots, the true kinetic currents (j_{kin}) were determined at −0.4 and −0.45 V vs RHE by correcting the currents at each potential (j) by the diffusion currents (j_{Diff}) using the modified Koutecký−Levich equation as previously described for the ORR.[31] The concentration of the CO_2/HCO_3^- was also determined at each temperature following the procedure described in the SI and shown in Figure S2. Figure S3 shows how the solubility of CO_2 increases as the temperature decreases. As a result of the increase in the solubility of CO_2, HCO_3^- is formed and the pH increases. The Arrhenius plots for the Cu(111) electrode at two different potentials, −0.4 V vs RHE, region I, and −0.45 V vs RHE, region II, and two rotation rates are shown in Figure 7. The kinetic constants were determined, taking into account that both CO_2 and HCO_3^- are reactive species in the CO_2 reduction reaction. As can be seen, the Arrhenius plots present two different slopes, positive slopes at temperatures greater than −5 °C and negative slopes at temperatures less −5 °C, independent of rotation rate and potential. At higher temperatures, greater than −5 °C, the calculated E_a values were E_a = 4.3 ± 0.3 kJ mol^{-1} at −0.4 V and E_a = 3.58 ± 0.04 kJ mol^{-1} at −0.45 V, and at temperatures lower than −5 °C, the Arrhenius plots show an anti-Arrhenius behavior with E_a = −1.25 ± 0.25 kJ mol^{-1} at −0.4 V and E_a = −1.52 ± 0.08 kJ mol^{-1} at −0.45 V.

Other kinetic parameters, such as Tafel plots and the electron transfer coefficient, could be extracted from the cyclic voltammetry; however, this manuscript does not include the kinetic analysis to avoid oversimplifying the process. Previous works have oversimplified the analysis of the kinetics of the CO_2 reduction reaction, typically assuming that the surface coverage of the intermediate species is constant.[32] However, this simplification leads to an incomplete description of the actual surface kinetics, in particular on Cu electrodes where the coverage of different reaction products and different intermediate adsorbed species varies with the applied potential.

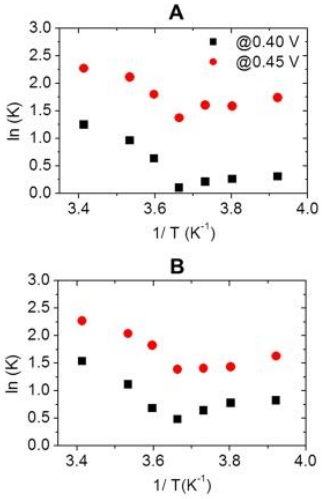


Figure 7. Arrhenius plots at −0.4 V (black square) and −0.45 V (red circle) on a Cu(111) electrode in a CO_2-saturated solution of 4.4 m $Mg(ClO_4)_2$. To obtain the ln(K), the kinetic currents (j_k) at each potential were corrected by the diffusion current (j_d) at −0.72 V according to the modified Koutecky−Levich equation. (A) Currents obtained at 250 rpm and (B) currents obtained at 1600 rpm.

Regarding the selectivity, results seen in Figure 4B show that on Cu(111) the HER decreases, and the formation of hydrocarbons, CH_4 and C_2H_4, increases as the temperature decreases from 20 to −18 °C. Similar trends were observed by Ahn et al. for the temperature range between 42 and 2 °C.[33] An increase in the CO production rate was also observed at low temperatures. It is important to note that the solubility of all these gases, CH_4, C_2H_4, and CO, increase at low temperature due to the formation of their respective gas hydrates. The NMR analysis, Table 1, shows that larger concentrations of formic acid and small amounts of methanol, gem-diol, and ethanol were detected after 20 min of electrolysis at −18 °C.

The changes in product selectivity during the CO_2RR can be attributed to different sources, and in fact, many of the reasons can be interlinked. As shown before, the decrease in the temperature results in a decrease of the HER, but also results

https://dx.doi.org/10.1021/acscatal.0c01676
ACS Catal. 2020, 10, 7464−7474

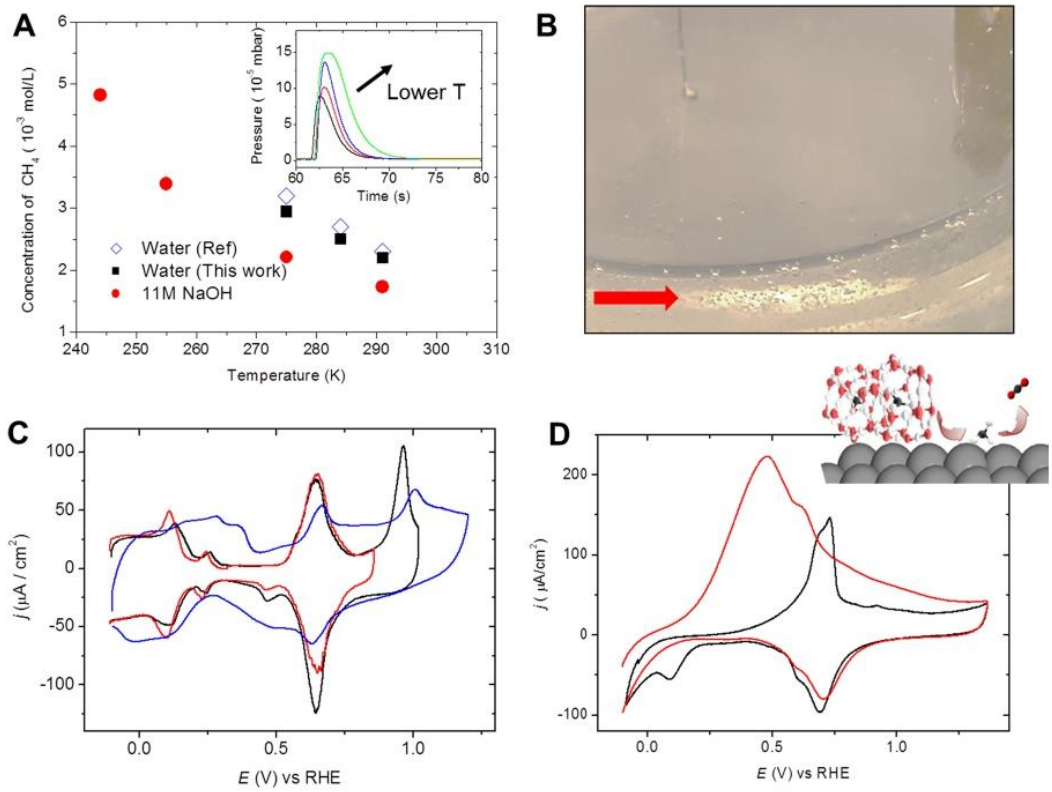


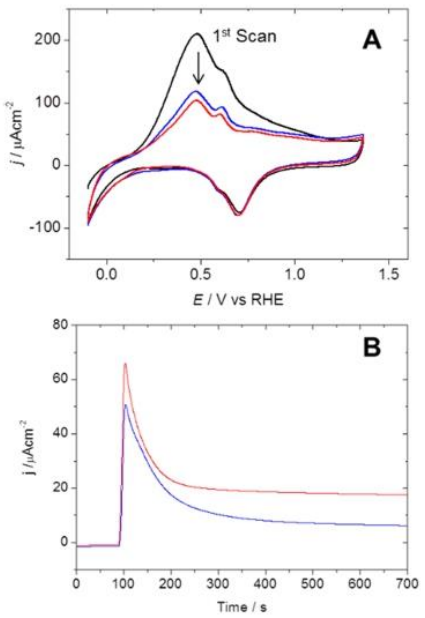
Figure 8. (A) Solubility curves of CH_4 as a function of the temperature in water and 11 m NaOH. The values of the solubility in water at different temperatures from Wiesenburg et al. and Duan et al. were included for validation of the method and proper comparison.[12,39] Inset: Pressure vs time curves obtained from MS measurements at different temperatures. (B) Photograph of the opaque gel formed upon bubbling CH_4 in 11 m NaOH solution at −35 °C. (C) Voltammetric profile of Pt(111) electrode in 11 m NaOH in absence of CH_4 at −18 °C (red curve), in the presence of CH_4 at −18 °C (black curve), and in the presence of CH_4 at −38 °C (blue curve). Scan rate, υ = 50 mV s^{-1}. (D) Voltammetric profile of Pd electrode in 11 m NaOH at −38 °C in the absence (black curve) and presence of CH_4 (red curve). Scan rate, υ = 50 mV s^{-1}. Inset shows a schematic cartoon of the oxidation of CH_4 hydrate to CO_2.

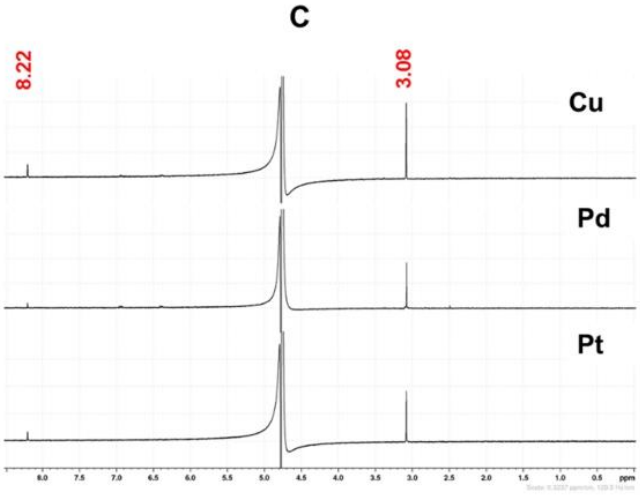
in an increase of the solubility of the CO_2 species. Koper's group reported that the water reduction pathway is specifically inhibited by adsorbed CO during the CO_2RR leading to high faradaic efficiency for CO_2 reduction on copper electrodes. This inhibition of the HER pathway becomes more pronounced at increased mass transport of CO_2.[30] In our system, the mass transport is not only affected by the decrease in the temperature but also by the viscosity of the highly concentrated electrolyte. Jaramillo's group reported that methane formation only occurs at potentials within a CO mass-transport-limited regime and the C2+ products are sensitive to the CO partial pressure.[34] While the mass transport effect has been mainly identified on high-surface-area nanostructured electrodes,[35] based on the results on HMRDE, mass transport effects on the product selectivity in our extended surface electrodes cannot be discarded. In addition, the solvation of the CO_2 and the intermediates by a more rigid structure of the water in the CO_2 hydrate might affect the product selectivity.

Previous works have demonstrated that in gas hydrate crystal structures, the arrangement of their hydrogen bond network is "ice-like" but with slight distortions. Further stabilized by encaging a guest molecule, the cage structures in gas hydrate crystals are considered relatively rigid and the lattice water molecules are largely restricted from rotation and translation.[36] The rigidity of the gas hydrate structure may influence different steps of the reaction mechanism. Studies performed by Luo et al. suggest that the hydrogenation of CO_{ads} to COH_{ads} or CHO_{ads} is a key step determining the selectivity of the reduction of CO_2 to hydrocarbons.[37] The formation of these intermediates depends on the coverage of CO and protons, which depends on the applied potential.

2.3. Electrochemical Oxidation of CH_4 in Brines at −40 °C. As previously mentioned, another interesting system to study is the electrochemistry of methane hydrates due to their abundance in deep ocean sediments and as icy brines on Mars.[38] Figure 8A shows the concentration of CH_4 in H_2O and 11 m NaOH as the temperature decreases. The concentration of CH_4 in water at temperatures between 20 and 0 °C is in agreement with previously reported values.[12,39] It was found that the concentration of CH_4 decreases upon increasing the salinity of the solution.[39] However, by increasing the concentration of NaOH, lower temperatures can be reached, so there is a net increase in CH_4 solubility at the lowest temperature of −38 °C. Upon bubbling CH_4 through an 11 m NaOH solution at −38 °C, the solution turned into a viscous emulsion−slurry solution[40] (Figure 8B). The voltammetric profile of Pt(111) in this solution is shown in Figure 8C. At this temperature, an oxidation wave is observed in the positive scan between 0.4 and 0.6 V vs RHE, confirming the oxidation

https://dx.doi.org/10.1021/acscatal.0c01676
ACS Catal. 2020, 10, 7464−7474





	1D ^{1}H
$HCOO^-$	8.22 ppm (singlet)
CH_3OH	3.08 ppm (singlet)

Figure 9. (A) Voltammetric profiles of consecutive scans, scan 1 (black curve) to scan 3 (red curve), of a Pd polyoriented electrode in 11 m NaOH at −35 °C in the presence of CH_4. Scan rate, υ = 50 mV/s. (B) Current transients at 0.5 V vs RHE recorded on Pt(111) (blue curve) and Pd(polycrystalline) (red curve) electrodes in 11 m NaOH in the presence of CH_4 at −38 °C. (C) 1D ^{1}H NMR spectrum recorded at 400 MHz for liquid samples collected after 20 min of electrolysis at 0.5 V vs RHE in CH_4-saturated solution of 10 m NaOH on (A) Cu(111), (B) Pd(polycrystalline), and (C) Pt. The table includes NMR chemical shifts and multiplicities for the different products of CH_4 oxidation in 10 m NaOH found in the 1D ^{1}H spectra.

of CH_4. At higher potentials the platinum oxide features are smaller than those in a solution without CH_4. This suggests the presence of adsorbed intermediate species, which are products of the oxidation of methane at lower potentials. The broadening of the double layer and the reduction currents in the negative going scan also suggest the presence of adsorbed intermediate species. At 20 °C under the same conditions of electrolyte concentration, the platinum electrode did not show any signal associated with the oxidation of CH_4. This is also true for temperatures ranging between 20 and −30 °C. The oxidation of methane was only observed between −30 and −38 °C upon the formation of the gel or slurry.

The same observation is true for the oxidation of CH_4 on palladium electrodes, where the oxidation of methane only took place upon the formation of the gel at −38 °C. As can be seen in Figure 8D, the onset of oxidation of CH_4 appears at 0.25 V, having a maximum at around 0.48 V vs RHE. Contrary to the observation on the platinum electrode, the reduction of palladium oxide is unaffected by the presence of CH_4 in solution. This indicates an absence of adsorbed poison species on the electrode and so a different reaction mechanism to platinum. Previous work in the gas phase and at higher temperatures has shown that oxygen-coated palladium surfaces favor the adsorption and dissociation of CH_4.[41] Consecutive scans (Figure 9A) show a decrease in the oxidation current of the methane on the Pd electrode, probably associated with the diffusion limitation of the gas toward the electrode through the viscous slurry. The oxidation of methane on Au(111) was also evaluated; however, no oxidation was observed at any temperature (Figure S12).

2.3.1. Product Characterization of the Electrochemical Reduction of CO_2 in Brines. Long-term electrolysis was performed in order to determine the oxidation products of the CH_4 on Pt and Pd electrodes. During electrolysis, the gas products were followed for a duration of 10 min using the modified OLEMS setup, and liquid samples were collected after 5 and 10 min. The current transients (Figure 9B) showed a fast decrease in the current, reaching a plateau after 2 min. This is probably associated with the limited diffusion of the CH_4 to the surface, as observed in the cyclic voltammetry, although the formation of poisonous species, which block active sites at the surface of the electrode, cannot be disregarded. No gas products were detected during the electrolysis; however, if CO_2 was formed, due to the highly alkaline media, the formation of carbonate is expected. The qualitative analysis of the liquid products was performed by NMR shown in Figure 9C. Methanol and formic acid were the main liquid products observed.

3. CONCLUSIONS

The use of brines as electrolytes is an efficient route to perform electrochemistry experiments at low temperatures. The large decrease in temperature greatly increases the solubility of nonpolar gases such as CO_2 and CH_4, opening the door to new routes of electrocatalysis.

It was found that in brines of NaOH, KOH, and $Mg(ClO_4)_2$ at low temperatures, the HER is hindered due to the formation of rigid ice-like structures at the interface between the electrode and electrolyte. In $Mg(ClO_4)_2$ brines at low temperatures, the HER from the water pathway competes with CO_2 reduction on a copper electrode at high overpotentials. At low overpotentials, the water reduction to H_2, where the proton reduction reaction is a diffusion-limited

https://dx.doi.org/10.1021/acscatal.0c01676
ACS Catal. 2020, 10, 7464−7474

process, hardly influences the reduction of CO_2 under mass transport conditions. Water reduction appears to be a slower process as the temperature decreases in comparison with the HER from protons. The combination of the high CO_2 concentration in solution and the decrease in the competitive HER results in a change in the product selectivity.

The electrochemical oxidation of CH_4 in NaOH brines was observed on Pt and Pd electrodes at temperatures below −35 °C and upon the formation of a gel/slurry type solution. Small amounts of CO_2 were observed, but the precise quantification of the products is not possible with the available techniques.

These systems open wide the door to many electrochemical applications in aqueous media where the reactions of interest are limited by the low solubility of the reactant species at high temperature or are limited by the HER.

We believe that a fundamental understanding, including modeling, of the formation of ice-like structures in these brines at the catalyst interface is very important and needs to be further explored.[42] In addition, further optimization of the parameters of gas pressure, temperature, and composition of the electrolyte will allow the implementation of these systems in electrocatalysis.

In addition, our results provide an alternative explanation for the discovery of organic molecules on Mars.[43] The presence of small organic molecules such as CH_4 could be the result of the photochemical hydrogenation of CO_2, from the CO_2-saturated aqueous brines,[6e] catalyzed by metal oxide semiconductors present in the Mars soil.[44] It is therefore relevant to extend these studies to photoelectrochemical systems and to those metals and metal oxides present on Mars, in order to complement this research.

4. EXPERIMENTAL METHODS

The working electrodes used in this work were Cu(111), Au(111), Pt(111), and Pt(100) bead-type single crystal electrodes from (icryst) and a Pd disk (Alfa Aesar, 99.995%). Prior to each experiment, the Cu electrodes were prepared as described in ref 45. The Au and Pt electrodes were prepared according to ref 46. The palladium working electrode was polished to a mirror finish using 1 μm diamond paste and then sonicated in Milli-Q water. The uncompensated solution resistance was measured as a function of the temperature using the positive feedback mode of the potentiostat, and all voltammetries have been corrected by the Ohmic drop.

In the experiments, a high-surface-area gold wire or a high-surface-area Pt wire was used as a counter electrode accordingly, and Hg/HgO was used as a reference electrode. All potentials are referenced to reversible hydrogen electrode, RHE. Electrochemical measurements were performed with an Autolab PGSTAT12.

Electrolyte solutions were prepared with high purity reagents (Sigma-Aldrich, KOH ≥ 85%, NaOH ≥ 99%, Fischer Scientific, $Mg(ClO_4)_2{\cdot}6H_2O$ Sigma-Aldrich 99%, K_2CO_3 ≥ 99%) and ultrapure water (Elga PureUltra, 18.2 MΩ cm^{-1}, 1 ppb total organic carbon). Electrolytes were purged with argon (Ar, N66), or saturated with methane (BOC, Research grade) or CO_2 (BOC, Research grade) for at least 20 min prior to the corresponding experiment. Details on calibration and experimental setup used for the determination of the solubility of the gases are included in the Supporting Information. The temperature control experiments were performed by immersing the electrochemical cell in a cooling medium of 1:1 glycerol:water and cooled to temperature using an HUBER TC45E-F immersion cooler. To accurately control the temperature of the electrolyte without contaminating the electrolyte inside the cell, the temperature was measured in a "shadow beaker" with a similar volume and placed next to the electrochemical cell inside the ice bath. The temperature was measured using a digital thermometer. In a control experiment, the temperatures of the solution inside the cell and of the ghost beaker were measured simultaneously to ensure that the cell and the shadow beaker were in thermal equilibrium.

Further details on the gas analysis (Figure S13) and product characterization and quantification can be found in the Supporting Information.

■ ASSOCIATED CONTENT

Supporting Information

The Supporting Information is available free of charge at https://pubs.acs.org/doi/10.1021/acscatal.0c01676.

Complementary experimental methods; product characterization by mass spectroscopy and NMR; determination of gas solubility; electrochemical measurements on Pt(111) in $Mg(ClO_4)_2$, on polycrystalline Pd in 10 m KOH and on Au(111) in 11m NaOH; GC showing purity of CH_4 (PDF)

■ AUTHOR INFORMATION

Corresponding Author

Paramaconi Rodriguez − *School of Chemistry, University of Birmingham, Edgbaston, Birmingham B15 2TT, United Kingdom*; orcid.org/0000-0002-1517-0964; Email: p.b.rodriguez@bham.ac.uk

Authors

Elizabeth Sargeant − *School of Chemistry, University of Birmingham, Edgbaston, Birmingham B15 2TT, United Kingdom*

Adam Kolodziej − *School of Chemistry, University of Birmingham, Edgbaston, Birmingham B15 2TT, United Kingdom*

Cécile S. Le Duff − *School of Chemistry, University of Birmingham, Edgbaston, Birmingham B15 2TT, United Kingdom*

Complete contact information is available at: https://pubs.acs.org/10.1021/acscatal.0c01676

Author Contributions

P.R. conceived the experiments. The electrochemical experiments and product characterization by mass spectrometry experiments were performed by E.S., A.K., and P.R. NMR characterization and analyses was performed by E.S. and C.L.D. All authors contributed to the analysis of the results, discussion, writing, and revision of the manuscript. All authors have given approval to the final version of the manuscript.

Notes

The authors declare no competing financial interest.

■ ACKNOWLEDGMENTS

E.S. acknowledges the University of Birmingham and the EPSRC Centre for Doctoral Training in Carbon Capture and Storage and Cleaner Fossil Energy for financial support through Ph.D. scholarships at the School of Chemistry. A.K. acknowledges the University of Birmingham for financial support through Ph.D. scholarships at the School of

https://dx.doi.org/10.1021/acscatal.0c01676
ACS Catal. 2020, 10, 7464−7474

Chemistry. P.R. acknowledges the University of Birmingham for financial support. The authors would also like to acknowledge the reviewers of the manuscript who, during the revision process, suggested including a discussion regarding mass transport, which resulted in the preparation of the HMRDE experiments and analysis.

REFERENCES

(1) Davy, H. I. The Bakerian Lecture. On Some of the Combinations of Oxymuriatic Gas and Oxygene, and on the Chemical Relations of These Principles, to Inflammable Bodies. *Philosophical Transactions of the Royal Society of London* **1811**, *101*, 1−35.

(2) Sloan, E. D., Jr Fundamental Principles and Applications of Natural Gas Hydrates. *Nature* **2003**, *426*, 353.

(3) Sloan, E. D. Gas Hydrates: Review of Physical/Chemical Properties. *Energy Fuels* **1998**, *12* (2), 191−196.

(4) (a) Koh, C. A.; Sloan, E. D. *Clathrate hydrtaes of Natural Gases*, 3rd ed.; CRC Press: Boca Raton, USA, 2008; pp 22. (b) Koh, C. A.; Sloan, E. D.; Sum, A. K.; Wu, D. T. Fundamentals and Applications of Gas Hydrates. *Annu. Rev. Chem. Biomol. Eng.* **2011**, *2* (1), 237−257.

(5) Hecht, M. H.; Kounaves, S. P.; Quinn, R. C.; West, S. J.; Young, S. M. M.; Ming, D. W.; Catling, D. C.; Clark, B. C.; Boynton, W. V.; Hoffman, J.; DeFlores, L. P.; Gospodinova, K.; Kapit, J.; Smith, P. H. Detection of Perchlorate and the Soluble Chemistry of Martian Soil at the Phoenix Lander Site. *Science* **2009**, *325* (5936), 64−67.

(6) (a) Safi, E.; Thompson, S. P.; Evans, A.; Day, S. J.; Murray, C. A.; Parker, J. E.; Baker, A. R.; Oliveira, J. M.; van Loon, J. T. Properties of CO2 Clathrate Hydrates Formed in the Presence of MgSO4 Solutions With Implications for Icy Moons. *Astron. Astrophys.* **2017**, *600*, A88. (b) Martínez, G. M.; Renno, N. O. Water and Brines on Mars: Current Evidence and Implications for MSL. *Space Sci. Rev.* **2013**, *175* (1), 29−51. (c) Martínez, G. M.; Newman, C. N.; De Vicente-Retortillo, A.; Fischer, E.; Renno, N. O.; Richardson, M. I.; Fairén, A. G.; Genzer, M.; Guzewich, S. D.; Haberle, R. M.; Harri, A.-M.; Kemppinen, O.; Lemmon, M. T.; Smith, M. D.; de la Torre-Juárez, M.; Vasavada, A. R. The Modern Near-Surface Martian Climate: A Review of In-situ Meteorological Data From Viking to Curiosity. *Space Sci. Rev.* **2017**, *212* (1), 295−338. (d) Marion, G. M.; Catling, D. C.; Zahnle, K. J.; Claire, M. W. Modeling Aqueous Perchlorate Chemistries With Applications to Mars. *Icarus* **2010**, *207* (2), 675−685. (e) Quinn, R. C.; Chittenden, J. D.; Kounaves, S. P.; Hecht, M. H. The oxidation-Reduction Potential of Aqueous Soil Solutions at the Mars Phoenix Landing Site. *Geophys. Res. Lett.* **2011**, *38* (14), 1.

(7) (a) Onstott, T. C.; McGown, D.; Kessler, J.; Lollar, B. S.; Lehmann, K. K.; Clifford, S. M. Martian CH4: Sources, Flux, and Detection. *Astrobiology* **2006**, *6* (2), 377−395. (b) Webster, C. R.; Mahaffy, P. R.; Atreya, S. K.; Moores, J. E.; Flesch, G. J.; Malespin, C.; McKay, C. P.; Martinez, G.; Smith, C. L.; Martin-Torres, J.; Gomez-Elvira, J.; Zorzano, M.-P.; Wong, M. H.; Trainer, M. G.; Steele, A.; Archer, D.; Sutter, B.; Coll, P. J.; Freissinet, C.; Meslin, P.-Y.; Gough, R. V.; House, C. H.; Pavlov, A.; Eigenbrode, J. L.; Glavin, D. P.; Pearson, J. C.; Keymeulen, D.; Christensen, L. E.; Schwenzer, S. P.; Navarro-Gonzalez, R.; Pla-García, J.; Rafkin, S. C. R.; Vicente-Retortillo, Á.; Kahanpää, H.; Viudez-Moreiras, D.; Smith, M. D.; Harri, A.-M.; Genzer, M.; Hassler, D. M.; Lemmon, M.; Crisp, J.; Sander, S. P.; Zurek, R. W.; Vasavada, A. R. Background Levels of Methane in Mars' Atmosphere Show Strong Seasonal Variations. *Science* **2018**, *360* (6393), 1093−1096.

(8) Muscatello, A.; Santiago-Maldonado, E. *Mars In Situ Resource Utilization Technology Evaluation; US* **2012**, 1−13.

(9) Duan, C.; Kee, R.; Zhu, H.; Sullivan, N.; Zhu, L.; Bian, L.; Jennings, D.; O'Hayre, R. Highly Efficient Reversible Protonic Ceramic Electrochemical Cells for Power Generation and Fuel Production. *Nat. Energy* **2019**, *4* (3), 230−240.

(10) Mimachi, H.; Takahashi, M.; Takeya, S.; Gotoh, Y.; Yoneyama, A.; Hyodo, K.; Takeda, T.; Murayama, T. Effect of Long-Term Storage and Thermal History on the Gas Content of Natural Gas Hydrate Pellets under Ambient Pressure. *Energy Fuels* **2015**, *29* (8), 4827−4834.

(11) (a) Conway, B. E.; Salomon, M. Studies on the Hydrogen Evolution Reaction Down to —150°C and the Role of Proton Tunneling. *J. Chem. Phys.* **1964**, *41* (10), 3169−3177. (b) Florit, M. I.; Arvia, A. J. The Voltammetric Behaviour of H and O Adatoms in the 189−292 K Range on Platinum in HClO4 • 5.5 H2O And H2SO4 • 12H2O. *J. Electroanal. Chem.* **1992**, *339* (1), 281−297. (c) Safford, L. K.; Weaver, M. J. The Evaluation of Rate Constants for Rapid Electrode Reactions Using Microelectrode Voltammetry: Virtues of Measurements at Lower Temperatures. *J. Electroanal. Chem.* **1992**, *331* (1), 857−876. (d) Frese, U.; Stimming, U. Hydrogen Evolution on Copper, Silver and Gold Electrodes in Aqueous Perchloric Acid 130 to 300 K. *J. Electroanal. Chem. Interfacial Electrochem.* **1986**, *198* (2), 409−416.

(12) Wiesenburg, D. A.; Guinasso, N. L. Equilibrium Solubilities of Methane, Carbon Monoxide, and Hydrogen in Water and Sea Water. *J. Chem. Eng. Data* **1979**, *24* (4), 356−360.

(13) Sanders, G. B. *In-Situ Resource Utilization (ISRU) Planning and Update*; National Aeronautics and Space Administration: Presentation to the NAC Technology, Innovation, and Engineering Committee Meeting, 2018. https://www.nasa.gov/sites/default/files/atoms/files/nac_tie_december_2018_gsanders_isru.pdf.

(14) Florit, M. I.; Martins, M. E.; Arvia, A. J. Comparative Voltammetric Behaviour of H- and O-Atoms on a Pt Electrode in Sulphuric Acid Solutions Within the 293 to 233 K Range. *J. Electroanal. Chem. Interfacial Electrochem.* **1989**, *269* (1), 209−216.

(15) deBethune, A. J.; Licht, T. S.; Swendeman, N. The Temperature Coefficients of Electrode Potentials. *J. Electrochem. Soc.* **1959**, *106* (7), 616.

(16) Markovic, N. M.; Schmidt, T. J.; Grgur, B. N.; Gasteiger, H. A.; Ross, P. N., Jr; Behm, R. J. The Effect of Temperature on the Surface Process at the Pt(111)-Liquid Inteface: Hydrogen Adsorption, Oxide Formation and CO Oxidation. *J. Phys. Chem. B* **1999**, *103*, 8568−8577.

(17) Frese, U.; Iwasita, T.; Schmickler, W.; Stimming, U. Hydrogen Evolution in Liquid and Frozen Aqueous Electrolyte. *J. Phys. Chem.* **1985**, *89* (7), 1059−1062.

(18) Tielrooij, K. J.; Garcia-Araez, N.; Bonn, M.; Bakker, H. J. Cooperativity in Ion Hydration. *Science* **2010**, *328* (5981), 1006−1009.

(19) (a) Conway, B. E.; Bai, L. State of Adsorption and Coverage by Overpotential-Deposited H in the H2 Evolution Reaction at Au and Pt. *Electrochim. Acta* **1986**, *31* (8), 1013−1024. (b) Schuldiner, S. Hydrogen Overvoltage on Bright Platinum: II. pH and Salt Effects in Acid, Neutral, and Alkaline Solutions. *J. Electrochem. Soc.* **1954**, *101* (8), 426−432. (c) Sheng, W.; Gasteiger, H. A.; Shao-Horn, Y. Hydrogen Oxidation and Evolution Reaction Kinetics on Platinum: Acid vs Alkaline Electrolytes. *J. Electrochem. Soc.* **2010**, *157* (11), B1529−B1536. (d) Schmidt, T. J.; Ross, P. N., Jr.; Markovic, N. M. Temperature Dependent Surface Electrochemistry on Pt Single Crystals in Alkaline Electrolytes: Part 2. The Hydrogen Evolution/Oxidation Reaction. *J. Electroanal. Chem.* **2002**, *524*−*525*, 252−260.

(20) Ledezma-Yanez, I.; Wallace, W. D. Z.; Sebastián-Pascual, P.; Climent, V.; Feliu, J. M.; Koper, M. T. M. Interfacial Water Reorganization as a pH-Dependent Descriptor of the Hydrogen Evolution Rate on Platinum Electrodes. *Nat. Energy* **2017**, *2*, 17031.

(21) Bai, D.; Chen, G.; Zhang, X.; Sum, A. K.; Wang, W. How Properties of Solid Surfaces Modulate the Nucleation of Gas Hydrate. *Sci. Rep.* **2015**, *5*, 12747.

(22) Opallo, M.; Prokopowicz, A. Electrochemical Hydrogen Evolution in Hydroxide Hydrate Down to 110 K. *Electrochem. Commun.* **2000**, *2* (1), 23−26.

(23) Chen, X.; McCrum, I. T.; Schwarz, K. A.; Janik, M. J.; Koper, M. T. M;, Co-adsorption of Cations as the Cause of the Apparent pH Dependence of Hydrogen Adsorption on a Stepped Platinum Single-Crystal Electrode. *Angew. Chem., Int. Ed.* **2017**, *56* (47), 15025−15029.

https://dx.doi.org/10.1021/acscatal.0c01676
ACS Catal. 2020, 10, 7464−7474

(24) Zhang, W.-S.; Zhang, X.-W.; Zhao, X.-G. Voltammograms of Thin Layer PdlH(D) Electrodes in the Coexistence of α and β Phases. *J. Electroanal. Chem.* **1998**, *458* (1), 107−112.
(25) (a) Zhou, F.; Li, H.; Fournier, M.; MacFarlane, D. R. Electrocatalytic CO2 Reduction to Formate at Low Overpotentials on Electrodeposited Pd Films: Stabilized Performance by Suppression of CO Formation. *ChemSusChem* **2017**, *10* (7), 1509−1516. (b) Humphrey, J. J. L.; Plana, D.; Celorrio, V.; Sadasivan, S.; Tooze, R. P.; Rodríguez, P.; Fermín, D. J. Electrochemical Reduction of Carbon Dioxide at Gold-Palladium Core−Shell Nanoparticles: Product Distribution versus Shell Thickness. *ChemCatChem* **2016**, *8* (5), 952−960.
(26) Duan, Z.; Sun, R. An Improved Model Calculating CO2 Solubility in Pure Water and Aqueous NaCl Solutions From 273 to 533 K and From 0 to 2000 bar. *Chem. Geol.* **2003**, *193* (3), 257−271.
(27) Kuhl, K. P.; Cave, E. R.; Abram, D. N.; Jaramillo, T. F. New Insights Into the Electrochemical Reduction of Carbon Dioxide on Metallic Copper Surfaces. *Energy Environ. Sci.* **2012**, *5* (5), 7050−7059.
(28) Min, X.; Kanan, M. W. Pd-Catalyzed Electrohydrogenation of Carbon Dioxide to Formate: High Mass Activity at Low Overpotential and Identification of the Deactivation Pathway. *J. Am. Chem. Soc.* **2015**, *137* (14), 4701−4708.
(29) (a) Rodriguez, P.; Feliu, J. M.; Koper, M. T. M. Unusual Adsorption State of Carbon monoxide on Single-Crystalline Gold Electrodes in Alkaline Media. *Electrochem. Commun.* **2009**, *11* (6), 1105−1108. (b) Rodriguez, P.; Garcia-Araez, N.; Koper, M. T. M. Self-Promotion Mechanism for CO Electrooxidation on Gold. *Phys. Chem. Chem. Phys.* **2010**, *12* (32), 9373−9380. (c) Rodriguez, P.; Garcia-Araez, N.; Koverga, A.; Frank, S.; Koper, M. T. M. CO Electroxidation on Gold in Alkaline Media: A Combined Electrochemical, Spectroscopic, and DFT Study. *Langmuir* **2010**, *26* (14), 12425−12432.
(30) Ooka, H.; Figueiredo, M. C.; Koper, M. T. M. Competition Between Hydrogen Evolution and Carbon Dioxide Reduction on Copper Electrodes in Mildly Acidic Media. *Langmuir* **2017**, *33* (37), 9307−9313.
(31) Ke, K.; Hiroshima, K.; Kamitaka, Y.; Hatanaka, T.; Morimoto, Y. An Accurate Evaluation for the Activity of Nano-Sized Electrocatalysts by a Thin-Film Rotating Disk Electrode: Oxygen Reduction on Pt/C. *Electrochim. Acta* **2012**, *72*, 120−128.
(32) Lee, C. W.; Cho, N. H.; Im, S. W.; Jee, M. S.; Hwang, Y. J.; Min, B. K.; Nam, K. T. New Challenges of Electrokinetic Studies in Investigating the Reaction Mechanism of Electrochemical CO_2 Reduction. *J. Mater. Chem. A* **2018**, *6* (29), 14043−14057.
(33) Ahn, S. T.; Abu-Baker, I.; Palmore, G. T. R. Electroreduction of CO2 on Polycrystalline Copper: Effect of Temperature on Product Selectivity. *Catal. Today* **2017**, *288*, 24−29.
(34) Wang, L.; Nitopi, S. A.; Bertheussen, E.; Orazov, M.; Morales-Guio, C. G.; Liu, X.; Higgins, D. C.; Chan, K.; Nørskov, J. K.; Hahn, C.; Jaramillo, T. F. Electrochemical Carbon Monoxide Reduction on Polycrystalline Copper: Effects of Potential, Pressure, and pH on Selectivity toward Multicarbon and Oxygenated Products. *ACS Catal.* **2018**, *8* (8), 7445−7454.
(35) (a) Lum, Y.; Yue, B.; Lobaccaro, P.; Bell, A. T.; Ager, J. W. Optimizing C−C Coupling on Oxide-Derived Copper Catalysts for Electrochemical CO2 Reduction. *J. Phys. Chem. C* **2017**, *121* (26), 14191−14203. (b) Nitopi, S.; Bertheussen, E.; Scott, S. B.; Liu, X.; Engstfeld, A. K.; Horch, S.; Seger, B.; Stephens, I. E. L.; Chan, K.; Hahn, C.; Nørskov, J. K.; Jaramillo, T. F.; Chorkendorff, I. Progress and Perspectives of Electrochemical CO2 Reduction on Copper in Aqueous Electrolyte. *Chem. Rev.* **2019**, *119* (12), 7610−7672.
(36) (a) Liang, S.; Liang, D.; Wu, N.; Yi, L.; Hu, G. Molecular Mechanisms of Gas Diffusion in CO2 Hydrates. *J. Phys. Chem. C* **2016**, *120* (30), 16298−16304. (b) Liang, S.; Liang, D.; Wu, N.; Yi, L.; Hu, G. Transient Translational and Rotational Water Defects in Gas Hydrates. *J. Phys. Chem. C* **2017**, *121* (33), 17595−17602.
(37) Luo, W.; Nie, X.; Janik, M. J.; Asthagiri, A. Facet Dependence of CO2 Reduction Paths on Cu Electrodes. *ACS Catal.* **2016**, *6* (1), 219−229.
(38) (a) Sohl, F.; Choukroun, M.; Kargel, J.; Kimura, J.; Pappalardo, R.; Vance, S.; Zolotov, M. Subsurface Water Oceans on Icy Satellites: Chemical Composition and Exchange Processes. *Space Sci. Rev.* **2010**, *153* (1), 485−510. (b) Marion, G. M.; Kargel, J. S.; Catling, D. C.; Lunine, J. I. Modeling Nitrogen-Gas, -Liquid, -Solid Chemistries at Low Temperatures (173−298K) With Applications to Titan. *Icarus* **2014**, *236*, 1−8.
(39) Duan, Z.; Møller, N.; Greenberg, J.; Weare, J. H. The Prediction of Methane Solubility in Natural Waters to High Ionic Strength From 0 to 250°C and From 0 to 1600 bar. *Geochim. Cosmochim. Acta* **1992**, *56* (4), 1451−1460.
(40) Gudmundsson, J. S.; Andersson, V.; Levik, O. I.; Mork, M. Hydrate Technology for Capturing Stranded Gas. *Ann. N. Y. Acad. Sci.* **2000**, *912* (1), 403−410.
(41) Hellman, A.; Resta, A.; Martin, N. M.; Gustafson, J.; Trinchero, A.; Carlsson, P. A.; Balmes, O.; Felici, R.; van Rijn, R.; Frenken, J. W. M.; Andersen, J. N.; Lundgren, E.; Grönbeck, H. The Active Phase of Palladium During Methane Oxidation. *J. Phys. Chem. Lett.* **2012**, *3* (6), 678−682.
(42) Factorovich, M. H.; Molinero, V.; Scherlis, D. A. Hydrogen-Bond Heterogeneity Boosts Hydrophobicity of Solid Interfaces. *J. Am. Chem. Soc.* **2015**, *137* (33), 10618−10623.
(43) ten Kate, I. L. Organic molecules on Mars. *Science* **2018**, *360* (6393), 1068−1069.
(44) (a) Rieder, R.; Economou, T.; Wänke, H.; Turkevich, A.; Crisp, J.; Brückner, J.; Dreibus, G.; McSween, H. Y. The Chemical Composition of Martian Soil and Rocks Returned by the Mobile Alpha Proton X-ray Spectrometer: Preliminary Results from the X-ray Mode. *Science* **1997**, *278* (5344), 1771−1774. (b) Bandfield, J. L.; Hamilton, V. E.; Christensen, P. R. A Global View of Martian Surface Compositions from MGS-TES. *Science* **2000**, *287* (5458), 1626−1630.
(45) Le Duff, C. S.; Lawrence, M. J.; Rodriguez, P. Role of the Adsorbed Oxygen Species in the Selective Electrochemical Reduction of CO_2 to Alcohols and Carbonyls on Copper Electrodes. *Angew. Chem. Int. Ed.* **2017**, *129* (42), 13099−13104.
(46) (a) Clavilier, J.; Armand, D.; Sun, S. G.; Petit, M. Electrochemical Adsorption Behaviour of Platinum Stepped Surfaces in Sulphuric Acid Solutions. *J. Electroanal. Chem. Interfacial Electrochem.* **1986**, *205* (1−2), 267−277. (b) Edens, G. J.; Hamelin, A.; Weaver, M. J. Mechanism of Carbon Monoxide Electrooxidation on Monocrystalline Gold Surfaces: Identification of a Hydroxycarbonyl Intermediate. *J. Phys. Chem.* **1996**, *100* (6), 2322−2329.

https://dx.doi.org/10.1021/acscatal.0c01676
ACS Catal. 2020, 10, 7464−7474

SUPPORTING INFORMATION

2.SI.1 Methods

The Ohmic drop between the working electrode and the reference electrode was determined using the positive feedback method at each temperature and necessary corrections made. Resistance values varied between 4-42 Ωcm^2 for $Mg(ClO_4)_2$ and 3-32 Ωcm^2 for NaOH.

2.SI.1.1 Product characterisation by Online Electrochemical Mass Spectrometry

Online Electrochemical Mass Spectrometry (OLEMS) was used to detect the gaseous products formed during the reaction. At low temperature, ice formation blocked the membrane, so the gases were detected in the gas phase with a slightly modified system, as shown in Figure S1. The reaction products at the electrode were collected with a small syringe tip positioned close to the electrode. The volume of the gas inside the cell depends on the size of the electrode and the meniscus. Due to this uncertainty and the different solubilities of the gases in the liquid phase, it is not possible to do a quantitative analysis of the gas products, only a qualitative analysis.

In order to determine the quantitative distinction of CO, N_2 and CO_2 during the reduction of CO_2, the calibration method described by Binninger *et al*. was implemented.[1]

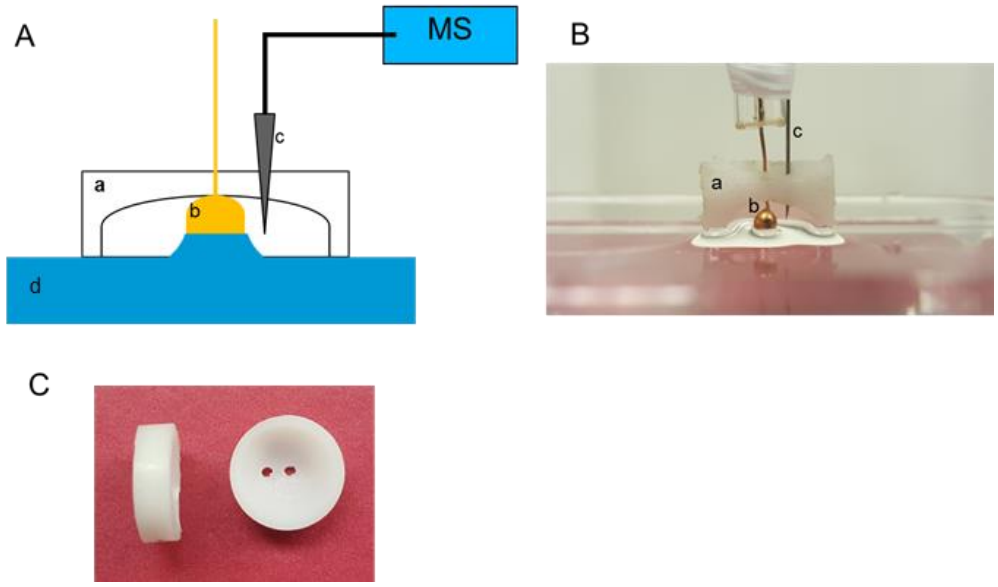


Figure S1. *(A) Cartoon representation of the side cut of the online electrochemical mass spectrometry used to identify the gas products. The system is formed by: (a) Teflon cell (b) single crystal electrode in meniscus configuration (c) syringe tip modified with Teflon membrane (d) solution. (B) Photography of the Teflon cell in the real configuration. The cell has been half cut to show the meniscus configuration and syringe position. (C) Top and lateral view of the Teflon cell for gas collection and analysis. The total volume of the cavity is approx.* $400\ \varepsilon L$.

2.SI.1.2 Determination of gas solubility in brines as a function of temperature

For the calibration of the system and the quantitative analysis, commercial mixtures of 1 % methane in hydrogen (Sigma-Aldrich) and 10 % methane in argon (Air liquid) were used. The mixtures of the gases were coupled with the MS system as previously reported.[2]

The concentration of CO_2 as a function of the temperature was measured using a similar protocol to that shown in Figure S2. However, given the $CO_2/HCO_3/CO_3$ equilibrium, a calibration was needed to determine the concentration of the species in solution. Solutions of different concentrations of $KHCO_3$ and K_2CO_3 were prepared and saturated with CO_2 for 20-30 min. After this time, the needle connected to the MS was inserted through the septum of the round bottomed flask. First, the CO_2 in the solution was detected until a stable baseline was reached. Then, an excess of 1 M H_2SO_4 was injected to decrease the pH and convert the HCO_3/CO_3 species to CO_2. A typical curve of the CO_2 signal (m/z=44) is shown in Figure S3(A) and the calibration curves for different concentrations of $KHCO_3$ and K_2CO_3 are shown in Figure S3(B). In order to obtain a quantitative analysis, the curves of the CO_2 signal were corrected by the change of the total pressure and the change water baseline associated to the injection of the 1 M solution of H_2SO_4.

In order to determine the concentration of CO_2 as a function of temperature, including the carbonate species, the CO_2 in solution was measured by saturating the solution at the given temperature for 20-30 minutes and following the same protocol as described above. To make sure no CO_2 remained in solution, the temperature was gradually increased to 50 $^{\circ}$C with a hot plate. Figure S3(C) show the curves of the concentration of CO_2 as a function of temperature in a solution 4.4 m $Mg(ClO_4)_2$. The CO_2 signals were corrected at the baseline for the increased water pressure associated to the change in temperature.

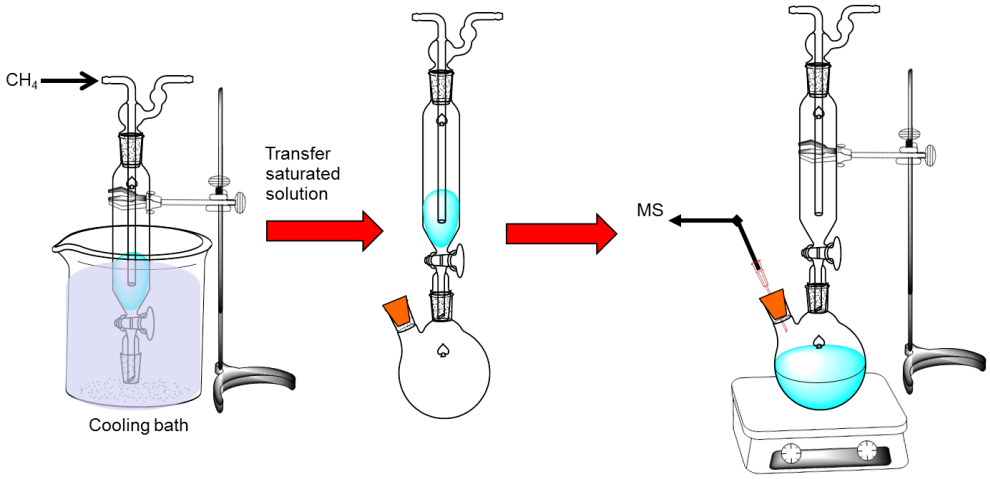


Figure S2. *Experimental setup and methodology used for the determination of the solubility of CH_4 in NaOH brines at different temperatures. The volume of the solution used for analysis was 5 mL. The solution was saturated with CH_4 with a pressure of 2 bar and a bubbling rate of 1 mL/s for 15 min.*

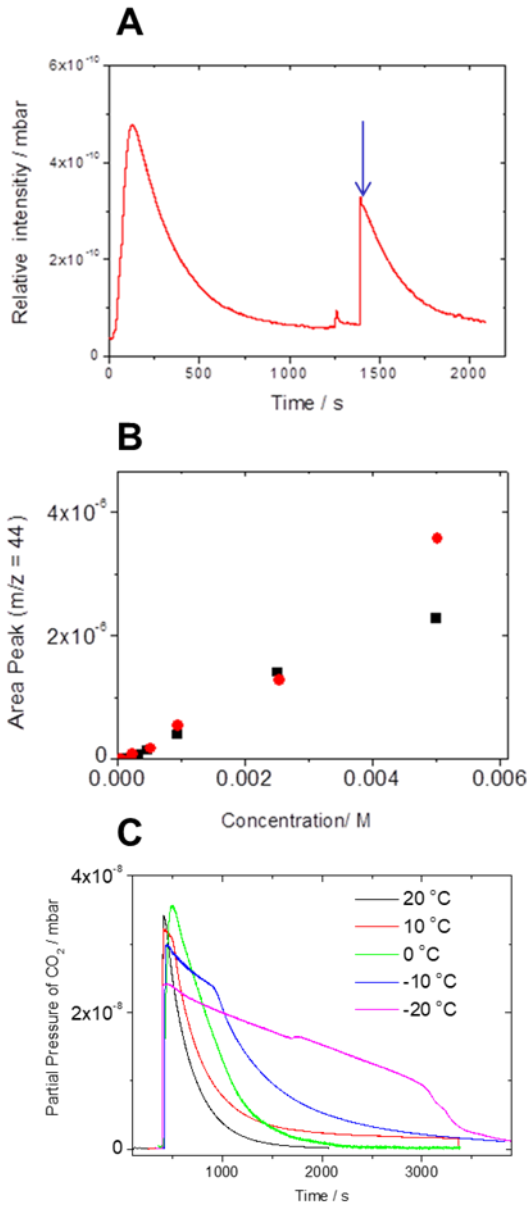


Figure S3. *(A) Example of the determination of the CO_2 solubility in equilibrium with HCO_3^- using head space mass spectrometry as detailed above. The spike at 1250 s correspond to the insertion of the needle in the septum and the arrow indicates the point of injection of 1 M H_2SO_4 for the formation of CO_2. (B) Calibration curve for the signals of CO_2 measured using the head space mass spectrometry as a function of the concentration of $KHCO_3$ and K_2CO_3 (C) Mass spectrometry curves for the concentration of CO_2 on a CO_2 saturated solution $Mg(ClO_4)_2$ as a function of temperature.*

2.SI.1.3 Product characterisation by NMR

A Bruker AVANCE NEO spectrometer console situated in an air-conditioned room equipped with a 9.4 T superconducting magnet operating at a frequency of 400 MHz fitted with a 5 mm nitrogen-cooled BBFO "SMART" probe, at a calibrated temperature of 298 K was used to measure all ^{1}H NMR.

1D ^{1}H NMR spectra were acquired using a pulse sequence with excitation sculpting and gradients to suppress the water (H_2O) peak;[3] a spectral width of 15 ppm with 32k complex data points was measured. 400 scans were acquired for each sample to increase the signal-to-noise ratio so that quantification of the products was possible. A delay (d1) of 40 s between scans was used. Data were zero-filled to 32k using a line broadening of 0.3 Hz to provide a final spectra resolution of 0.19 Hz per point and chemical shifts were indirectly referenced to TMS at 0 ppm.

To enable quantification of all analytes and ensuring the d1 delay was long enough to get full signal recovery, T1 data were measured using the Bruker inverse recovery pulse sequence. A spectral width of 15 ppm with 131k complex data points and 128 scans was measured for each of the 7 delays (0.001, 0.1, 0.33, 1, 3.33, 10 and 33 s). Data were zero filled to 131k using a line broadening of 1.0 Hz to give a final spectral resolution of 0.05 Hz per point and chemical shifts were indirectly referenced to TMS at 0 ppm. The longest T1 of 8 s was measured for formate in 4.4 m $Mg(ClO_4)_2$, hence a d1 of 40 s was used for quantification measurements.

A Bruker AVANCE NEO spectrometer console situated in an air-conditioned room equipped with a 11.74 T superconducting magnet operating at a frequency of 500 MHz, fitted with a 5 mm nitrogen-cooled "Prodigy" BBFO probe, at a calibrated temperature of 298 K, was used to measure ^{13}C data.

For the ^{1}H-decoupled 1D ^{13}C spectra, a sweep width of 250 ppm with 119k complex data points was measured. A minimum of 10,000 scans was used but for the weaker samples up to 18,000 scans were acquired. Due to the high sensitivity of the nitrogen-cooled probe, a broad background signal from its composing materials was present in the spectra; using a back linear prediction using 30 points was good enough to process out this small background signal. The final resolution from those spectra was 0.24 Hz per point using a line broadening of 2 Hz. For the coupled 1D ^{13}C NMR spectrum, 36,000 scans were measured in order to have a sensitivity good enough to determine the number of ^{1}H attached to each carbon detected in the ^{1}H-decoupled 1D ^{13}C spectrum. A small number of points from the fid (30) were also back predicted while processing this 1D ^{13}C spectrum in order to achieve a good baseline.

All data were processed and plotted using TOPSPIN 4.0.6 software and T1 data was analysed using Dynamics Centre 2.5.6

2.SI.1.4 Product Quantification by NMR

In order to quantify the products, the area of the peaks was compared to internal standards. Phenol (Sigma Aldrich, 99+%) and DMSO (Fischer, 99.7%) were chosen as the standards.[4] The area of the formate peak was compared to the phenol triplet at 7.40 ppm. Methanol and ethanol were compared to the area of the DMSO peak at 2.78 ppm. The ethanol triplet at 1.24 ppm was used for quantification since the quartet signal at 3.75 ppm was within the water suppression region and so, less accurate.

Calibration curves were constructed using purchased chemicals (Fluka Analytical, ethanol >99.8%, VWR Chemicals, formic acid 98%, Sigma Aldrich, Methanol, >99.9%) dissolved in 4.4 m $Mg(ClO_4)_2$ and measuring spectra at concentrations 0.0025, 0.05, 0.1, 0.25, 0.5, 0.75 and 1 mM. See Figure S4 and Figure S5. The average signals from 3 different samples were measured, integrated and the standard deviation was calculated.

Each sample contained:

- 75 µL of 0.1 mol dm^{-3} phenol in 4.4 m $Mg(ClO_4)_2$
- 15 µL of 0.1 mol dm^{-3} DMSO in 4.4 m $Mg(ClO_4)_2$
- 150 µL of D_2O (for lock purposes)

For the calibration curve, stock solution of each concentration was added to get a total volume of 1500 µL. For analysis of electrolysis products, the electrolyte was used. Each sample was sonicated to ensure mixing and 600 µL was pipetted into the NMR tube.

Table S1: *NMR shifts and multiplicities for the different products of CO_2 reduction in 4.4 m $Mg(ClO_4)_2$ found in the 1D ^{1}H and ^{13}C NMR spectra*

	1D ^{1}H	**1D ^{13}C**
$HCOO^-$	8.38 ppm (singlet)	171.5 ppm (doublet in 1D-coupled 13C spectrum)
CH_3CH_2OH	3.75 ppm (quartet); 1.24 ppm (triplet)	82.0 ppm; 16.9 ppm
CH_3OH	3.45 ppm (singlet)	49.5 ppm (peak too weak to clearly identify multiplicity in 1H-coupled 13C spectrum, expected to be a quartet)
$CH_2(OH)_2$	Not visible – peak suppressed under water peak (previously reported as 4.7 to 4.88 ppm)	82.2 ppm (triplet in 1H-coupled 13C spectrum)
CH_3COO^-	1.81 ppm to 1.77 ppm (singlet)	
phenol	7.40 ppm (triplet), 7.08 (triplet), 6.99 ppm (doublet)	-
DMSO	2.78 ppm (singlet)	-

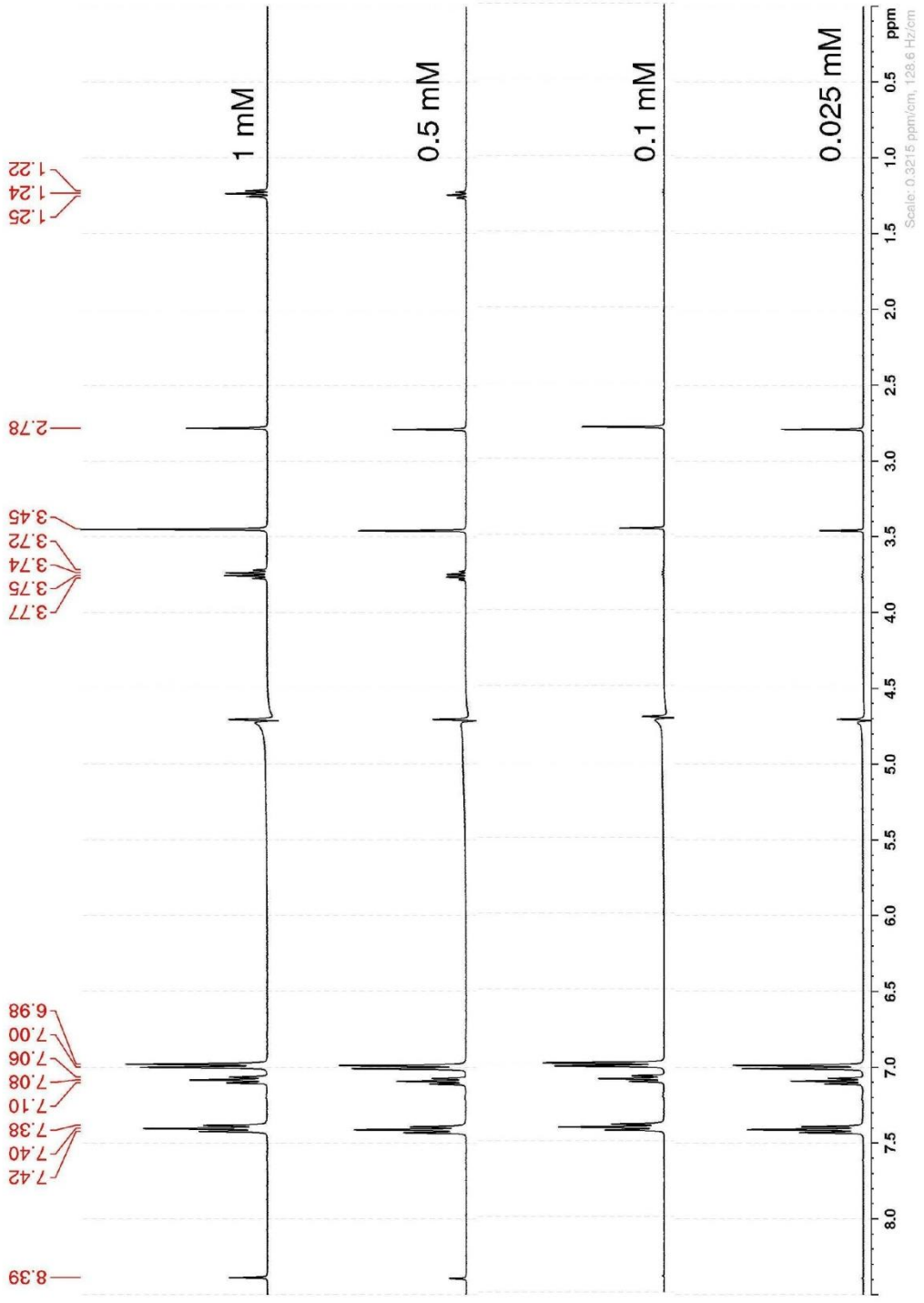


Figure S4. *1D ^{1}H NMR spectra recorded at 400 MHz used for calibration curve using phenol and DMSO as internal references. Signal at 4.7 ppm results from the suppressed H_2O peak.*

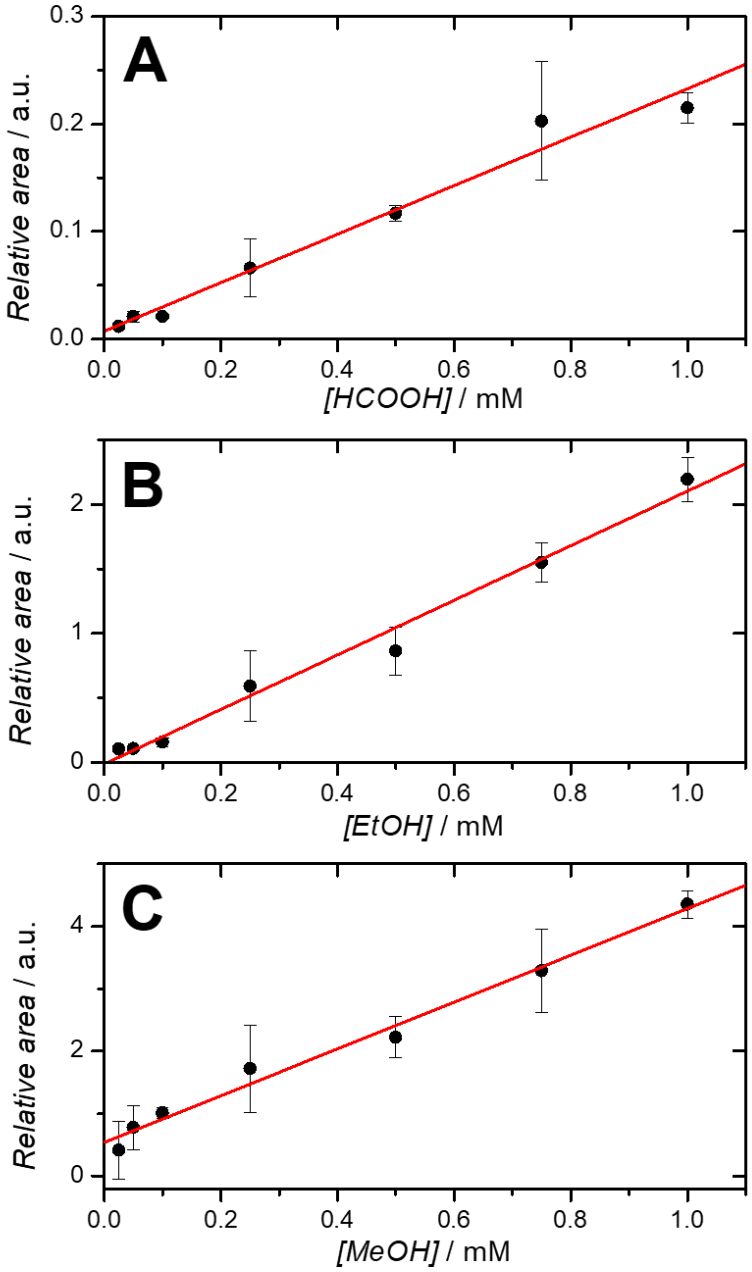


Figure S5. *Calibration curves measured for the integrals of the signals of formic acid (8.39 ppm), ethanol (1.24 ppm) and methanol (3.45 ppm) with respect the signal of phenol and DMSO as a function of concentration of the species*

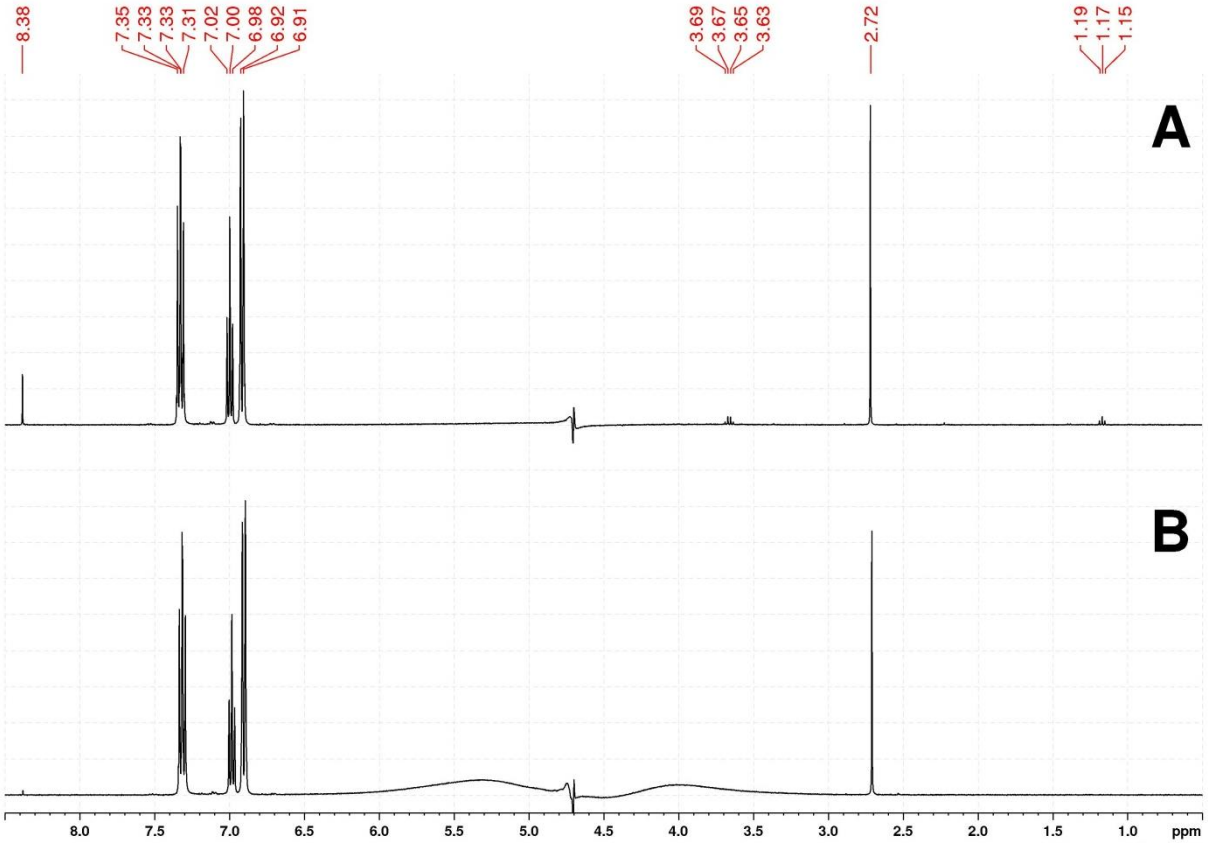


Figure S6. *^{1}H NMR spectrum recorded at 400 MHz for liquid samples collected after 30 min of electrolysis, at -0.6 V in a CO_2-saturated solution of 4.4 m $Mg(ClO_4)_2$ on Pd(polycrystalline) (A) -18 °C and (B) 20 °C*

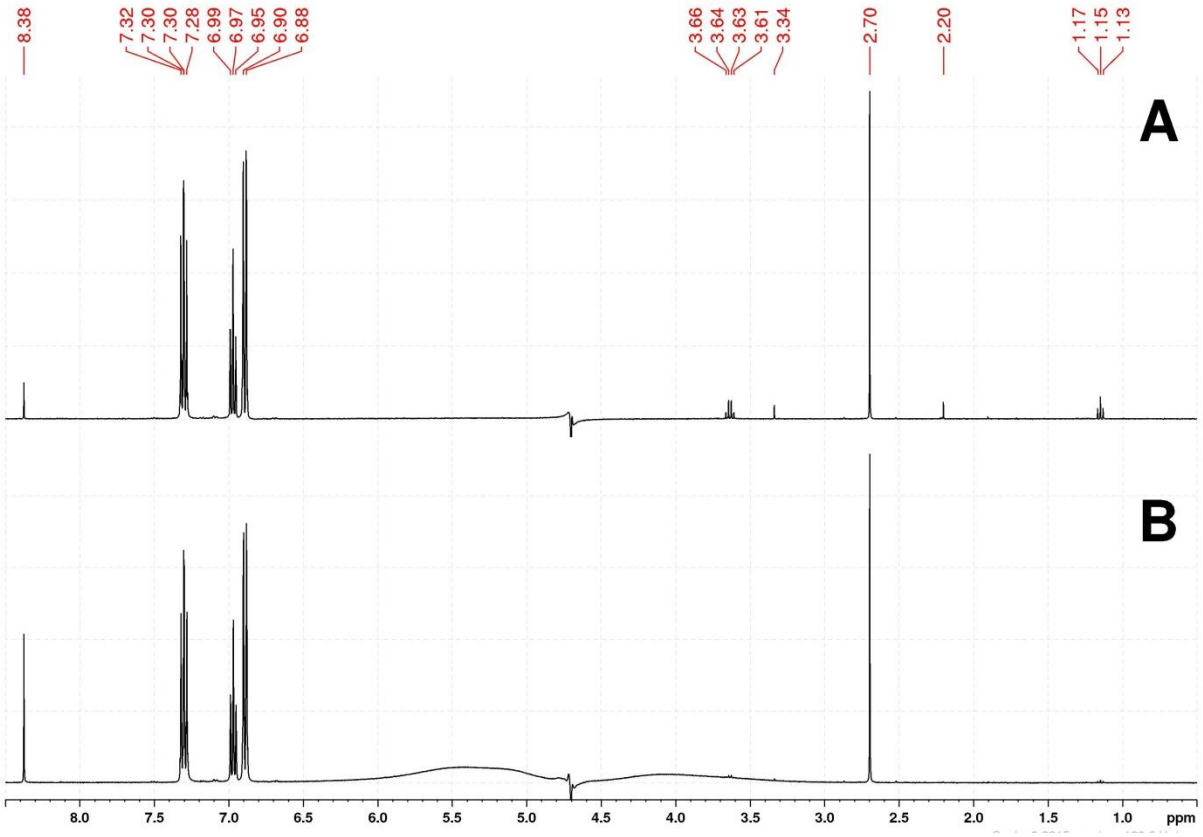


Figure S7. *^{1}H NMR spectrum recorded at 400 MHz for liquid samples collected after 30 min of electrolysis, at -0.6 V in a CO_2-saturated solution of 4.4 m $Mg(ClO_4)_2$ on Cu(111) (A) -18 ¯C (B) 20 ¯C*

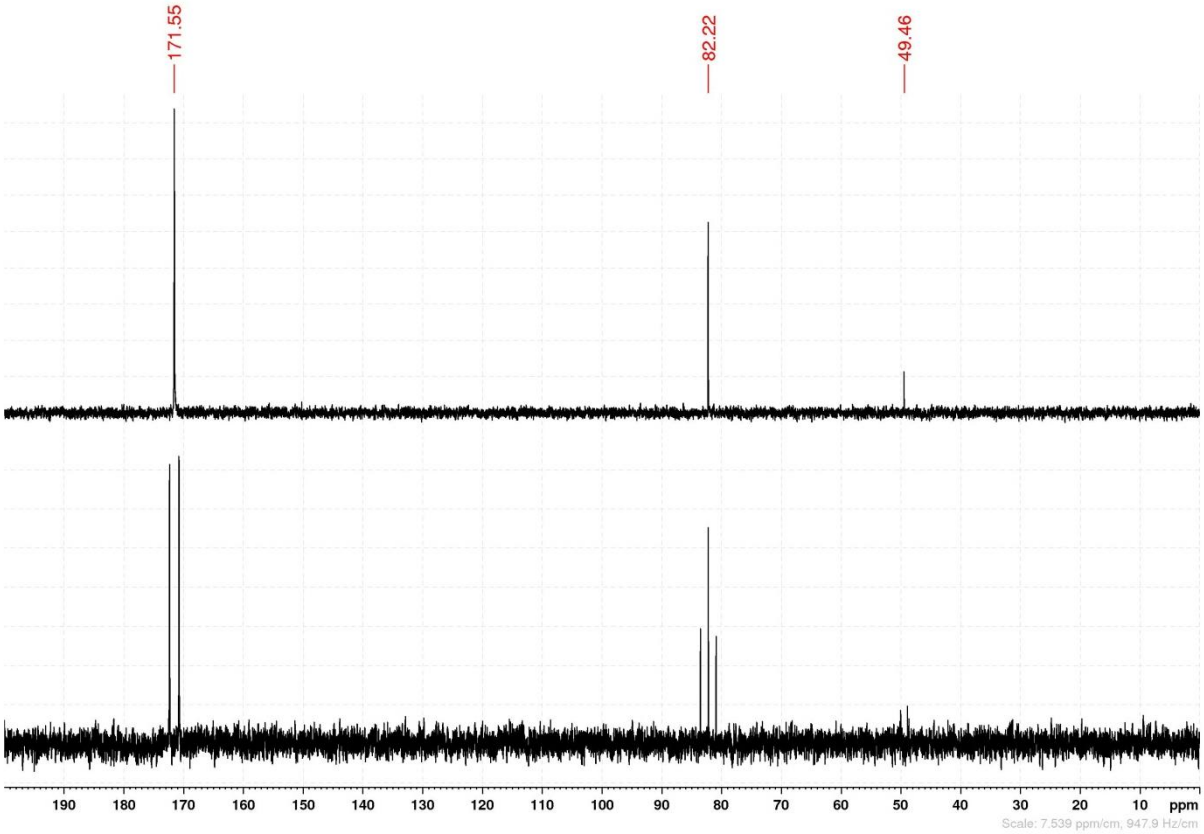


Figure S8. *1D ^{13}C spectra recorded at 125 MHz for liquid sample collected after 10 min of electrolysis on Cu(111) at 20 °C; the top spectrum shows the ^{1}H-decoupled spectrum while the bottom spectrum shows the ^{1}H-coupled ^{13}C spectrum*

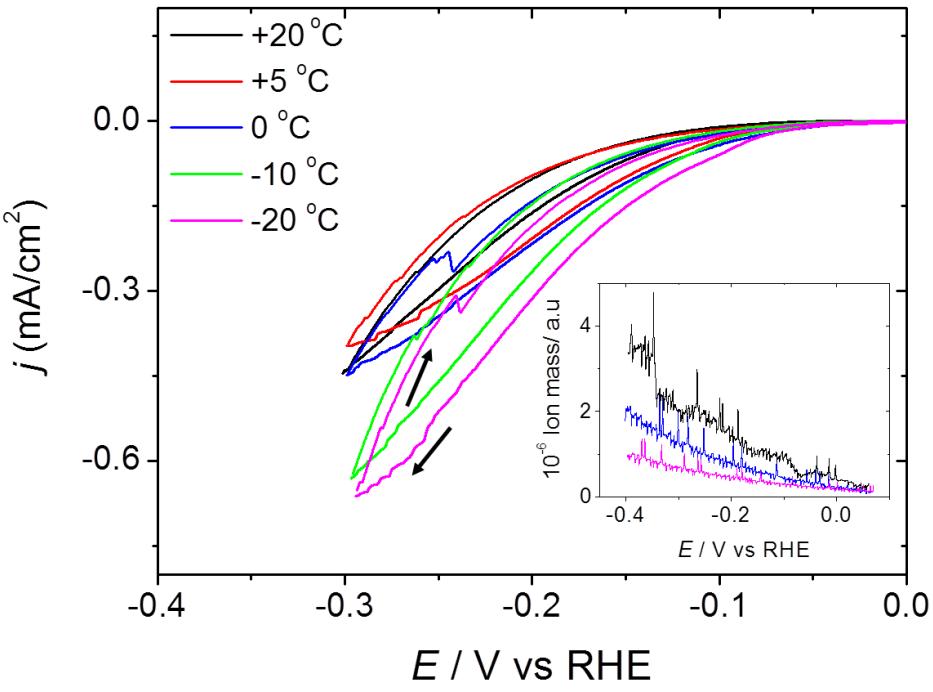


Figure S9. *Voltammetric profiles of Pt(111) in CO_2-saturated 4.4 m solution of $Mg(ClO_4)_2$, different temperatures as indicated in the figure. The arrows indicate the direction of the scan. Inset: Ion mass curves for the m/z=2 during the CO_2 reduction at 20 °C (magenta curve), 0 °C (blue curve) and -20 °C (black curve).*

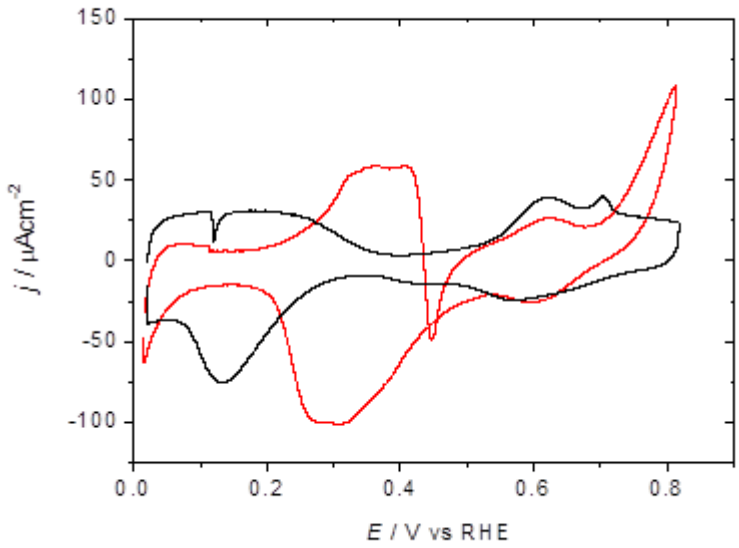


Figure S10. *Voltammetric profiles of Pt(111) (black curve) and Pt(100) (red curve) in a 4.4 m $Mg(ClO_4)_2$ solution [from ACS granular quality, Alfa Aesar] at 20 °C. The arrows indicate the initial potential and direction of the scan.*

The signal at 0.45V vs RHE on the Pt(100) is associated to the reduction of contaminants from the salt on specific (100) sites. High purity electrolytes had to be used for the experiments.

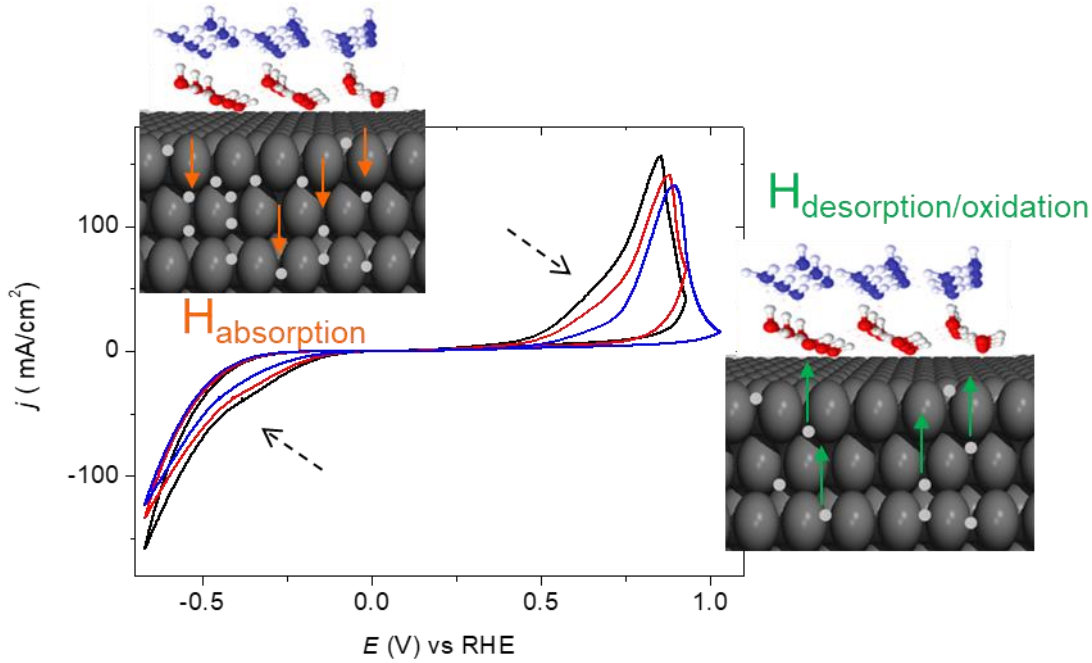


Figure S11. *Voltammetric profiles of polycrystalline Pd in 10 m solution of KOH at +20 °C (black curve), +2 °C (red curve) and -18 °C (blue curve).*

The oxidation of hydrogen shifts towards more positive potentials as the temperature decreases. The change in the intensity of the peaks associated to the hydrogen oxidation is related to different rates of diffusion of the hydrogen through the two distinct palladium hydride phases, *α*- and *β*-, and the transformation between these phases.[5] This transformation is a shift from an *α*-phase, of low hydrogen content, to a *β*-phase containing up to 0.8 atoms of hydrogen per atom of palladium in the matrix.[6] In alkaline media, the effect of the cations on the adsorption of hydrogen and formation of the different phases of the palladium hydride is not trivial.[7–9] It has been shown that the adsorption of cations has an effect on the oxidation rate of the hydrogen by increasing the stability of the hydrogen phase just below the surface.[7–10]

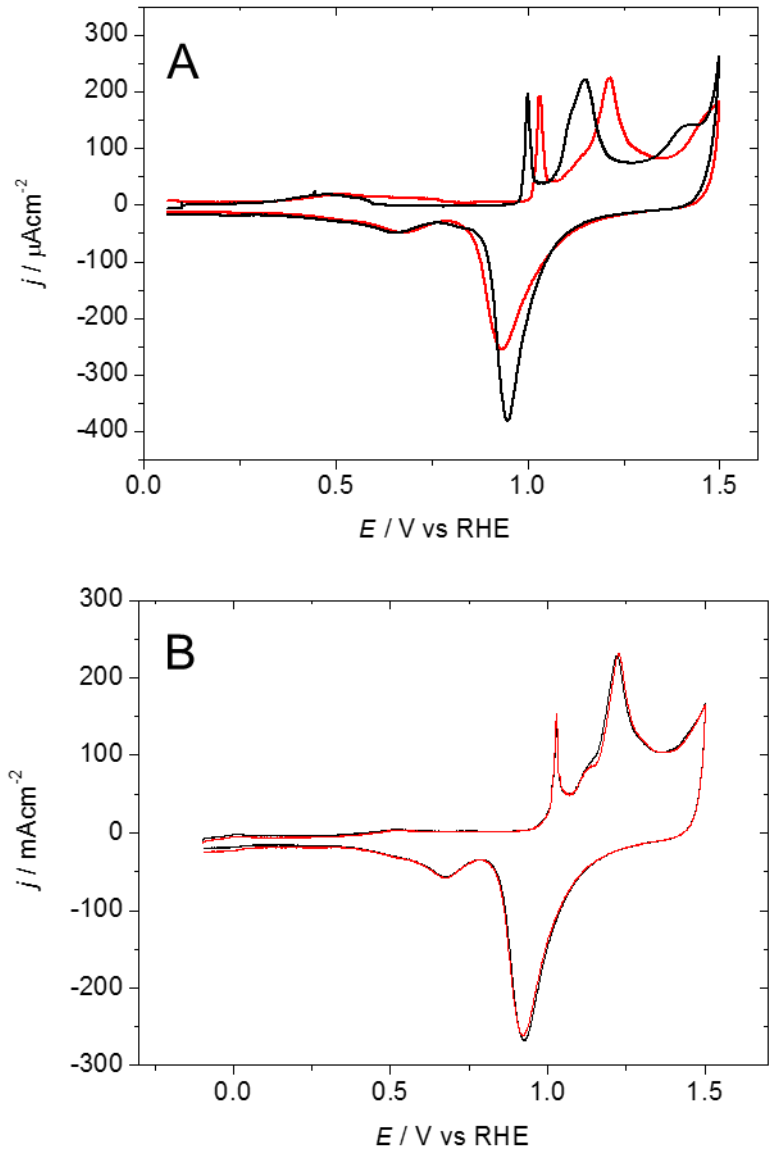


Figure S12. *(A) Voltammetric profile of Au(111) in 11 m NaOH at 18 °C (black) and -35 °C (red). Scan rate ɜ = 50 mV/s. (B) Voltammetric profile of Au(111) in 11 m NaOH at -35 °C in absence (black) and presence of CH_4 (red). Scan rate ɜ = 50 mV/s*

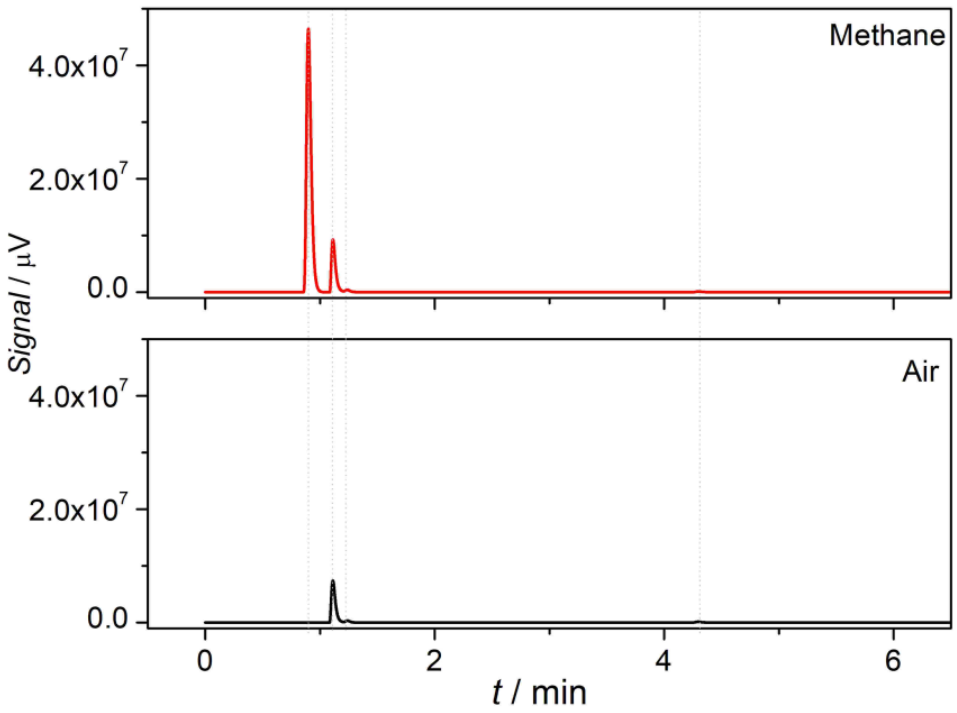


***Figure S13**. Gas chromatography of the CH_4 bottle.*

2.SI.2 References

1 T. Binninger, B. Pribyl, A. Pătru, P. Ruettimann, S. Bjelić and T. J. Schmidt, *J. Mass Spectrom.*, 2018, **53**, 1214–1221.

2 J. Monzó, Y. Malewski, R. Kortlever, F. J. Vidal-Iglesias, J. Solla-Gullón, M. T. M. Koper and P. Rodriguez, *J. Mater. Chem. A*, 2015, **3**, 23690–23698.

3 T. L. Hwang and A. J. Shaka, *J. Magn. Reson. Ser. A*, 1995, **112**, 275–279.

4 K. P. Kuhl, E. R. Cave, D. N. Abram and T. F. Jaramillo, *Energy Environ. Sci.*, 2012, **5**, 7050–7059.

5 W.-S. Zhang, X.-W. Zhang and X.-G. Zhao, *J. Electroanal. Chem.*, 1998, **458**, 107–112.

6 S. Majorowski and B. Baranowski, *J. Phys. Chem. Solids*, 1982, **43**, 1119–1127.

7 O. Yamazaki, H. Yoshitake, N. Kamiya and K. Ota, *J. Electroanal. Chem.*, 1995, **390**, 127–133.

8 M. H. Martin and A. Lasia, *Electrochim. Acta*, 2008, **53**, 6317–6322.

9 A. Czerwiński, M. Czauderna, G. Maruszczak, I. Kiersztyn, R. Marassi and S. Zamponi, *Electrochim. Acta*, 1997, **42**, 81–86.

10 A. Czerwiński, I. Kiersztyn and M. Grdeń, *J. Solid State Electrochem.*, 2003, **7**, 321–326.

Additions to the Supporting Information

Reference Electrode Conversion

The experiments were carried out using a Hg/HgO reference electrode and then reported vs the Reference Hydrogen Electrode. Conversion between the reference electrodes was carried out using equation S1.

$$E_{RHE} = E_{Hg/HgO} + 0.059 \times pH + 0.098 \quad \text{(S1)}$$

Where E_{RHE} (V) is the potential vs RHE, $E_{Hg/HgO}$ (V) is the potential *vs*. the Hg/HgO reference electrode.

Additional NMR parameters

Wilmad 400 MHz 5 mm NMR tubes were used for each experiment. For the calibration curves the average of three measurements used and the standard deviation in the measurements used for the error bars. The zgesgp water suppression pulse program from Topspin was used. For each -180° pulse the pulse duration was 2 mS and for each gradient the pulse duration was 1 mS. The delay between each scan was 40s. 4 dummy scans and 400 acquisition scans were recorded. For the pulse sequence the receiver gain was 101.

CHAPTER 3

Determination of kinematic viscosity of $Mg(ClO_4)_2$ and KOH brines saturated with CO_2 at Sub-Zero Temperatures

E. Sargeant and P. Rodríguez

Submitted to Journal of Chemical and Engineering Data

Declaration

E.S. and P.R. conceived the experiments. E.S. carried out the experiments and wrote the manuscript. Both authors contributed to the analysis of the results, discussion, and revision of the manuscript.

Abstract

The current race for space exploration has hastened the development of electrochemical technologies for *in-situ* utilisation of planetary resources for the synthesis of vital chemicals such O_2 and fuels. Understanding the physicochemical properties, such as density and kinematic viscosity, of aqueous solutions is essential for the design of electrochemical devices for electrolysis of water and CO_2, particularly at low temperature. Density and kinematic viscosity of highly concentrated $Mg(ClO_4)_2$ and KOH solutions have been determined, both at low temperatures and in the presence of CO_2 gas. It was found that for all solutions, independent of the concentration or nature of the electrolyte, as the temperature was decreased to 255 K, the density and the viscosity of the solutions increased. Upon saturation with CO_2, no significant change to the density and viscosity of $Mg(ClO_4)_2$,at all temperatures measured, was observed. Conversely, CO_2 saturated solutions of KOH show significant changes in density and viscosity at all temperatures, likely due to the formation of carbonates. The effects of these changes on the diffusion coefficient for dissolved CO_2 is also discussed.

3.1 Introduction

Current exploration of extra-terrestrial surfaces relies on unmanned probes such as Curiosity on the surface of Mars, Rosetta and its associated lander, Philae, which landed on the comet Churyumov–Gerasimenko and, the Voyager probes. However, human exploration and colonisation to the farthest reaches of our solar system, faces many challenges, which need to be overcome. To explore and colonise other planets for extended periods of time, human astronauts will need essential supplies such as oxygen and chemicals that can be used as fuels. However, there are prohibitive weight limits to space travel and therefore the practice of *in-situ* resource utilisation to generate products with local materials is essential in this endeavour. For example, future plans for exploration of the Martian surface by humans involve refuelling the ascent vehicles on the surface using *in-situ* resources. Transporting the

necessary fuel from Earth would require almost 40 Mt of oxygen and methane which clearly poses a significant challenge in weight transport.[1,2] However, the first experiments to generate oxygen on the surface have already taken place. By December 2021, the Mars Oxygen *In Situ* Resource Utilisation experiment (MOXIE) had generated around 50 g of O_2 via a solid oxide fuel cell at 800 °C from the compressed Martian atmosphere.[1]

Other electrocatalytic processes could be carried out to produce necessary chemicals, such as hydrogen or methane, by electrolysis of CO_2 dissolved in water.[3,4] The Phoenix lander observed gulley formations on the surface of Mars, likely caused by the flow of liquid over the surface, which, coupled with soil analysis, led to the conclusion that perchlorate brines exist under certain conditions on the surface of Mars.[5–9] Previous research has shown that lowering the temperature below 0 °C increases the production of CH_4 and CO and decreases the production of H_2 when CO_2 is electrocatalytically reduced in brines of $Mg(ClO_4)_2$.[3] The non-standard temperature and pressure conditions of extra-terrestrial regions need to be considered when designing catalytic processes and they can sometimes be advantageous.

It has been demonstrated that electrochemical processes can be carried out in solid aqueous electrolyte[10,11], however by increasing the electrolyte concentration, the freezing point of the solution can be depressed to maintain a liquid phase, which is more technologically advantageous. Blagden's Law, equation (1), can be used to estimate the depression in freezing point of the electrolyte, φT, where K is the cryoscopic constant of the solvent, m is the molality (moles solute per kg solvent) and i is the Van't Hoff factor.

ŸŽ‖ سي ╚ عي □ عي ▒ (1)

Care should be taken when using, equation (1) as it does not account for the chemical activity of the ions and is only applicable for ideal solutions. Equation (1) can be used for general approximations, such as for the freezing point of sea water, but at high concentration, non-linear behaviour occurs and the freezing point begins to rise again.[12,13] Using brines as electrolytes enables the depression of the freezing point whilst, in theory, also favouring the

increase in the solubility of certain gases such CO_2, methane and O_2.[14] As such the increase of the reactants might also increase the rate of electrochemical reaction involving these gases. For example, in $Mg(ClO_4)_2$ brines as the temperature is lowered to -35 °C, the solubility of O_2 increases to around 1.1 mM and the current due to O_2 reduction increases.[15] In previous works we have also reported an increase of the reaction rate of the electrochemical conversion of CO_2 and methane at sub-zero temperatures in aqueous brines of $Mg(ClO_4)_2$ and KOH.[3]

Changes in temperature not only have an effect on the solubility of CO_2 in aqueous electrolyte, they will also have a marked effect on the dynamic viscosity, *q* and the density, *µ* . These factors are not only important in the engineering of future technology but also for fundamental processes such as mass transport of ions. The Nernst-Plank equation, (2) is used to describe the mass transfer to an electrode, encompassing the processes of diffusion, convection, and migration.

$$J_i(x) = -D_i \frac{\partial C_i(x)}{\partial x} - \frac{z_i F}{RT} D_i C_i \frac{\partial \phi(x)}{\partial x} + C_i v(x) \qquad (2)$$

Where at a distance *x* from an electrode for a species *i* , *J* is the flux (mol s^{-1} cm^{-2}), *D* is the diffusion coefficient (cm^2 s^{-1}) , *C* is the concentration (mol cm^{-3}), *z* is the charge, *F* is the Faraday constant, *R* is the gas constant, *T* is the temperature (K), *ű* is the electrostatic potential (V), and *v* is the velocity (cm s^{-1}). The diffusion coefficient, *D*, can be derived from the Einstein-Stokes equation (3),

$$D = \frac{k_B T}{6\pi \eta r_{eff}} \qquad (3)$$

where, k_B is the Boltzmann constant, r_{eff} is the effective radius of the species (m), and *q* is the dynamic viscosity of the solution (Pa s). The dynamic viscosity is derived from the kinematic viscosity, *ɜ*, (m^2 s^{-1}) and the density via equation (4).

$$\eta = \nu \rho \qquad (4)$$

When designing electrolysers for any catalytic process involving a liquid reaction media, the viscosity of the media is important for the physical design aspects, since viscosity will affect the flow through components. However, as equation (2) shows, the flux of any reactants or products of the reaction is heavily influenced by the diffusion coefficient which is, in-turn, heavily affected by the viscosity. Given the importance of the viscosity for mass transport during electrochemical reactions, such as CO_2 conversion[16–19] and water splitting[20], herein we report the values of density and dynamic viscosity at sub-zero temperatures down to 255 K for $Mg(ClO_4)_2$ and KOH brines in the absence of, and upon saturation with, CO_2 gas.

These results can then be used to better understand the anti-Arrhenius behaviour seen during the electrochemical conversion of CO_2 and the oxidation of methane at temperatures below -5 °C reported in our previous work.[3] A more complete understanding of electrochemical conversion of CO_2 at low temperatures will further promote the design of electrochemical devices for space exploration and colonization.

3.2 Methodology

3.2.1 Preparation of materials

Solutions of KOH (Sigma Aldrich > 85 %) and $Mg(ClO_4)_2$ (Alfa Aesar > 95 %) were prepared by weighing out the required mass of solid using an analytical balance (measuring to 0.01 mg) and dissolving in a weighed mass of ultrapure water (Millipore Milli-Q® Integral 3, 18.2 MΩ cm^{-1}, <5 ppb total organic carbon) to make the correct concentration in mol kg^{-1}. All solutions were left in a temperature controlled 1:1 glycerol: water bath, cooled using a HUBER TC45E cooler with a temperature control ±0.5 K until they reached the desired temperature. Solutions were saturated with CO_2 (BOC, N4 grade) by bubbling for 20 minutes at room temperature and then for another 10 minutes at each temperature before each measurement was taken. Given the units involved in equation (1), all the concentrations in the manuscript are reported in molality (moles solute per kg solvent).

3.2.2 Density measurements

Pycnometers were acquired from Fisher Scientific and calibrated using acetonitrile (Fisher Scientific, 99.9%, Extra Dry over Molecular Sieves) at 298 K, 273 K, 263 K and 255 K. For density measurements, the pycnometers were filled with solutions that had been pre-cooled in the temperature-controlled bath and then left again to reach the desired temperature before measurements were taken (usually > 10 mins). Reported densities for 8.5 m KOH and 3.8 m $Mg(ClO_4)_2$ are an average of at least 12 measurements from three different samples. The reported error is the calculated via root sum of the squares of the error in the pycnometer and the error in the calibration curve fit (error in volume of pycnometer ± 3 x 10^{-4} cm^{-3}).

3.2.3 Viscosity measurements

To measure the kinematic viscosity an Ubbelohde viscometer (Paragon Scientific) suspended in the same temperature-controlled bath was used. When solutions were introduced to the viscometer, the sample was again left to cool to temperature before any measurement took place. The flow time was measured with a digital stopwatch capable of measuring ±0.1 s. Kinematic viscosity (*ɜ*) was calculated using the equation,

$$ɜ = At \quad (5)$$

Where *t* is the flow time and *A* is the calibration constant of the viscometer. Kinematic viscosities are an average of at least 15 measurements from three different samples and the standard deviation of the measurements taken as the error.

The measured kinematic viscosity, *ɜ*, was converted to the dynamic viscosity, *ɖ*, via equation (4) and the errors propagated via root sum of the squares. The error increases at low temperature due to uncertainty in the end point of measurement.

3.2.4 Methodology validation

To validate the methodology, density and viscosity measurements were determined for pure water and KOH solutions and are compared to previous works. As can be seen in Table

1, in the case of water, both the density and the dynamic viscosity are within 1 % of the literature results.[21] For 8.5 m KOH, the density value reported in this work is within 1% of the literature value, however, the dynamic viscosity has a 4% deviation.[22] Such error can be associated to the hygroscopic nature of KOH solutions decreasing the concentration of the solutions during measurement of the viscosity.

Table 1. *Comparison between density and viscosity measurements obtained in this work and in previous reports. [a] Reference 21. [b] Calculated from reference 22.*

	ρ at 25 °C / g cm^{-3}		η at 25 °C / mPa s	
	This work	literature	This work	literature
water	1.0005 ± 0.0008	0.997[a]	0.900 ± 0.004	0.890[a]
8.5 m KOH	1.3024 ± 0.0010	1.309[b]	2.271 ± 0.008	2.362[b]

3.3 Results and Discussion

3.3.1 Determination of the density of $Mg(ClO_4)_2$ and KOH solutions as a function of temperature

Figure 1 shows the densities of $Mg(ClO_4)_2$ and KOH solutions as a function of the temperature. As expected, the density of all solutions increases linearly with decreasing temperature. At 255 K, 3.8 mol kg^{-1} is close to the saturation of the $Mg(ClO_4)_2$ solution and below this temperature precipitation of $6H_2O.Mg(ClO_4)_2$ occurs[12] which is the most stable form under Martian conditions.[23] Upon CO_2 saturation, the solution of 3.8 m $Mg(ClO_4)_2$ showed no

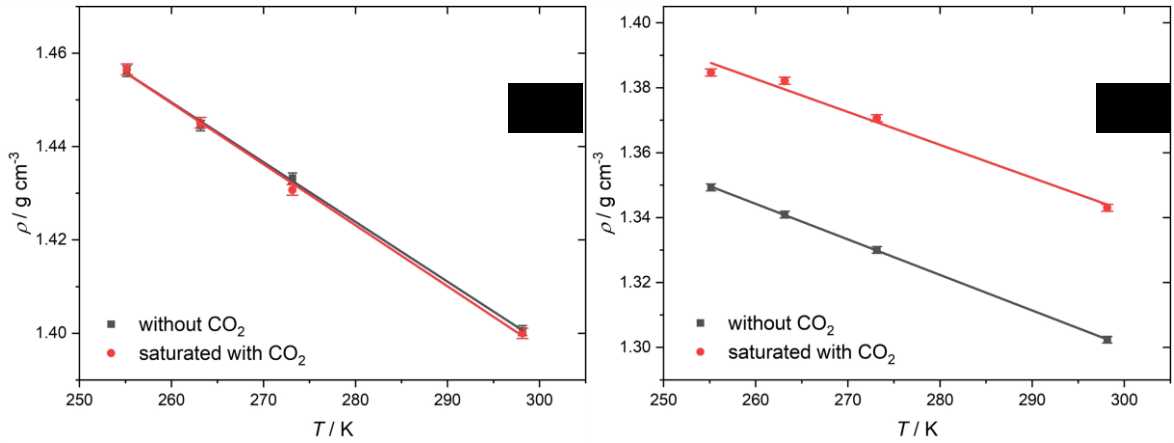


Figure 1. *Density as a function of temperature between 255 K and 298 K with CO_2 (red) and without CO_2 (black). (A) Results from 3.8 m $Mg(ClO_4)_2$. (B) Results from 8.5 m KOH.*

Table 2. *Measured density of 3.8 m $Mg(ClO_4)_2$ and 8.5 m KOH solutions, with and without CO_2 saturation.*

	3.8 m $Mg(ClO_4)_2$	CO_2 sat. 3.8 m $Mg(ClO_4)_2$	8.5 m KOH	CO_2 sat. 8.5 m KOH
T / K		ρ / g cm^{-3}		
298	1.4006 ± 0.0011	1.4000 ± 0.0011	1.3024 ± 0.0010	1.3430 ± 0.0011
273	1.4332 ± 0.0011	1.4307 ± 0.0011	1.3300 ± 0.0010	1.3706 ± 0.0011
263	1.4445 ± 0.0011	1.4451 ± 0.0011	1.3409 ± 0.0011	1.3821 ± 0.0011
255	1.4562 ± 0.0012	1.4566 ± 0.0012	1.3493 ± 0.0011	1.3847 ± 0.0011

significant change in the density at any T measured suggesting little absorption of CO_2 in the solution. These results are in agreement with the poor solubility of CO_2 at the pH of the $Mg(ClO_4)_2$ solutions (pH=8). Previous work by our group using mass spectroscopy found that, in the same electrolyte, the concentration of CO_2 increased from 1.12 mM at 293.15 K to 5.08 mM at 253 K.[3] However, such small changes of concentration of CO_2 in the solution are below the detection limit and within the standard deviation of the measurements using the methodology used in this work.

Upon saturation with CO_2, the density of 8.5 m KOH increases by 0.04 g cm^{-3} across all the measured temperatures. This indicates that the amount of CO_2 absorbed is constant over all temperatures in this range. Alternatively, as in the case of the $Mg(ClO_4)_2$, the variation in concentration of CO_2 is again, too small to be seen via this methodology. In this regard, previous works have shown that at room temperature, the concentration of absorbed CO_2 increases with concentration of KOH[24], due to the formation of (bi)carbonates, but at very high concentrations of the electrolyte, the CO_2 solubility is limited due to the so called the “salting out” effect.[25,26] The balance between these factors, (bi) carbonate formation and salting out effect, and the expected increase in CO_2 solubility due to the lower temperature, may account for the observed constant CO_2 concentration across the temperatures measured.

3.3.2 Determination of the viscosity of the $Mg(ClO_4)_2$ and KOH solutions as a function of temperature

The measured kinematic viscosity, *ɜ*, was converted to the dynamic viscosity, *ɖ*, via equation (4) and the results are shown in Table 3. Over the temperature range investigated, the values of viscosity for both $Mg(ClO_4)_2$ and KOH solutions fit an Arrhenius relationship, equation (6),

$$\text{—سي ÖΩ}^{\text{ثريخ}}_{\text{بي}} \qquad (6)$$

Where *R* is the gas constant, *A* is the preexponential factor (Pa s), and E_a is the activation energy (kJ mol^{-1}). The Arrhenius plots are shown in Figures 2A and 2B. Figure 2A shows little difference between *ɖ* for the CO_2 saturated and unsaturated $Mg(ClO_4)_2$ solution. This agrees with the interpretation of the *ɟ* results where there is little absorption of CO_2.

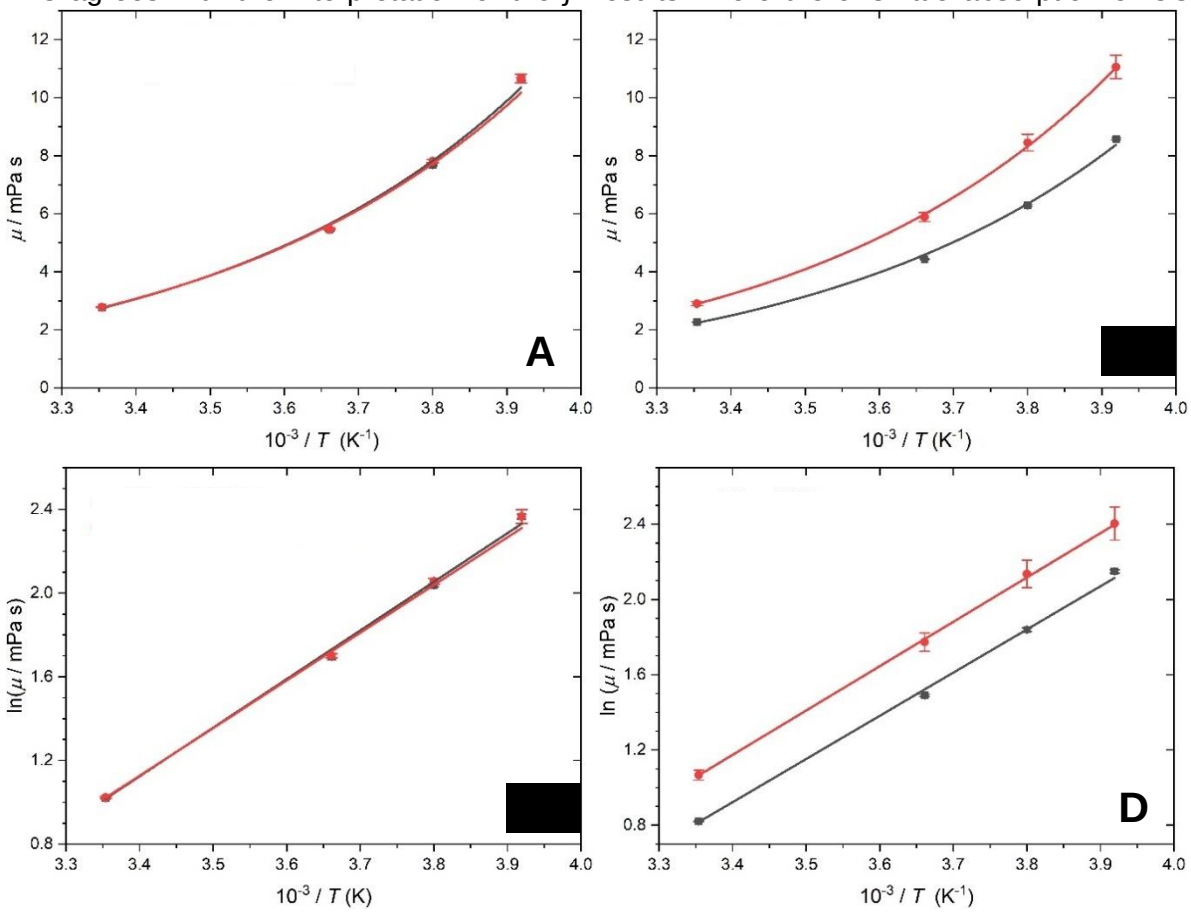


Figure 2. *Viscosity as a function of temperature (black) without CO_2 and (red) upon saturation with CO_2. (A) and (C) Results from 3.8 m $Mg(ClO_4)_2$. (B) and (D) Results from 8.5 m KOH.*

Table 3. *Calculated ɖ values for $Mg(ClO_4)_2$ and KOH solutions with and without saturation with CO_2.*

	3.8 m $Mg(ClO_4)_2$	CO_2 sat. 3.8 m $Mg(ClO_4)_2$	8.5 m KOH	CO_2 sat. 8.5 m KOH
T / K		*ɖ* / mPa s		
298	2.77 ± 0.04	2.78 ± 0.04	2.27 ± 0.03	2.91 ± 0.08
273	5.45 ± 0.09	5.48 ± 0.07	4.44 ± 0.06	5.89 ± 0.18
263	7.67 ± 0.10	7.82 ± 0.11	6.29 ± 0.09	8.45 ± 0.31
255	10.65 ± 0.14	10.66 ± 0.2	8.58 ± 0.11	11.06 ± 0.43

Previous work has attributed the increase in viscosity for concentrated $Mg(ClO_4)_2$ solutions to the formation of solvation spheres on a picosecond timescale around the ions which act as suspended spheres in solution which in turn increases the viscosity.[27]

On the other hand, Figure 2B shows an increase in the difference in *ɖ* for the unsaturated and CO_2 saturated KOH solutions as the temperature decreases . Since, ɟ indicates that the concentration of CO_2 is constant across the temperature range, then the change in *ɖ* must be due to changes in the strength of the intermolecular forces of attraction. When the CO_2 dissolves, it reacts with the available water and sets up an equilibrium between CO_3^{2-}, HCO_3^- and H_2CO_3. In concentrated KOH, the most abundant ion is HCO_3^-, which causes an associated lowering of the pH.[24] The carbonate ions can form hydrogen bonds and interact with the wider water network which therefore increases the intermolecular forces of attraction and therefore the viscosity.

In other to obtain the activation energy of the system, Figures 2C and 2D show the Arrhenius linear representation of the measured values of the viscosity as a function of the temperature, using equation (7).

ì ÎسÌ Î ط ئ ٰ ٣ا (7)

η_∞, can be interpreted as the viscosity in the absence of an activation energy (Pa s), and E_a is the energy input needed for molecules in the solution to flow past each other. These parameters are derived for each of the solutions, Table 4. There is a small increase in E_a when KOH is saturated with CO_2 which supports that there is an increase in the strength of the interactions between the ions.

Table 4. *Viscosity at infinite temperature and the activation energy for each solution derived from the linear fit in Figures 2C and D*

solution	$10^{-3}\ \eta_\infty$ / mPa s	E_a / kJ mol^{-1}	R^2 values for Figure 2C & D
3.8 m $Mg(ClO_4)_2$	1.14 ± 0.03	19.3 ± 0.4	0.999
CO_2 sat. 3.8 m $Mg(ClO_4)_2$	1.32 ± 0.04	19.0 ± 0.4	0.998
8.5 m KOH	1.03 ± 0.03	19.1 ± 0.5	0.998
CO_2 sat. 8.5 m KOH	1.07 ± 0.02	19.6 ± 0.3	0.999

3.3.3 Determination of the diffusion coefficient of CO_2 in $Mg(ClO_4)_2$ and KOH

Using the values for η determined in the previous section and equation (3) the values for D were calculated and the results shown in Table 5. The hydrodynamic radius of the CO_2 was assumed to be the same as in pure water[28] but loosely dependent on temperature.[29] As T decreases, the diffusion coefficient also decreases in both solutions. The larger η values for 8.5 m KOH correspond with lower D values compared to 3.8 m $Mg(ClO_4)_2$. According to equation (2), lower values of the diffusion coefficient, indicate a lower flux and a decrease in mass transport of CO_2 through the solutions.

Table 5. *Calculated diffusion coefficient for CO_2 in $Mg(ClO_4)_2$ and KOH at various temperatures*

	CO_2 sat. 3.8 m $Mg(ClO_4)_2$	CO_2 sat. 8.5 m KOH
T / K	D / 10^{-10} m^2 s^{-1}	
298	7.01	6.71
273	3.43	6.71
263	2.37	3.19
255	1.71	2.19

Interestingly, our previous work showed an increase in the electrochemical conversion of CO_2 in brines at sub-zero temperatures, with and without mass transport control. Therefore, even though the physicochemical properties of the solution, such as density and viscosity, influence the diffusion of the gaseous reactant species, other intrinsic parameters are promoting Anti-Arrhenius behaviour so that at low temperatures the catalytic activity increases.

3.4 Conclusions

The density and dynamic viscosity of highly concentrated KOH and $Mg(ClO_4)_2$ solutions, was measured and reported at temperatures below 273 K. The high electrolyte concentration results in the depression of the freezing point of the aqueous solution down to 255 K. It was found that as the temperature decreased, d and μ for all solutions increased. μ increased linearly and d followed an Arrhenius relationship. Given the importance of these solutions for the development of electrolysers on other planetary object, the density and dynamic viscosity of the same KOH and $Mg(ClO_4)_2$ solutions saturated with CO_2 is also reported.

3.8 m $Mg(ClO_4)_2$ shows no significant differences in d or μ at any measured temperature after saturation with CO_2. The results are associated to the poor solubility of CO_2 at the pH of the $Mg(ClO_4)_2$. Conversely, 8.5 m KOH solutions show marked changes in physicochemical behaviour upon saturation with CO_2. A constant increase in μ is observed, at the same time a much greater increase is observed in d at lower temperatures. We conclude that the formation of (bi) carbonate species, due to the reaction between the CO_2 and the KOH, increase in the strength of the interactions between the ions resulting in a larger change in the viscosity at lower temperatures.

At low temperature, the diffusion coefficient of CO_2 is significantly reduced in these solutions which will result in less mass transport through the electrolyte. This indicates that the increase in CO_2 reduction current at low temperature seen in our previous work is not due to

an increase in transport of CO_2 to the electrode surface but more likely other factors such as overall CO_2 concentration.[3] However, the benefit in increased activity at low temperature is finely balanced with the disadvantageous increase in viscosity of the solutions and the decrease in diffusion of CO_2.

3.5 Acknowledgments

E.S. acknowledges the University of Birmingham and the EPSRC Centre for Doctoral Training in Carbon Capture and Storage and Cleaner Fossil Energy for financial support through Ph.D. scholarships at the School of Chemistry. P.R. acknowledges the University of Birmingham for financial support through the Ikerbasque foundation.

3.6 References

1. Hoffman, J. A. *et al.* Mars Oxygen ISRU Experiment (MOXIE)-Preparing for human Mars exploration. *Sci. Adv.* **8**, 1–7 (2022).
2. Hecht, M. H. *et al.* Mars Oxygen ISRU Experiment (MOXIE). *Space Sci. Rev.* **217**, 9, (2021).
3. Sargeant, E., Kolodziej, A., Le Duff, C. S. & Rodriguez, P. Electrochemical Conversion of CO 2 and CH 4 at Subzero Temperatures. *ACS Catal.* **10**, 7464–7474 (2020).
4. Gayen, P., Sankarasubramanian, S. & Ramani, V. K. Fuel and oxygen harvesting from Martian regolithic brine. *Proc. Natl. Acad. Sci. U. S. A.* **117**, 31685–31689 (2020).
5. Hecht, M. H. *et al.* Detection of Perchlorate and the Soluble Chemistry of Martian Soil at the Phoenix Lander Site. *Science.* **325**, 64–67 (2009).
6. Smith, P. H. *et al.* H_2O at the Phoenix Landing Site. *Science.* **325**, 58–61 (2009).
7. Toner, J. D. & Catling, D. C. Chlorate brines on Mars: Implications for the occurrence of liquid water and deliquescence. *Earth Planet. Sci. Lett.* **497**, 161–168 (2018).
8. Primm, K. M., Gough, R. V., Chevrier, V. F. & Tolbert, M. A. Freezing of perchlorate and chloride brines under Mars-relevant conditions. *Geochim. Cosmochim. Acta* **212**, 211–220 (2017).
9. Chevrier, V. F., Fitting, A. B. & Rivera-Valentín, E. G. Limited Stability of Multicomponent Brines on the Surface of Mars. *Planet. Sci. J.* **3**, 125 (2022).
10. Frese, U., Iwasita, T., Schmickler, W. & Stimming, U. Hydrogen evolution in liquid and frozen aqueous electrolyte. *J. Phys. Chem.* **89**, 1059–1062 (1985).
11. Borkowska, Z., Cappadonia, M. & Stimming, U. Interfacial and bulk electrolyte properties in frozen electrolyte studies. *Electrochim. Acta* **37**, 565–568 (1992).
12. Pestova, O. N., Myund, L. A., Khripun, M. K. & Prigaro, A. V. Polythermal Study of the Systems M(ClO4)2-H2O (M2+ = Mg2+, Ca2+, Sr2+, Ba2+). *Russ. J. Appl. Chem.* **78**, 409–413 (2005).
13. Haynes, W. Concentrative properties of aqueous solutions: density, refractive index, freezing point depression, and viscosity. *CRC Handb. Chem. Phys.* 5–128 (2012).
14. Diamond, L. W. & Akinfiev, N. N. Solubility of CO2 in water from -1.5 to 100°C and from 0.1 to 100 MPa: Evaluation of literature data and thermodynamic modelling. *Fluid Phase Equilib.* **208**, 265–290 (2003).
15. Elliott, J., Ngamchuea, K., Batchelor-McAuley, C. & Compton, R. G. Martian Redox Chemistry: Oxygen Reduction in Low-Temperature Magnesium Perchlorate Brines. *J. Phys. Chem. Lett.* **8**, 6171–6175 (2017).
16. Gupta, N., Gattrell, M. & MacDougall, B. Calculation for the cathode surface concentrations in the electrochemical reduction of CO2 in KHCO3 solutions. *J. Appl. Electrochem.* **36**, 161–172 (2006).
17. Varela, A. S., Kroschel, M., Reier, T. & Strasser, P. Controlling the selectivity of CO2 electroreduction on copper: The effect of the electrolyte concentration and the importance of the local pH. *Catal. Today* **260**, 8–13 (2016).
18. Raciti, D., Mao, M. & Wang, C. Mass transport modelling for the electroreduction of CO2 on Cu nanowires. *Nanotechnology* **29**, (2018).
19. Zhang, B. A., Ozel, T., Elias, J. S., Costentin, C. & Nocera, D. G. Interplay of Homogeneous Reactions, Mass Transport, and Kinetics in Determining Selectivity of the Reduction of CO2 on Gold Electrodes. *ACS Cent. Sci.* **5**, 1097–1105 (2019).
20. Goyal, A. & Koper, M. T. M. Understanding the role of mass transport in tuning the hydrogen evolution kinetics on gold in alkaline media. *J. Chem. Phys.* **155**, (2021).
21. Lide, D. R. *CRC handbook of chemistry and physics*. (CRC press, 2004).
22. Sipos, P. M., Hefter, G. & May, P. M. Viscosities and Densities of Highly Concentrated Aqueous MOH Solutions (M + = Na + , K + , Li + , Cs + , (CH 3) 4 N +) at 25.0 °C. *J. Chem. Eng. Data* **45**, 613–617 (2000).
23. Robertson, K. & Bish, D. Stability of phases in the Mg(ClO4)2·nH 2O system and

implications for perchlorate occurrences on Mars. *J. Geophys. Res. Planets* **116**, 1–7 (2011).
24. Zhong, H., Fujii, K., Nakano, Y. & Jin, F. Effect of CO 2 Bubbling into Aqueous Solutions Used for Electrochemical Reduction of CO 2 for Energy Conversion and Storage. *J. Phys. Chem. C* **119**, 55–61 (2015).
25. Dinh, C.-T. *et al.* CO 2 electroreduction to ethylene via hydroxide-mediated copper catalysis at an abrupt interface. *Science.* **360**, 783–787 (2018).
26. Gilbert, K., Bennett, P. C., Wolfe, W., Zhang, T. & Romanak, K. D. CO2 solubility in aqueous solutions containing Na+, Ca2+, Cl-, SO42- and HCO3-: The effects of electrostricted water and ion hydration thermodynamics. *Appl. Geochemistry* **67**, 59–67 (2016).
27. Omta, A. W., Kropman, M. F., Woutersen, S. & Bakker, H. J. Negligible Effect of Ions on the Hydrogen-Bond Structure in Liquid Water. *Science.* **301**, 347–349 (2003).
28. Cadogan, S. P., Hallett, J. P., Maitland, G. C. & Trusler, J. P. M. M. Diffusion Coefficients of Carbon Dioxide in Brines Measured Using 13 C Pulsed-Field Gradient Nuclear Magnetic Resonance. *J. Chem. Eng. Data* **60**, 181–184 (2015).
29. Cadogan, S. P., Maitland, G. C. & Trusler, J. P. M. M. Diffusion Coefficients of CO 2 and N 2 in Water at Temperatures between 298.15 K and 423.15 K at Pressures up to 45 MPa. *J. Chem. Eng. Data* **59**, 519–525 (2014).

CHAPTER 4

Investigating the stabilising effects of the electrolyte on CO_2 reduction intermediates using DFT calculation

Abstract

The electrode-electrolyte interface, and in particular the nature of the cation, has considerable effects on the activity and product selectivity of the electrochemical reduction of CO_2. In order to improve the selectivity of this challenging reaction, it is paramount to understand the cation effect on the reaction mechanism. Here, DFT calculations are used to assess the different effects of K^+, Na^+, and Mg^{2+}, on single carbon CO_2 reduction intermediates and the results are illustrated using scaling relations. From these relations, it is shown that K^+ and Na^+ influence intermediates similarly, while Mg^{2+} interacts differently, likely due to its greater charge. These results are then applied to the reduction of CO_2 to CO on three different catalytic surfaces (Au, Cu and Pd) and the change in selectivity highlighted.

4.1 Introduction

Density Functional Theory, DFT, calculations are a useful tool for investigating chemical reactions. They calculate an approximate solution to the Schrödinger equation for a many-body system and the technique provides a good balance between accuracy and computational resources.[1] Herein, DFT calculations are used to investigate the stabilisation of key CO_2 reduction intermediates by experimentally relevant species, namely water and metal cations.

DFT calculations have been used in the past to develop a deeper understanding of experimental results. For example, on Cu(100) at low overpotentials, only C_2 products are observed, and the formation of ethylene is shown to be independent of pH.[2] Results from DFT calculations showed that at low overpotential, the formation of a $C_2O_2^-$ intermediate (which was observed in its hydrogenated form in IR experiments), via a decoupled proton-electron transfer step, is the potential determining step for the production of ethylene on this surface.[3,4] Further calculations proposed that at high overpotential, the reaction mechanism changes and the C_2 intermediate is formed from the dimerization of *CO and *CHO.[5] The protonation of *CO is considered one of the potential limiting steps and forms either *CHO or *COH, see Figure 1.

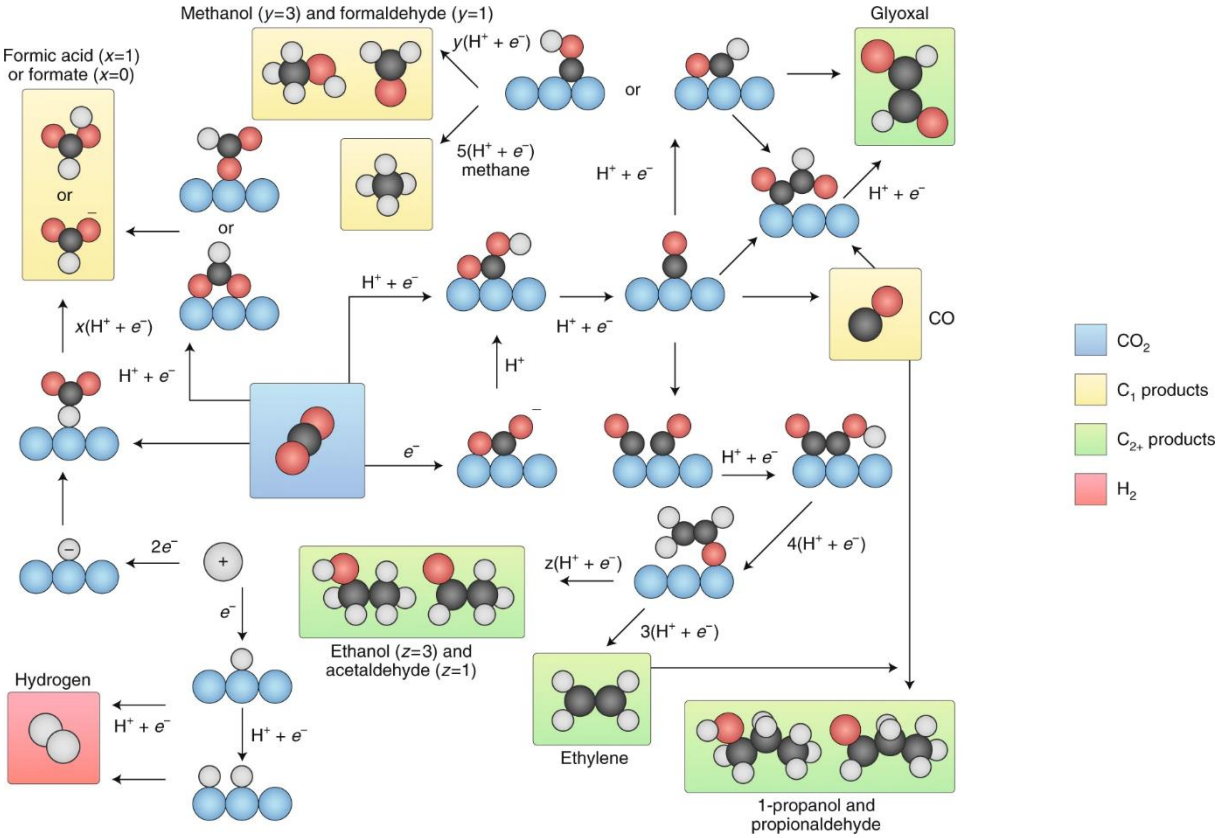


Figure 1. *Schematic showing the reduction of CO_2 on Cu catalysts to its various products. Reprinted from reference.* [44]

DFT screening of various facets of transition metals was able to show that *COH and *CHO are stabilised differently by different surfaces and so different strategies are required to stabilise each intermediate.[6,7] This highlights the difficultly in optimising the CO_2RR since there may be no single approach which will stabilise all intermediates appropriately.

Scaling relations are a method of screening many surfaces for catalytic purposes.[8] The adsorption energy of similar intermediates correlates in a linear fashion, for example, *OH and *OOH which are key intermediates in oxygen catalysis,[9,10] and C, S, N and O with their respective hydrogenated forms.[8] These scaling relations allow for the production of Sabatier-like volcano plots where the most active catalysts sit at the apex. However, scaling relations cause intrinsic limitations to the minimisation of the overpotential for reactions in which more than two electrons are transferred due to the constant separation of energy between intermediates that scale together.[10] For CO_2 reduction, there has been some progress in

detecting[7,11] and understanding how to "break" these scaling relations[12,13] but also criticism that there is insufficient consideration given to solvent effects.[14]

The simplest DFT calculations of an absorbate on a surface take place as if in a vacuum and so there are often discrepancies between theoretical and experimental results. There are multiple ways to include solvent and/or electrolyte effects to try to improve the predictions of DFT calculations. There are two commonly used methods to mimic the effect of the surrounding solution. Implicit solvation treats the surrounding liquid as a continuous media and generally relies on the experimentally measured dielectric screening constant.[15–17] This method is computationally cheap but, because it does not account for hydrogen bonding to adsorbates, it can be inaccurate.[18] Explicit solvation models include explicit water molecules in the calculations and although these models have a greater accuracy they are very computationally demanding.[19] For the calculations within this chapter, an affordable model where calculated solvation corrections determined from a micro-solvated adsorbate are applied which provides a good approximation to experimental results.[20] In other studies, electrolyte ions have been included and shown to affect the selectivity and the activity of the CO_2 reduction reaction. On Ag electrodes, larger cations promoted CO production over H_2 production[21] and increased the current density due to formation of CO and $HCOO^-$.[22] On Cu electrodes, increasing cation size also favours CO_2 reduction over H_2 evolution as well as promoting C_2 products rather than C_1.[23] DFT calculations have provided an explanation by showing that larger cations provide greater stabilisation to C_2 intermediates.[24]

This chapter aims to look at how C_1 intermediates are stabilised by water solvation effects and cations. The main body of the work looks at whether there is variation in how K^+, Na^+, and Mg^{2+} cations affect the intermediates and scaling relations are constructed to determine this. The specific effects of the cations on the first steps of CO_2 reduction, namely CO_2 reduced to *CO via *COOH, on experimentally relevant metals is then discussed.

4.2 Methodology

All calculations were performed using the Vienna ab-initio Simulation package[25] using the PBE exchange-correlation functional[26] and the projector augmented-wave (PAW) method[27] to describe the ion-electron interactions. Geometry optimisation was carried out using the conjugate gradient method with a plane-wave cut-off of 450 eV. For calculations of slabs with adsorbates, relaxation was stopped when the maximal residual forces on all atoms was less than 0.05 eV/Å. The Methfessel-Paxton smearing method[28] was used where the Fermi level was smeared to a width of 0.2 eV and all energies were extrapolated to 0 K. The vertical distance between slabs was greater than 12 Å and dipole corrections were added to avoid spurious electrostatic interactions between vertically stacked images.

The gas phase energies of molecules were either taken from the literature or calculated in the same way where Gaussian smearing was used with a Fermi level smearing width of 0.001 eV and again, all energies were extrapolated to 0 K.[7] For gas-phase calculations a 15 Å box was used and the Brillouin zone was sampled using a (1x1x1) Monkhorst-Pack mesh.[29]

4.2.1 Reaction energies

For the reduction of CO_2 to CO, the reaction energy, $q\Delta G$, in vacuum was calculated using the equation (1).

ŸŸOسي ŸŸO ـ ٠ طا ŸŸO ئ طيْ ¨YŸŸY (1)

Where $q\Delta E_{DFT}$ is the calculated DFT reaction energy, $q\Delta E_{ZPE}$ is the zero-point energy and $q\Delta S$ is the entropic contribution. $q\Delta E_{ZPE}$ was calculated with DFT using the vibrational frequencies from the simple harmonic oscillator approximation. For gas and liquid molecules, $q\Delta S$ was taken from standard entropies reported in the literature.[30] A liquid phase correction was applied to $q\Delta S$ for water.[3,30,31] For adsorbed intermediates, $q\Delta S$ includes only the vibrational contribution. Heat capacity effects were not included since their effects are negligible on formation energies at 298.15 K.[32] To account for the errors intrinsic to DFT calculation of gas

phase energies, for CO_2 and CO specifically, semiempirical corrections have been applied.[33] When solvation or cationic corrections are applied, it is assumed that any changes in qpE_{ZPE} and qpS are negligible since all species remain adsorbed.[20] To verify this, solvation corrections for *K on adsorbed CO was calculated with DFT energies and reaction energies and the difference was shown to be less than 0.05 eV.

4.2.2 Effect of solvation on CO_2 reduction to CO

When investigating the effect of solvation on the reduction of CO_2 to CO, (3×3) slabs were used of the (111), (100), and (211) surfaces. 4 layers of atoms were used where the bottom 2 layers were fixed at the optimised bulk distance. Again, a Monkhorst-Pack mesh was used to sample the Brillouin zone but with grid size (6×6×1).

VASPsol was used to calculate stabilisation by implicit solvation.[15,16] For explicit solvation, step wise addition of H_2O molecules was used.[20] The additional stabilising energy provided by each additional water molecule solvating the CO_2 reduction intermediate, q_w^n, is compared to the stabilising energy provided when the water molecule is solvated by other water molecules, $q_{H2O,}$, and if $q_w^n < q_{H2O}$ it is assumed that the intermediate, *w*, is solvated.

E_{H_2O} is the energy of a H-bond between two water molecules in a micro-solvation environment and is calculated in the following manner. Equation (2) describes 4 water molecules being adsorbed onto a surface in a micro-solvating configuration, where the square brackets signify species interacting with one another on a surface.

$$[H_2O]_{ads} + [H_2O]_{ads} \rightarrow [(H_2O)_2]_{ads} \qquad (2)$$

To calculate the stabilising energy of a single water-water interaction, equation (3) is used.

$$E_{H_2O} = \frac{1}{2}E_{ads}[(H_2O)_2] - E_{ads}[H_2O] \qquad (3)$$

Where, $E_{ads}[(H_2O)_2]$ is the adsorption energy of 4 water molecules being adsorbed into a micro-solvation configuration where one water is stabilised by three surrounding water molecules,

described in equation (2). The energy is an average of three configurations where one of the O-H bonds of the central water molecule is either pointing, up, down, or parallel to the surface. E_{ads} is the adsorption energy of a single water molecule in a vacuum described in equation (4).

$$E_{ads} = E_{slab+H_2O} - E_{slab} - E_{H_2O} \quad (4)$$

The stabilisation provided by the micro-solvation environment is the difference between E_{int} and E_{ads}. This energy is divided by 3, as in equation (3), to give the stabilisation of a single H-bond.

4.2.3 Effect of cations on C_1 intermediates

To investigate the effect of cations on CO_2 reduction intermediates, (4×4) (111) slabs were used. These were large enough to avoid lateral interactions between adsorbates. Due to computational resource limits, 3 layers of atoms were used, where the bottom layer was fixed at the optimised bulk distances and the top two layers and any absorbates were allowed to fully relax. The Brillouin zone was sampled using a (3×3×1) Monkhorst-Pack mesh. Ag, Au, Co, Cu, Ni, Ir, Pt, Pd and Rh surfaces were used in their spin restricted fcc configuration. Previous work shows that this configuration is acceptable for Co and that, although there are differences in the spin restricted and unrestricted values for Co and Ni surfaces, the trends are unaffected.[7]

To calculate the binding energy, qE_W, for each intermediate equation (5) was used.

$$qE_W = E_{*W} - E_{*} - E_W \quad (5)$$

Where, E_* is the energy of the metal surface, E_{*W} is the energy of the surface with the adsorbed intermediate (*COOH, *CO, *COH, *CHO, *C, *CH, *CH_2, *CH_3) and E_W is the energy of the adsorbate in its gas form ($COOH_{(g)}$, $CO_{(g)}$, $COH_{(g)}$, $CHO_{(g)}$, $C_{(g)}$, $CH_{(g)}$, $CH_{2(g)}$, or $CH_{3(g)}$).

The stabilisation of each intermediate by a cation is modelled using equation (6), with *K used as an example.

$$^{z}\text{ن طى }^{z}\text{ن }^{O\,z}\text{ ن طى ن طى }^{z} \qquad (6)$$

And so, the stabilisation energy provided by *K, q_{*K}, is given by equation (7),

$$\text{ŋ}_{z}\text{ أ سي }'O_{z}\text{ ـد ٨ أ طى }'O_{z}\text{طي }'O_{z}\text{ـد طي }'O_{z}\text{أ} \qquad (7)$$

Where $E_{*[W+K]}$ is the energy of the intermediate with a co-adsorbed K, and E_{*K} is the energy of adsorbed K.

4.3 Results and Discussion

4.3.1 Scaling relations

Scaling relations for CO_2 reduction intermediates are shown in Figure 2. The results for each intermediate are plotted vs. $\breve{Y}O_{z}$ using the linear equation (8).

$$\breve{Y}O_{\text{ـد}}\text{ سي ά }\breve{Y}O_{z}\text{ طى ''Ω} \qquad (8)$$

The gradient of the line can be calculated using a simple electron counting relation, ά سي ŭ$_{\text{ـد}}$ j ŭ, where ŭ$_{\text{ـد}}$ is the number of electrons required for an intermediate, *w*, to reach a full outer shell and ŭ is the number of electrons for C to complete its outer shell, that is 4. This relation is applicable in many situations where the interaction between the surface and each species is similar. For example, atoms with the same number of valence electrons (e.g. C and Si) scale linearly with a gradient of 1,[34] and step-wise hydrogenation causes the same change in gradient irrespective of whether the central atom is S or O, so that the slope of the SH vs S scaling relation is similar to that of OH vs O.[8] However, other factors can influence the gradient such as solvation or covalent character in the interaction between the adsorbed intermediate and the surface.[14] Besides, scaling relations may or may not exist depending on the chemical nature of the adsorbates and the composition and coordination number of the adsorption sites.[35]

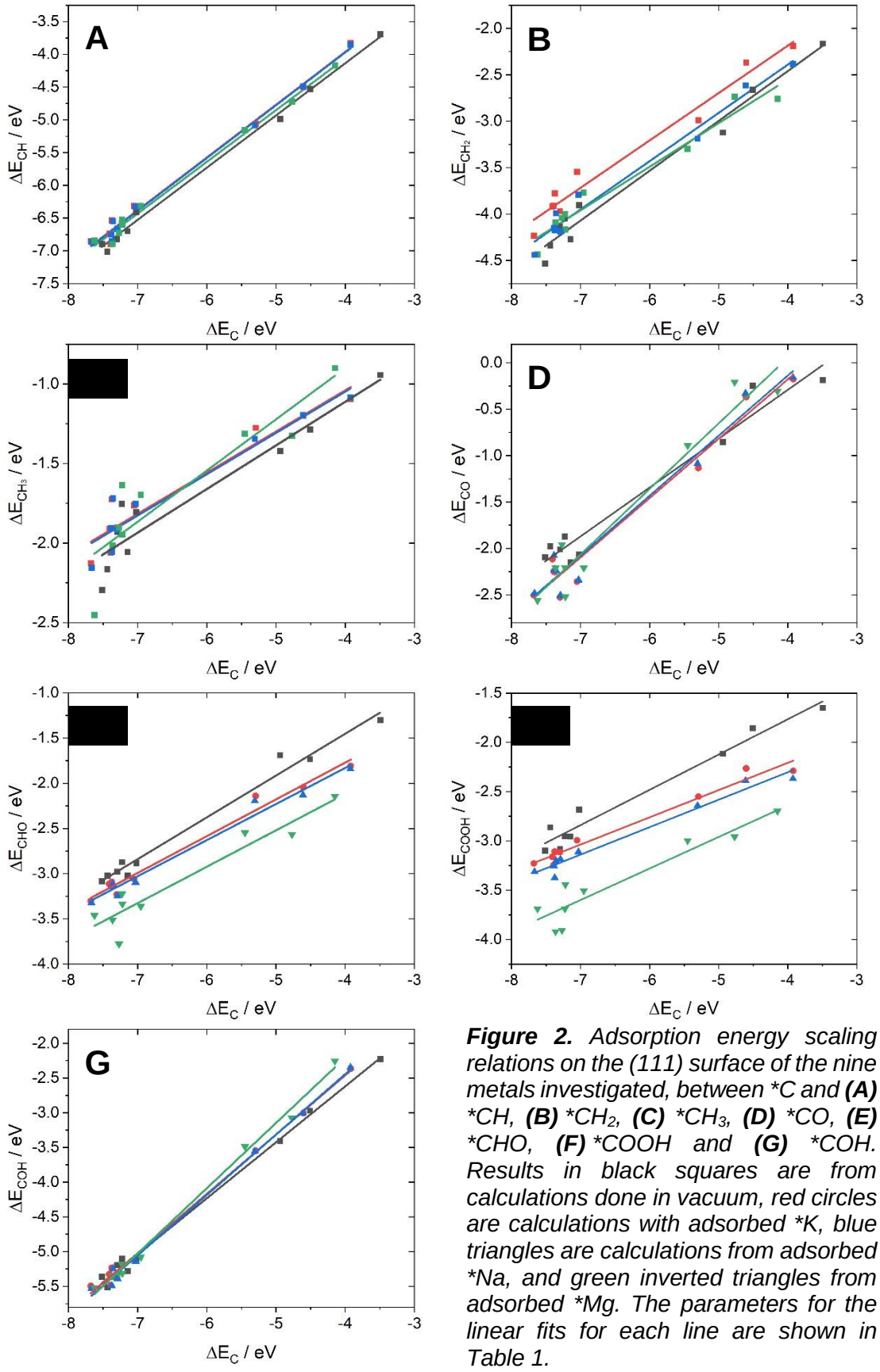


Figure 2. *Adsorption energy scaling relations on the (111) surface of the nine metals investigated, between *C and* ***(A)*** **CH,* ***(B)*** **CH_2,* ***(C)*** **CH_3,* ***(D)*** **CO,* ***(E)*** **CHO,* ***(F)*** **COOH and* ***(G)*** **COH. Results in black squares are from calculations done in vacuum, red circles are calculations with adsorbed *K, blue triangles are calculations from adsorbed *Na, and green inverted triangles from adsorbed *Mg. The parameters for the linear fits for each line are shown in Table 1.*

Table 1. *Parameters from the linear fits in Figure 2.*

parameter	*cation*	*adsorbed intermediate*						
		CH	**CH_2**	**CH_3**	**CO**	**COOH**	**COH**	**CHO**
m	-	0.80	0.54	0.27	0.53	0.36	0.81	0.46
	*K	0.81	0.51	0.26	0.64	0.28	0.85	0.41
	*Na	0.81	0.52	0.26	0.65	0.28	0.87	0.40
	*Mg	0.79	0.47	0.32	0.71	0.32	0.94	0.40
i / eV	-	-0.95	-0.31	-0.01	1.81	-0.33	0.61	0.40
	*K	-0.74	-0.14	0.00	2.38	-1.10	0.95	-0.14
	*Na	-0.75	-0.31	-0.01	2.45	-1.19	1.03	-0.23
	*Mg	-0.90	-0.67	0.39	2.88	-1.36	1.55	-0.50
R^2	-	0.994	0.974	0.900	0.957	0.965	0.995	0.983
	*K	0.991	0.970	0.921	0.965	0.971	0.995	0.981
	*Na	0.993	0.977	0.920	0.964	0.971	0.996	0.990
	*Mg	0.993	0.956	0.821	0.947	0.886	0.995	0.907

Table 1 shows that for the intermediates alone on the surface, shown in black in Figure 2, the gradients follow the literature and abide by the expected valence electron relationship. Intermediates where N_w is 3, (*CH and *COH) have gradients close to 0.75, where N_w is 2 (*CH_2, *CO, and *CHO) the gradient is close to 0.5 and where N_w is 1 (*CH_3 and *COOH) the gradient is close to 0.33. Upon co-adsorption of cations, *K shown in red, *Na shown in blue, and *Mg shown in green respectively in Figure 2, there is no significant change (<0.1 eV) in the gradient for any intermediate, except for CO. For CO, as the electronegativity of the cation increases, the gradient increases from close to 0.5 to close to 0.75 suggesting a loss of the double bond character in CO and a change from 2 to 1 electron needed to complete the valence shell. Previous work has shown that the stretching vibration, which is inversely proportional to the bond strength, for CO is affected by approaching cations, which supports the change in bond order observed here.[24,36]

Significant changes are observed in the offset on addition of a co-adsorbed cation. The offset of scaling relations is generally dependent on the coordination number of the surface adsorption site.[6,37] On addition of the cation, there is no observed change in the coordination of the carbon intermediate, since the preferred adsorption site for the intermediate does not

change. Thus, the changes to the offset must be due to stabilisation by the cations. The stabilisation provided by the cation is denoted with q_{*X} where *X is the cation. Figures 3A and 3B, illustrate how the stabilisation varies depending on the cation.

Figure 3A shows how the difference in binding energy between the sole intermediate and the intermediate in the presence of *K, q_{*K}, compares to the presence of *Na, q_{*Na}, for each of the intermediates. If the ions affect the intermediates in the same manner, then there will be a linear relationship between q_{*K} and q_{*Na} with a gradient of 1. To show the expected

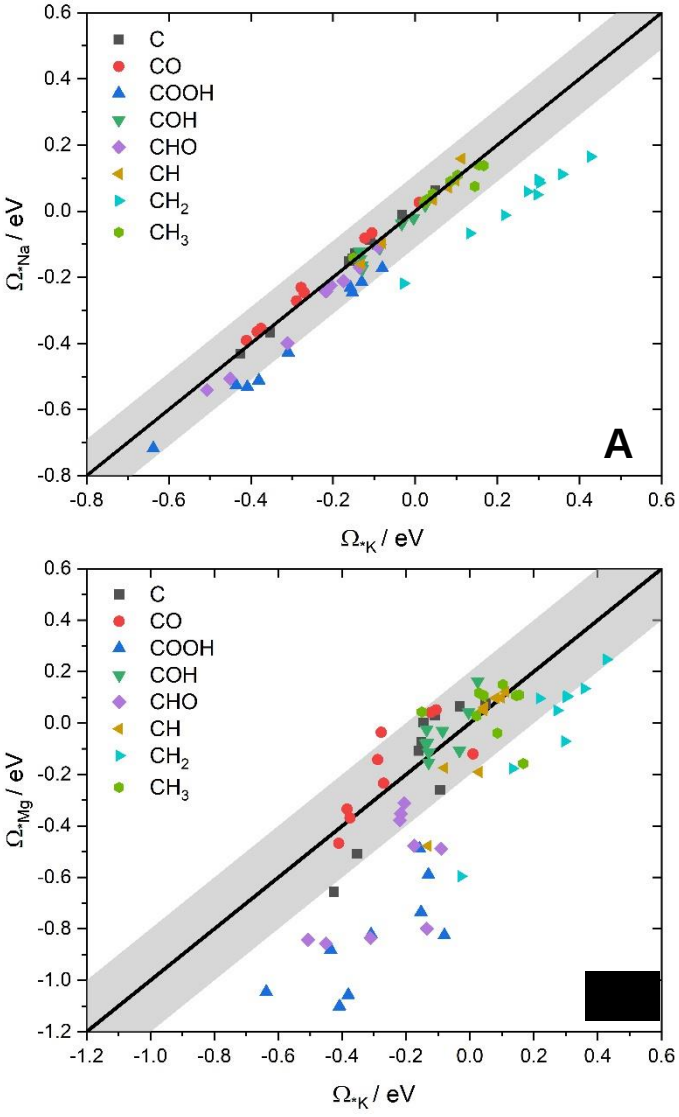


Figure 3. *Energy stabilisation provided by (A) *Na (q_{*Na}) and (B) *Mg (q_{*Mg}) plotted against energy stabilisation provided by *K (q_{*K}) for C_1 intermediates in the reduction of CO_2. The trendlines show the parity line y = x.*

Table 2. *Parameters for the linear fits shown in Figure 3 for q_{*Mg} vs. q_{*K} for each intermediate.*

	CH	CH_2	CH_3	CO	COOH	COH	CHO
m	2.28	1.75	-0.14	0.98	0.86	1.11	1.02
i	-0.10	-0.46	0.06	0.06	-0.58	0.05	-0.33
R^2	0.788	0.855	-0.121	0.526	0.495	0.491	0.280

relationship, a guideline of $y = x$ is included with an error bar twice the mean absolute error (MAE) with respect to the parity line. For this correlation, the MAE is 0.06 eV. All the intermediates, apart from $*CH_2$, follow this correlation indicating that the intermediates are stabilised in a similar way by both *K and *Na. $*CH_2$ is stabilised more by *Na than *K.

The same analysis is carried out to determine the correlation between stabilisation by *Mg and *K and the results plotted in Figure 3B. Here, the MAE was 0.2 eV which is twice the intrinsic error of DFT calculations, estimated to be around 0.1 eV. Therefore, the shaded band around $y = x$ is twice the error in the DFT method. For each intermediate, the parameters for the linear fit for q_{*Mg} vs. q_{*K} are shown in Table 2. It is clear from the R^2 correlation coefficients that none of the intermediates follow closely the linear relationship, except perhaps for $*CH_2$, indicating that *Mg affects the intermediates differently to *K.

4.3.2 Application to reduction of CO_2 to CO

The reduction of CO_2 to form CO via *COOH is the first step (except for formic acid which is formed via *OCHO) common to the production of all CO_2 reduction products. To illustrate the electrocatalytic effects of different methods of stabilisation the results are applied to the reduction of CO_2 to CO on three experimentally relevant surfaces. Cu, Pd and Au were the metals used in our previous work[38] and so these surfaces have been highlighted in Figure 4. The black line shows the reaction energy, $q\Delta G$, for the intermediates without any external stabilisation. For all three surfaces, the adsorption of CO_2 to form *COOH is the potential limiting step and then the further reduction to *CO is a favourable step. For Pd(111), the desorption step is very thermodynamically unfavourable which accounts for Pd catalysts

being poisoned by *CO, reducing their efficiency.[39] On Au(111) however, this final step is favourable hence $CO_{(g)}$ is the main product of CO_2 reduction.[40] The desorption step on Cu(111) is only 0.12 eV which is a relatively small barrier to overcome and so at low potentials, CO is a major product on Cu, but CO can stay adsorbed to the surface and react further.[40,41]

Stabilisation of intermediates by the solvent is a more developed subject of investigation than stabilisation by cations. In Figure 4, established methods have been used to show solvent stabilisation effects. The yellow line shows the stabilisation provided by implicit solvation. This stabilisation, $q_{solv,imp}$, was calculated using the VASPsol programme which simulates the dielectric screening of the surrounding solvent.[15,16] However, $q_{solv,imp}$ does not account for the additional stabilisation provided by H-bonds between the surrounding water molecules and the intermediate. The explicit solvation method used applies solvent

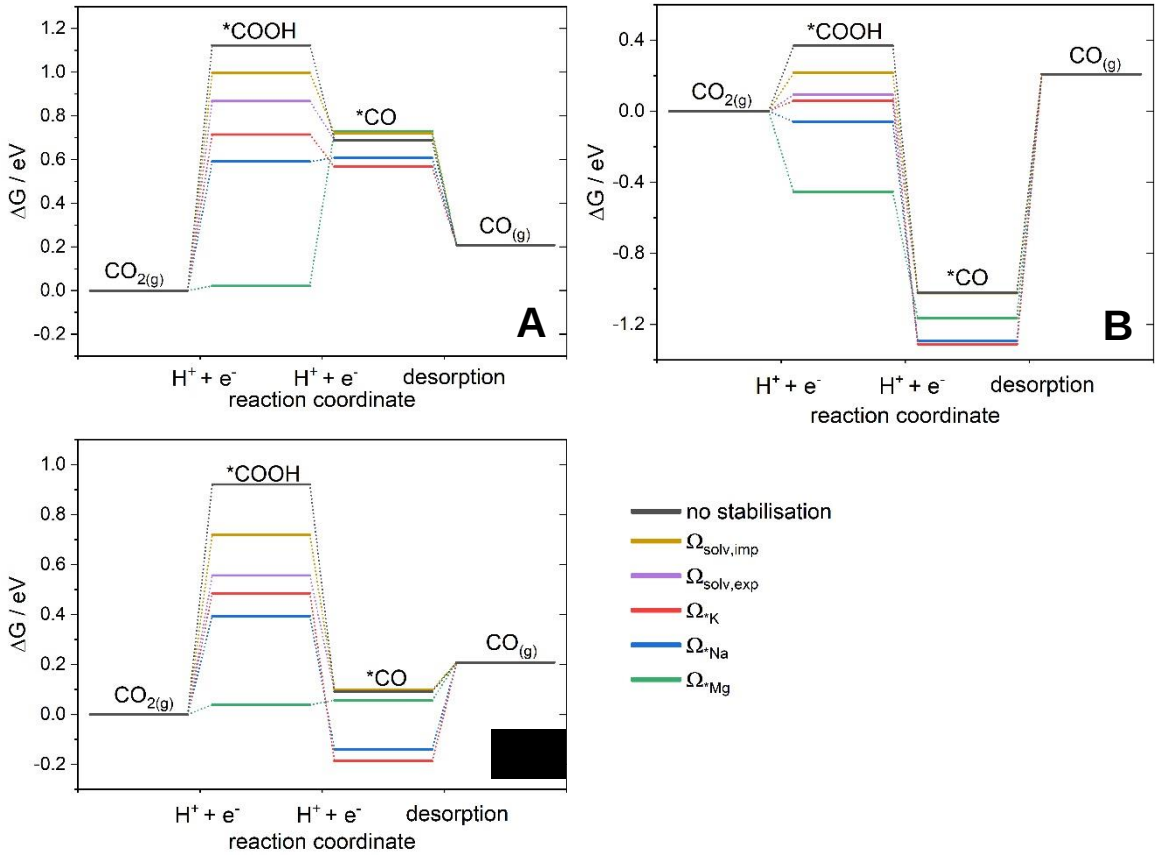


Figure 4. *Energy diagrams for reduction of CO_2 to CO on **(A)** Au(111) **(B)** Pd(111) **(C)** Cu(111). Black line shows reaction energies with no stabilisation of intermediates. Red shows stabilisation by *K. Blue shows stabilisation by *Na. Green shows stabilisation by *Mg. Lilac shows stabilisation by explicit solvation. Yellow shows stabilisation by implicit solvation.*

corrections, $q_{solv,exp}$, only if there is an H-bond formed and the results are shown as the lilac line in Figure 4.[20] For this reason, $q_{solv,exp}$ corrections are greater for *COOH than *CO.

Cation stabilisation affects both intermediates to a greater extent on all surfaces. Stabilisation by *K, q_{*K} , is shown in red, stabilisation by *Na, q_{*Na}, is shown in blue, and stabilisation by *Mg, q_{*Mg}, is shown in green. For *CO, q_{*K} is greater than q_{*Na}, but for *COOH, q_{*Na} is greater than q_{*K}. In turn, q_{*Mg} is greater for both intermediates than q_{*K} and q_{*Na}. Recent work has shown that in the absence of alkali metal cations, CO_2 reduction does not take place since the electrostatic stabilisation provided by the cations is essential for the initial adsorption of CO_2.[42] In other work, *K has been shown to stabilise the *COOH intermediate and strengthen the bond between the central C and the metal surface.[43] *COOH is more polarisable than *CO,[22] hence it is stabilised to a greater extent by the electrostatic interactions with the more electronegative *Na and *Mg.

4.4 Conclusions and Future Work

The work in this chapter has reiterated the importance of having a picture which is as complete as possible when undertaking DFT calculations. For the reduction of CO_2 to CO, solvent corrections dramatically change the stability of *COOH. However, the addition of cations stabilises *COOH further and also stabilises *CO, since cations stabilise the intermediates via electrostatic interactions rather than direct H-bonding. These results are in accordance with previous works where K^+ has been shown to stabilise *COOH more than *CO[43] and addition of H-bonding to calculations provides additional stabilisation to certain intermediates compared to implicit solvation[20] but in this work they are extended to more surfaces and include the divalent Mg^{2+}. K^+ and Na^+ seem to affect intermediates similarly and to the same extent, but the results from the scaling relations show that Mg^{2+} interacts in a dramatically different manner.

If there were more computational time available, the additive effect of water and cations together on intermediates would have been investigated. This would show whether *COOH can interact with both the cation and form an H-bond with water, and whether this interaction is more energetically favourable than just interacting with the cation. In reality, cations are not bare on the surface of the electrode and would have some form of solvation shell. Further calculations would look at this by both explicitly solvating the cation with water and via implicit solvation with VASPsol. Of course, C_1 intermediates are only part of the full story of CO_2 reduction and later calculations would expand this work to C_2 intermediates.

4.5 References

1 K. Capelle, *A bird's-eye view of density-functional theory*, 2002.
2 K. J. P. Schouten, Y. Kwon, C. J. M. van der Ham, Z. Qin and M. T. M. Koper, *Chem. Sci.*, 2011, **2**, 1902.
3 F. Calle-Vallejo and M. T. M. Koper, *Angew. Chemie Int. Ed.*, 2013, **52**, 7282–7285.
4 E. Pérez-Gallent, M. C. Figueiredo, F. Calle-Vallejo and M. T. M. Koper, *Angew. Chemie*, 2017, **129**, 3675–3678.
5 J. D. Goodpaster, A. T. Bell and M. Head-gordon, , DOI:10.1021/acs.jpclett.6b00358.
6 F. Calle-Vallejo and M. T. M. Koper, *ACS Catal.*, 2017, **7**, 7346–7351.
7 M. J. Kolb, D. Loffreda, P. Sautet and F. Calle-Vallejo, *J. Catal.*, 2021, **395**, 136–142.
8 F. Abild-Pedersen, J. Greeley, F. Studt, J. Rossmeisl, T. R. Munter, P. G. Moses, E. Skúlason, T. Bligaard and J. K. Nørskov, *Phys. Rev. Lett.*, 2007, **99**, 4–7.
9 V. Viswanathan, H. A. Hansen, J. Rossmeisl and J. K. Nørskov, *ACS Catal.*, 2012, **2**, 1654–1660.
10 M. T. M. Koper, *J. Electroanal. Chem.*, 2011, **660**, 254–260.
11 A. A. Peterson and J. K. Nørskov, *J. Phys. Chem. Lett.*, 2012, **3**, 251–258.
12 H. Li, Y. Li, M. T. M. Koper and F. Calle-Vallejo, *J. Am. Chem. Soc.*, 2014, **136**, 15694–15701.
13 Y. Li and Q. Sun, *Adv. Energy Mater.*, 2016, **6**, 1600463.
14 F. Calle-Vallejo, A. Krabbe and J. M. García-Lastra, *Chem. Sci.*, 2016, **8**, 124–130.
15 K. Mathew, R. Sundararaman, K. Letchworth-Weaver, T. A. Arias and R. G. Hennig, *J. Chem. Phys.*, 2014, **140**, 1–9.
16 K. Mathew, V. S. C. Kolluru, S. Mula, S. N. Steinmann and R. G. Hennig, *J. Chem. Phys.*, 2019, **151**, 1–8.
17 A. V Marenich, C. J. Cramer and D. G. Truhlar, *J. Phys. Chem. B*, 2009, **113**, 6378–6396.
18 Q. Zhang and A. Asthagiri, *Catal. Today*, 2019, **323**, 35–43.
19 H. H. Heenen, J. A. Gauthier, H. H. Kristoffersen, T. Ludwig and K. Chan, *J. Chem. Phys.*, 2020, **152**, 144703.
20 A. Rendón-Calle, S. Builes and F. Calle-Vallejo, *Appl. Catal. B Environ.*, 2020, **276**, 119147.
21 M. R. Thorson, K. I. Siil and P. J. A. Kenis, *J. Electrochem. Soc.*, 2012, **160**, F69–F74.
22 J. Resasco, L. D. Chen, E. Clark, C. Tsai, C. Hahn, T. F. Jaramillo, K. Chan and A. T. Bell, *J. Am. Chem. Soc.*, 2017, **139**, 11277–11287.
23 A. Murata and Y. Hori, *Bull. Chem. Soc. Jpn.*, 1991, **64**, 123–127.
24 E. Pérez-Gallent, G. Marcandalli, M. C. Figueiredo, F. Calle-Vallejo and M. T. M. Koper, *J. Am. Chem. Soc.*, 2017, **139**, 16412–16419.
25 G. Kresse and J. Furthmüller, *Phys. Rev. B*, 1996, **54**, 11169–11186.
26 J. P. Perdew, K. Burke and M. Ernzerhof, *Phys. Rev. Lett.*, 1996, **77**, 3865–3868.
27 G. Kresse and D. Joubert, *Phys. Rev. B*, 1999, **59**, 1758–1775.
28 M. Methfessel and A. T. Paxton, *Phys. Rev. B*, 1989, **40**, 3616–3621.
29 H. J. Monkhorst and J. D. Pack, *Phys. Rev. B*, 1976, **13**, 5188–5192.
30 D. R. Lide, *CRC handbook of chemistry and physics*, CRC press, 85th edn., 2004.
31 J. K. Nørskov, J. Rossmeisl, A. Logadottir, L. Lindqvist, J. R. Kitchin, T. Bligaard and H. Jónsson, *J. Phys. Chem. B*, 2004, **108**, 17886–17892.
32 C. J. Bartel, A. W. Weimer, S. Lany, C. B. Musgrave and A. M. Holder, *npj Comput. Mater.*, 2019, **5**, 4.
33 L. P. Granda-Marulanda, A. Rendón-Calle, S. Builes, F. Illas, M. T. M. Koper and F. Calle-Vallejo, *ACS Catal.*, 2020, **10**, 6900–6907.
34 F. Calle-Vallejo, J. I. Martínez, J. M. García-Lastra, J. Rossmeisl and M. T. M. Koper, *Phys. Rev. Lett.*, 2012, **108**, 1–5.
35 A. Brito Ravicini and F. Calle-Vallejo, *Exploration*, 2022, **2**, 20210062.

36 G. Hussain, L. Pérez-Martínez, J.-B. Le, M. Papasizza, G. Cabello, J. Cheng and A. Cuesta, *Electrochim. Acta*, 2019, **327**, 135055.

37 F. Calle-Vallejo, D. Loffreda, M. T. M. Koper and P. Sautet, *Nat. Chem.*, 2015, **7**, 403–410.

38 E. Sargeant, A. Kolodziej, C. S. Le Duff and P. Rodriguez, *ACS Catal.*, 2020, **10**, 7464–7474.

39 X. Min and M. W. Kanan, *J. Am. Chem. Soc.*, 2015, **137**, 4701–4708.

40 Y. Hori, H. Wakebe, T. Tsukamoto and O. Koga, *Electrochim. Acta*, 1994, **39**, 1833–1839.

41 K. P. Kuhl, E. R. Cave, D. N. Abram and T. F. Jaramillo, *Energy Environ. Sci.*, 2012, **5**, 7050–7059.

42 M. C. O. Monteiro, F. Dattila, B. Hagedoorn, R. García-Muelas, N. López and M. T. M. Koper, *Nat. Catal.*, 2021, **4**, 654–662.

43 M. Liu, Y. Pang, B. Zhang, P. De Luna, O. Voznyy, J. Xu, X. Zheng, C.-T. Dinh, F. Fan, C. Cao, F. P. G. de Arquer, T. S. Safaei, A. Mepham, A. Klinkova, E. Kumacheva, T. Filleter, D. Sinton, S. O. Kelley and E. H. Sargent, *Nature*, 2016, **537**, 382–386.

44 Y. Y. Birdja, E. Pérez-Gallent, M. C. Figueiredo, A. J. Göttle, F. Calle-Vallejo and M. T. M. Koper, *Nat. Energy*, 2019, **4**, 732–745.

CHAPTER 5

Final Conclusions and Future Work

5.1 Conclusions

This thesis has shown that electrochemical reduction of CO_2 at sub-zero temperatures is not only feasible but can have tangible benefits. However, this work also shows that a complete understanding of the effects of temperature, electrolyte concentration, and CO_2 concentration are essential before the system can be scaled up. As with any new technology a clear picture of limitations on the small scale can help pre-empt problems on a large scale.

Reviewing the current literature, alternative electrolytes may have significant advantages for CO_2RR when the target products are not hydrocarbons, for example CO and carbon. However, when hydrocarbons are the focus, a proton source is essential which reintroduces the HER as a competing reaction. An ideal electrolyte balances efficiency, expense, and safety. Ionic liquids can have very high CO_2 concentrations but are expensive to manufacture, molten carbonates use non-precious metal electrodes but require very high operating temperatures, and organic solvents can degrade and be hazardous to health. Hence the argument can therefore be made that the benefits of these alternative electrolytes do not outweigh the affordability and accessibility of aqueous electrolytes.

Experimental work in Chapter 2 showed that using brines of KOH and $Mg(ClO_4)_2$, CO_2RR can be carried out at sub-zero temperatures and in these conditions, the CO_2RR is promoted and the HER is hindered. Untangling the cause of these results is essential for further development. Rotating disk electrode experiments in $Mg(ClO_4)_2$ confirmed that the current due to the CO_2RR increased at low temperatures, independently of mass transport. Further experiments in Chapter 3 highlighted that the mass transport of CO_2 can vary greatly between room temperature and temperatures below 0 °C. As the temperature decreases, the physical parameter of viscosity increases and influences the diffusion coefficient of CO_2 such that the mass transport would be reduced. Together these results seem to indicate that under undefined mass transport conditions, increases in the current are not due to high mass transport of CO_2 to the electrode surface, but more likely an increase in the CO_2 concentration.

One of the central ideas in this thesis is that CO_2 concentration increases at low temperatures. The increase in the density of KOH at low temperatures supports this hypothesis. However, for $Mg(ClO_4)_2$ there are contradictory results. There was no measured change in density using the methodology in Chapter 3, but using OLEMS in Chapter 2, which is more sensitive, there was a small increase in CO_2 concentrations. This merits further investigation since it could be that the concentration of $Mg(ClO_4)_2$ used is so close to the saturation point, that the salting out effect, limits the CO_2 absorption to negligible amounts, even at low temperatures.

Not only does the concentration of the electrolyte affect the physical characteristics, the computational calculations in Chapter 4 indicate that reaction intermediates are affected differently by ions, and so the increased concentration of ions can change the selectivity of the reaction. The effect of alkali metal cations on the selectivity of the CO_2RR is already observed in the literature, but the calculations here show that Mg^{2+} has dissimilar effects to K^+ and Na^+. This result could be utilised for changing selectivity in conventional dilute aqueous electrolytes.

This body of work has shown that for the electrochemical reduction of CO_2, the parameters of low temperatures and high electrolyte concentration are under-explored pathways with recognisable benefits. Space exploration missions could use these reactions to synthesis useful chemicals directly on the surface of Mars. For environmental remediation on Earth, CO_2RR for carbon capture and utilisation could take advantage of high cation concentrations, which are shown here to change the selectivity of the reaction. An alternative pathway for this research is for detection of CO_2 in deep sea clathrate structures since the size of the CO_2 reduction current can be correlated to the concentration. However, further research is needed, and the next experiments are described below.

5.2 Future work

The parameters of temperature, electrolyte concentration and CO_2 concentration need to be effectively disentangled. The density and viscosity measurements of Chapter 3 should be conducted at different concentrations of electrolyte and then with increasing concentrations of CO_2. Then the effect of each parameter can on the viscosity of the electrolyte and the diffusion coefficient of CO_2 can be seen independently. Once this is determined, further rotating electrode experiments should be carried out to determine the kinetics of the reaction at low temperatures.

In order to vary the concentration of CO_2 in solution, experiments on varying the CO_2 bubbling time or pressure should be carried out. However, a consistent methodology for measuring CO_2 concentration first needs to be established so that its influence can be isolated from the influence of temperature and electrolyte concentration. From the work presented here, OLEMS seems to be more sensitive but alternatively, pycnometers with a larger volume could be explored. Larger volumes of electrolyte would have larger changes in mass on saturation with CO_2, which may then be measurable using an analytical balance. This methodology is faster and does not utilise the assumption that all dissolved CO_2 is released into its gaseous form used for analysis of OLEMS experiments.

Further computational calculations should look at the stabilisation of C_2 products by Mg^{2+} and also how solvated cations interact with the intermediates. This would provide a full picture of the stabilisation of all intermediates along the reaction pathway to hydrocarbons. Extending the scaling relations to key C_2 intermediates, such as the adsorbed CO dimer, will allow for general predictions on the products on different metal catalysts.

The other major area that needs to be explored is the oxidation reaction happening at the anode. Oxygen evolution from water is the reaction taking place under these experimental conditions and on the surface of Mars, this would be exceptionally useful as O_2 is needed for astronaut survival and as fuel. If this reaction is dramatically hindered under the low

temperature, high electrolyte concentration conditions, then the overall efficiency of the electrolyser will be reduced.